

ISSN 1881-7831 Online ISSN 1881-784X

DD & T

Drug Discoveries & Therapeutics

Volume 11, Number 5
October, 2017



www.ddtjournal.com

DD&T

Drug Discoveries & Therapeutics



ISSN: 1881-7831
Online ISSN: 1881-784X
CODEN: DDTRBX
Issues/Year: 6
Language: English
Publisher: IACMHR Co., Ltd.

Drug Discoveries & Therapeutics is one of a series of peer-reviewed journals of the International Research and Cooperation Association for Bio & Socio-Sciences Advancement (IRCA-BSSA) Group and is published bimonthly by the International Advancement Center for Medicine & Health Research Co., Ltd. (IACMHR Co., Ltd.) and supported by the IRCA-BSSA and Shandong University China-Japan Cooperation Center for Drug Discovery & Screening (SDU-DDSC).

Drug Discoveries & Therapeutics publishes contributions in all fields of pharmaceutical and therapeutic research such as medicinal chemistry, pharmacology, pharmaceutical analysis, pharmaceuticals, pharmaceutical administration, and experimental and clinical studies of effects, mechanisms, or uses of various treatments. Studies in drug-related fields such as biology, biochemistry, physiology, microbiology, and immunology are also within the scope of this journal.

Drug Discoveries & Therapeutics publishes Original Articles, Brief Reports, Reviews, Policy Forum articles, Case Reports, News, and Letters on all aspects of the field of pharmaceutical research. All contributions should seek to promote international collaboration in pharmaceutical science.

Editorial Board

Editor-in-Chief:

Kazuhisa SEKIMIZU
Teikyo University, Tokyo, Japan

Co-Editors-in-Chief:

Xishan HAO
Tianjin Medical University, Tianjin, China
Munehiro NAKATA
Tokai University, Hiratsuka, Japan

Chief Director & Executive Editor:

Wei TANG
The University of Tokyo, Tokyo, Japan

Senior Editors:

Guanhua DU
Chinese Academy of Medical Science and Peking Union Medical College, Beijing, China
Xiao-Kang LI
National Research Institute for Child Health and Development, Tokyo, Japan
Masahiro MURAKAMI
Osaka Ohtani University, Osaka, Japan
Yutaka ORIHARA
The University of Tokyo, Tokyo, Japan
Tomofumi SANTA
The University of Tokyo, Tokyo, Japan
Hongbin SUN
China Pharmaceutical University, Nanjing, China

Fengshan WANG
Shandong University, Ji'nan, China

Managing Editor:

Hiroshi HAMAMOTO
Teikyo University, Tokyo, Japan

Web Editor:

Yu CHEN
The University of Tokyo, Tokyo, Japan

Proofreaders:

Curtis BENTLEY
Roswell, GA, USA
Thomas R. LEBON
Los Angeles, CA, USA

Editorial and Head Office:

Pearl City Koishikawa 603,
2-4-5 Kasuga, Bunkyo-ku,
Tokyo 112-0003, Japan
Tel.: +81-3-5840-9697
Fax: +81-3-5840-9698
E-mail: office@ddtjournal.com

Drug Discoveries & Therapeutics

Editorial and Head Office

Pearl City Koishikawa 603, 2-4-5 Kasuga, Bunkyo-ku,
Tokyo 112-0003, Japan

Tel: +81-3-5840-9697, Fax: +81-3-5840-9698
E-mail: office@ddtjournal.com
URL: www.ddtjournal.com

Editorial Board Members

Alex ALMASAN <i>(Cleveland, OH)</i>	Rodney J. Y. HO <i>(Seattle, WA)</i>	Xingyuan MA <i>(Shanghai)</i>	Yuhong XU <i>(Shanghai)</i>
John K. BUOLAMWINI <i>(Memphis, TN)</i>	Hsing-Pang HSIEH <i>(Zhunan, Miaoli)</i>	Ken-ichi MAFUNE <i>(Tokyo)</i>	Bing YAN <i>(Ji'nan, Shandong)</i>
Jianping CAO <i>(Shanghai)</i>	Yongzhou HU <i>(Hangzhou, Zhejiang)</i>	Sridhar MANI <i>(Bronx, NY)</i>	Yun YEN <i>(Duarte, CA)</i>
Shousong CAO <i>(Buffalo, NY)</i>	Yu HUANG <i>(Hong Kong)</i>	Tohru MIZUSHIMA <i>(Tokyo)</i>	Yasuko YOKOTA <i>(Tokyo)</i>
Jang-Yang CHANG <i>(Tainan)</i>	Hans E. JUNGINGER <i>(Marburg, Hesse)</i>	Abdulla M. MOLOKHIA <i>(Alexandria)</i>	Takako YOKOZAWA <i>(Toyama, Toyama)</i>
Fen-Er CHEN <i>(Shanghai)</i>	Amrit B. KARMARKAR <i>(Karad, Maharashtra)</i>	Yoshinobu NAKANISHI <i>(Kanazawa, Ishikawa)</i>	Rongmin YU <i>(Guangzhou, Guangdong)</i>
Zhe-Sheng CHEN <i>(Queens, NY)</i>	Toshiaki KATADA <i>(Tokyo)</i>	Weisan PAN <i>(Shenyang, Liaoning)</i>	Guangxi ZHAI <i>(Ji'nan, Shandong)</i>
Zilin CHEN <i>(Wuhan, Hubei)</i>	Gagan KAUSHAL <i>(Philadelphia, PA)</i>	Rakesh P. PATEL <i>(Mehsana, Gujarat)</i>	Liangren ZHANG <i>(Beijing)</i>
Shaofeng DUAN <i>(Lawrence, KS)</i>	Ibrahim S. KHATTAB <i>(Kuwait)</i>	Shivanand P. PUTHLI <i>(Mumbai, Maharashtra)</i>	Lining ZHANG <i>(Ji'nan, Shandong)</i>
Chandradhar DWIVEDI <i>(Brookings, SD)</i>	Shiroh KISHIOKA <i>(Wakayama, Wakayama)</i>	Shafi qur RAHMAN <i>(Brookings, SD)</i>	Na ZHANG <i>(Ji'nan, Shandong)</i>
Mohamed F. EL-MILIGI <i>(6th of October City)</i>	Robert Kam-Ming KO <i>(Hong Kong)</i>	Adel SAKR <i>(Cairo)</i>	Ruiwen ZHANG <i>(Amarillo, TX)</i>
Hao FANG <i>(Ji'nan, Shandong)</i>	Nobuyuki KOBAYASHI <i>(Nagasaki, Nagasaki)</i>	Gary K. SCHWARTZ <i>(New York, NY)</i>	Xiu-Mei ZHANG <i>(Ji'nan, Shandong)</i>
Marcus L. FORREST <i>(Lawrence, KS)</i>	Norihiro KOKUDO <i>(Tokyo, Japan)</i>	Yuemao SHEN <i>(Ji'nan, Shandong)</i>	Yongxiang ZHANG <i>(Beijing)</i>
Takeshi FUKUSHIMA <i>(Funabashi, Chiba)</i>	Toshiro KONISHI <i>(Tokyo)</i>	Brahma N. SINGH <i>(New York, NY)</i>	
Harald HAMACHER <i>(Tübingen, Baden-Württemberg)</i>	Chun-Guang LI <i>(Melbourne)</i>	Tianqiang SONG <i>(Tianjin)</i>	<i>(As of February 2017)</i>
Kenji HAMASE <i>(Fukuoka, Fukuoka)</i>	Minyong LI <i>(Ji'nan, Shandong)</i>	Sanjay K. SRIVASTAVA <i>(Amarillo, TX)</i>	
Junqing HAN <i>(Ji'nan, Shandong)</i>	Xun LI <i>(Ji'nan, Shandong)</i>	Chandan M. THOMAS <i>(Bradenton, FL)</i>	
Xiaojiang HAO <i>(Kunming, Yunnan)</i>	Jikai LIU <i>(Kunming, Yunnan)</i>	Murat TURKOGLU <i>(Istanbul)</i>	
Kiyoshi HASEGAWA <i>(Tokyo)</i>	Xinyong LIU <i>(Ji'nan, Shandong)</i>	Hui WANG <i>(Shanghai)</i>	
Waseem HASSAN <i>(Rio de Janeiro)</i>	Yuxiu LIU <i>(Nanjing, Jiangsu)</i>	Quanxing WANG <i>(Shanghai)</i>	
Langchong HE <i>(Xi'an, Shaanxi)</i>	Hongxiang LOU <i>(Jinan, Shandong)</i>	Stephen G. WARD <i>(Bath)</i>	

Original Articles

- 230 - 237 **Structural analysis of an innate immunostimulant from broccoli, *Brassica oleracea* var. *italica*.**
Makoto Urai, Keiko Kataoka, Satoshi Nishida, Kazuhisa Sekimizu
- 238 - 245 **Characterization of the chemical structure and innate immunestimulating activity of an extracellular polysaccharide from *Rhizobium* sp. strain M2 screened using a silkworm muscle contraction assay.**
Makoto Urai, Tomoko Aizawa, Katsutoshi Imamura, Hiroshi Hamamoto, Kazuhisa Sekimizu
- 246- 252 **Glycyrrhizin inhibits human parainfluenza virus type 2 replication by the inhibition of genome RNA, mRNA and protein syntheses.**
Kae Sakai-Sugino, Jun Uematsu, Miyuki Kamada, Hiroe Taniguchi, Saori Suzuki, Yumiko Yoshimi, Sahoko Kihira, Hidetaka Yamamoto, Mitsuo Kawano, Masato Tsurudome, Myles O'Brien, Makoto Itoh, Hiroshi Komada
- 253 - 258 **Skin permeability of tulobuterol in two transdermal formulations and their followability.**
Yuichi Takizawa, Takeshi Goto, Shuji Sato, Naoya Ohmori, Kenji Mori, Yayoi Shimada, Kuei-Chen, Takamitsu Miyagi, Fumio Fukai
- 259 - 266 **Two-spotted cricket as an animal infection model of human pathogenic fungi.**
Yuto Kochi, Yasuhiko Matsumoto, Kazuhisa Sekimizu, Chikara Kaito
- 267 - 275 **Isolation of antibiotic-producing *Pseudomonas* species with lowtemperature cultivation of temperate soil.**
Shuhe Mitsutomi, Kazuhisa Sekimizu, Chikara Kaito
- 276 - 280 **Effect of methyl p-hydroxybenzoate on the culture of mammalian cell.**
Hidenori Tani, Jun-ichi Takeshita, Hiroshi Aoki, Kaoru Nakamura, Ryosuke Abe, Akinobu Toyoda, Yasunori Endo, Sadaaki Miyamoto, Masashi Gamo, Masaki Torimura, Hiroaki Sato
- 281 - 287 **Ethanol extracts of *Aster yomena* (Kitam.) Honda inhibit adipogenesis through the activation of the AMPK signaling pathway in 3T3-L1 preadipocytes.**
Min Ho Han, Ji-Suk Jeong, Jin-Woo Jeong, Sung Hyun Choi, Sung Ok Kim, Su Hyun Hong, Cheol Park, Byung Woo Kim, Yung Hyun Choi

CONTENTS

(Continued)

Brief Report

- 288 - 290 **Evaluation of the innate immune-stimulating activity of amazake using a silkworm muscle contraction assay.**
Hiroko Maruki-Uchida, Masahiko Sai, Kazuhisa Sekimizu

Case Report

- 291 - 292 **Early small bowel perforation due to aflibercept.**
Toufic Moussallem, Chetana Lim, Michael Osseis, Francesco Esposito, Eylon Lahat, Liliana Fuentes, Chady Salloum, Daniel Azoulay

Erratum

E1

Guide for Authors

Copyright

Structural analysis of an innate immunostimulant from broccoli, *Brassica oleracea* var. *italica*

Makoto Urai¹, Keiko Kataoka², Satoshi Nishida², Kazuhisa Sekimizu^{1,2,3,*}

¹ Graduate School of Pharmaceutical Sciences, The University of Tokyo, Tokyo, Japan;

² Genome Pharmaceuticals Institute Co., Ltd., Tokyo, Japan;

³ Teikyo University Institute of Medical Mycology, Tokyo, Japan.

Summary

Vegetables are eaten as part of a healthy diet throughout the world, and some are also applied topically as a traditional medicine. We evaluated the innate immunostimulating activities of hot water extracts of various vegetables using the silkworm muscle contraction assay system, and found that broccoli, *Brassica oleracea* var. *italica*, contains a strong innate immunostimulant. We purified the innate immunostimulant from broccoli, and characterized the chemical structure by chemical analyses and NMR spectroscopy. The innate immunostimulant comprised galacturonic acid, galactose, glucose, arabinose, and rhamnose, and had a pectic-like polysaccharide structure. To determine the structural motif involved in the innate immunostimulating activity, we modified the structure by chemical and enzymatic treatment, and found that the activity was attenuated by pectinase digestion. These findings suggest that a pectic-like polysaccharide purified from broccoli has innate immunostimulating activity, for which the polygalacturonic acid structure is necessary.

Keywords: Innate immune stimulating activity, pectic polysaccharide, polygalacturonic acid, silkworm muscle contraction assay, structure, vegetable

1. Introduction

Innate immunity is an animal's first line of defense against microbe infection or tumor development. Stimulation of innate immunity may be an effective method of preventing infectious diseases or cancer. An agent that stimulates innate immunity may help to maintain health, especially in aging humans. Medicinal herbs and mushrooms are a potential source of antitumor and immunomodulating agents based on their empirical drug actions, and active substances have been extracted (1). Few studies, however, have evaluated the innate immune-stimulating activity of compounds from natural sources by wide screening using a convenient method.

We advocate the use of silkworm larvae, *Bombyx mori*, as an animal model for the discovery of drug

candidates (2), and previously isolated lysocin E, a bactericidal antibiotic from the cultured supernatant of the soil bacterium *Lysobacter* sp. RH2180-5, using a silkworm model of infection (3). Injection of yeast β -glucans and bacterial peptidoglycans into the silkworm *Bombyx mori* induces maturation of the insect cytokine paralytic peptide, which results in muscle contraction of the larvae (4,5). We established an assay using the silkworm based on muscle contraction, which is associated with activation of innate immunity (6), and purified a polysaccharide with innate immunostimulating activity from green tea extracts (7). We also evaluated the activities of polysaccharides from natural origins using the silkworm muscle contraction assay (8). The silkworm muscle contraction assay has several advantages for evaluating innate immunostimulants (6-8). The system does not respond to lipopolysaccharide (LPS) due to presence of LPS-absorbing proteins in the hemolymph, and thus potential LPS contamination of the assay is negligible. Furthermore, the method is based on a bioassay using the silkworm body, and compounds with toxic activities or poor pharmacokinetics can be excluded from the candidate compounds.

Vegetables, which contain high amounts of nutrients,

Released online in J-STAGE as advance publication October 11, 2017.

*Address correspondence to:

Dr. Kazuhisa Sekimizu, Teikyo University Institute of Medical Mycology, 359 Otsuka, Hachioji, Tokyo 192-0395, Japan.

E-mail: sekimizu@main.teikyo-u.ac.jp

vitamins, minerals, and dietary fiber, are eaten as part of a healthy diet throughout the world. Some vegetables are also applied topically as a traditional medicine. We hypothesized that vegetables contribute to human health not only through their nutritional value, but also through their innate immunostimulant activity, similar to medicinal herbs. Vegetables are considered harmless to humans, empirically. In the present study, we evaluated the innate immune-stimulating activities of hot water extracts of various vegetables using the silkworm muscle contraction assay system, and found that broccoli, *Brassica oleracea* var. *italica*, contains a strong innate immunostimulant. Furthermore, we purified the innate immunostimulant from a hot water extract of broccoli, and characterized its chemical structure. We also determined the structural motif involved in the innate immunostimulating activity.

2. Materials and Methods

2.1. Hot water extraction of vegetables

The vegetables used in this study were purchased from local markets in Japan, and are listed in Table 1. The edible parts of the vegetables were cut into small pieces and autoclaved at 121°C for 15 min in 1 L of water (7,9). The sample was cooled and then centrifuged at 8000× g for 10 min at 4°C. The supernatant was lyophilized.

2.2. Silkworm muscle contraction assay

Eggs of silkworms (*Bombyx mori*, HuYo Tukuba Ne) were purchased from Ehime Sanshu (Ehime, Japan), and larvae were reared on an artificial diet (Silkmate 2S, Nihon Nosan, Yokohama, Japan) at 27°C. The silkworm muscle contraction assay was performed to evaluate innate immunity activation as previously described (4). Samples were dissolved in sterile saline, and 100 µL of each sample was injected into the body fluid of a specimen. The muscle contraction value was calculated by measuring the maximum length of each specimen before (x cm) and after (y cm) the injection according to the following formula: $(x - y)/x$. One unit of activity was defined as that causing muscle contraction with a value of 0.15. The specific activities of the samples were determined by creating a titration curve with diluted samples.

2.3. Purification of an innate immunostimulant from broccoli

Before the hot water extraction described above, edible parts (inflorescences and stems) of broccoli were heated in a microwave oven (600 W) for 5 min, and washed with MilliQ water (9). Two volumes of ethanol were added to the hot water extract, and the mixture was centrifuged. Precipitate dissolved in MilliQ water was

dialyzed against MilliQ water, and lyophilized. The lyophilized sample was dissolved in 10 mM Tris-HCl buffer (pH 8.0) and subjected to DEAE-cellulose column chromatography (DE-52, Whatman). After washing the column with 10 mM Tris-HCl buffer (pH 8.0), it was eluted with a linear gradient (0-0.4 M) of NaCl in the same buffer. Fractions containing carbohydrate were monitored by the phenol-H₂SO₄ method (10), combined, dialyzed against MilliQ water, and lyophilized.

2.4. Monosaccharide analysis

Samples were hydrolyzed by 4 M trifluoroacetic acid at 100°C for 3 h. Monosaccharides were labeled with aminobenzoic acid ethyl ester (ABEE) using an ABEE labeling kit (Seikagaku Corporation, Tokyo, Japan), and the ABEE-labeled saccharides were separated on an ODS column (Honenpak C18, 75 mm × 4.60 mm, Seikagaku Corporation, Tokyo, Japan) by high-performance liquid chromatography (HPLC; 1500 HPLC system, Waters, Milford, MA) according to the supplier's instructions.

2.5. Nuclear magnetic resonance (NMR) experiments

All NMR spectra were recorded at 500 MHz (¹H) and 125 MHz (¹³C) with an ECA 500 instrument (JEOL Ltd. Tokyo, Japan). Chemical shifts were given in δ units, with acetone (δ ¹H 2.23, δ ¹³C 31.1) used as an internal reference for samples measured in D₂O solutions. Signals were assigned based on two-dimensional homonuclear correlation spectroscopy, total correlated spectroscopy, heteronuclear multiple quantum coherence, and heteronuclear multiple bond coherence experiments. ¹H NMR chemical shifts of overlapping signals were obtained from the center of the cross-peaks in the two-dimensional (2D) spectra.

2.6. Methylation analysis

Before the methylation reaction, galacturonic acid in the sample was methyl-esterified, and reduced to (6,6-dideutero)galactose using NaBD₄ as described previously (11). Methylation of the polysaccharide was performed according to the Ciucanu method using sodium hydroxide and CH₃I (12). The methylated polysaccharide was then hydrolyzed, reduced, and acetylated before analysis by gas chromatography/mass spectroscopy (GLC-MS). The GLC-MS analysis was performed with a QP-2010 plus instrument (Shimadzu, Kyoto, Japan) fitted with a fused silica capillary column (Rtx-5, 30 m × 0.25 mm × 0.25 µm; Restek, Shimadzu).

2.7. Structural modifications of the innate immunostimulant

The arabinofuranose residue in the sample was hydrolyzed with oxalic acid, selectively (13). The

hydrolysate was neutralized, dialyzed against MilliQ water, and lyophilized.

The polygalacturonic acid moiety was digested using pectinase from *Aspergillus niger* (Sigma-Aldrich) according to the manufacturer's protocol. The hydrolyzed material was fractionated by gel-filtration column chromatography on a Bio-Gel P-4 (900 × 15 mmφ) with 0.2 M acetic acid as the eluent. Fractions containing carbohydrate were monitored by the phenol-H₂SO₄ method, combined, and lyophilized.

3. Results

3.1. Evaluation of innate immune-stimulating activity of hot water extracts of various vegetables

The edible parts of 17 vegetables purchased from local markets in Japan were extracted by hot water. The innate immune-stimulating activity of hot water extracts was evaluated by the silkworm muscle contraction assay. The activities varied according to the species of vegetables, and the extract from broccoli, *Brassica oleracea* var. *italica*, exhibited the highest activity among them with 7 units/mg of specific activity (Table 1). Next, we tried to purify the active compound from broccoli.

3.2. Purification of innate immunostimulant from broccoli

The innate immunostimulant was purified from a hot

water extract of the edible parts (inflorescences and stems) of broccoli by monitoring the silkworm muscle contraction activity. The purification of the innate immunostimulant from broccoli is summarized in Table 2. First, the activity was recovered by ethanol precipitation against the hot water extract. This suggests that the active substrate is a high molecular-weight compound, probably a polysaccharide. Next, we performed DEAE-cellulose column chromatography eluted with a linear gradient of NaCl, and carbohydrate-eluted fractions were detected by the phenol-H₂SO₄ method. This procedure produced two major peaks at 0 M (non-absorbed fraction) and ~0.2 M concentration of NaCl (acidic fraction, AF), and the fractions contained in these peaks were combined, dialyzed, and lyophilized (data not shown). The activity was recovered in both peaks. Because the AF may comprise a homogeneous polysaccharide as described below, we characterized this fraction further. Analysis of the non-absorbed fraction may be presented elsewhere. The specific activity was increased in the AF as 130 units/mg (Table 2).

3.3. Structural analysis of the innate immunostimulant from broccoli

The monosaccharide content of the AF was determined by trifluoroacetic acid hydrolysis followed by HPLC analysis. Consequently, galacturonic acid (GalA), arabinose (Ara), galactose (Gal), rhamnose (Rha), and glucose (Glc) were detected (Figure 1) in molar ratios of 12: 7.3: 4.9: 1.2: 1.0. These results suggest that the structure of the innate immunostimulant in the AF is a pectic-like polysaccharide (14).

We performed further structural analysis by NMR. ¹H and ¹³C NMR analysis showed that the pattern of detected signals in the AF was a polysaccharide, not a protein or lipid (Figure 2). Assignments of major signals could be made from 2D NMR experiments (Table 3). The spin system of the GalA residue, the most abundant constituent in AF according to monosaccharide analysis, was strongly detected. The chemical shifts of the anomeric proton and carbon of GalA were detected at 5.07 and 99.8 ppm, respectively, suggesting that the GalA residue has an α configuration. The chemical shifts of this spin system revealed that the GalA residue exists in this fraction as α-1,4-polygalacturonic acid with a pyranose form (15,16). Methyl signals of the GalA methyl ester, a characteristic structure of homogalacturonan in a plant pectin, were not detected.

Table 1. Muscle contraction activity of hot water extracts of various vegetables

Vegetables	Specific activity (units/mg)
<i>Allium fistulosum</i> (Leek)	1
<i>Allium sativum</i> (Garlic)	0.0
<i>Brassica oleracea</i> var. <i>capitata</i> (Cabbage)	< 0.4
<i>Brassica oleracea</i> var. <i>italica</i> (Broccoli)	7
<i>Brassica rapa</i> var. <i>glabra</i> (Chinese cabbage)	0.3
<i>Capsicum annuum</i> var. <i>grossum</i> (Green pepper)	0.3
<i>Cucumis sativus</i> (Cucumber)	0.8
<i>Cucurbita moschata</i> (Pumpkin)	< 0.1
<i>Daucus carota</i> (Carrot)	0.6
<i>Lycopersicon esculentum</i> (Cherry tomato)	0.5
<i>Petroselinum crispum</i> (Parsley)	0.7
<i>Pisum sativum</i> (Pea)	< 0.2
<i>Raphanus sativus</i> var. <i>longipinnatus</i> (Japanese radish)	0.2
<i>Siraitia grosvenorii</i> (Arhat fruit)	0.6
<i>Solanum melongena</i> (Eggplant)	0.5
<i>Spinacia oleracea</i> (Spinach)	< 0.2
<i>Zingiber officinale</i> (Ginger)	< 0.3

Table 2. Summary of the purification of the innate immunostimulant from broccoli

Fraction	Total activity (units)	Amount (mg)	Specific activity (units/mg)
Hot water extract	50,000	800	63
Ethanol extract	11,000	250	44
DEAE-cellulose chromatography (Acidic fraction)	13,000	100	130

The chemical shift of the carbonyl carbon of GalA detected at 176.2 ppm also suggested that the residue is not methyl-esterified (15,16). A small amount of acetyl ester was detected at ~2 ppm in ^1H NMR and 20 ppm in ^{13}C NMR analysis (Figure 2). The spin system of the

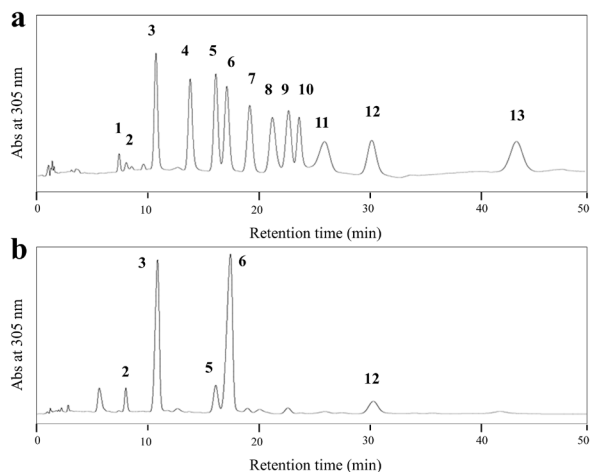


Figure 1. HPLC elution profile of acid hydrolysate of the acidic fraction. Panel (a), standard samples; and (b), AF. Standard samples: 1, D-glucuronic acid; 2, D-galacturonic acid; 3, D-galactose; 4, D-mannose; 5, D-glucose; 6, L-arabinose; 7, D-ribose; 8, *N*-acetyl-D-mannosamine; 9, D-xylose; 10, *N*-acetyl-D-glucosamine; 11, L-fucose; 12, L-rhamnose; and 13, *N*-acetyl-D-galactosamine.

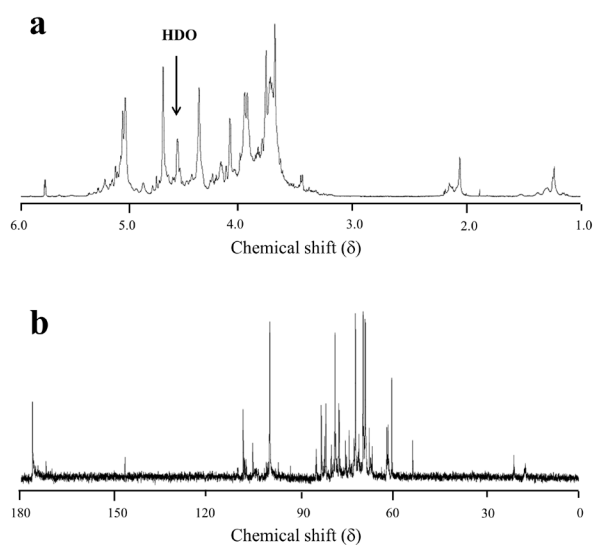


Figure 2. NMR spectra of the acidic fraction. (a), 500 MHz ^1H NMR; (b), 125 MHz ^{13}C NMR spectrum recorded in D_2O at 40°C .

Ara residue, the second-most abundant constituent in the AF, was partially assigned, and the chemical shifts of the detected signals revealed that the Ara residue exists in the AF as α -1,5-arabinan with a furanose form (15,16). We could not assign the weak signals belonging to the other sugar residues present in small amounts in the AF.

We then performed methylation analysis to elucidate the detailed connectivity of sugar residues detected by the monosaccharide analysis. Thirteen peaks of the partially methylated alditol acetate derivatives were detected by gas liquid chromatography-mass spectrometry analysis (Supplementary Figure 1). According to the retention times and mass fragmentation patterns of the detected peaks, the connectivity of the sugar residues was determined (Table 4). The datasets of the detected sugar connectivity suggest that the structure of the innate immunostimulant in AF is a pectic-like polysaccharide, composed of a homogalacturonan with a rhamnagalacturonan I (RG-I) structure, as described below. Based on the pectin structure reported previously (14), we propose the structural model of the innate immunostimulant from broccoli shown in Figure 3. The abundance of 4-GalpA and 5-Araf residues was consistent with the results of the NMR analysis, and these results suggest that the 4-GalpA residue has an α -1,4-polygalacturonic acid structure, and the 5-Araf residue has an α -1,5-arabinan structure. Detection of the 2,4-Rhap residue suggests that the AF has an RG-I structure; *i.e.* $\rightarrow 4$ - α -GalpA-(1 \rightarrow 2)- α -Rhap-(1 \rightarrow), with the Rha residue substituted for by galactan and arabinan chains at the C-4 position (14,17). The presence of T-Araf, 3-Araf, and 3,5-Araf residues suggest that the α -1,5-arabinan chains are partially branched at the C-3 position (14,17). Detection of T-Galp, 4-Galp, 3-Galp, 6-Galp, and 3,6-Galp suggest the presence of β -1,4-galactan and β -1,3/6-galactan structures in the AF (14,17). We cannot propose the binding sites of the T-Rhap and T-Glcp residues detected as a minor components based on the methylation analysis.

3.4. Effects of structural modifications on the activity of the innate immunostimulant from broccoli

To determine the structural motif involved in the innate immunostimulating activity, we modified the structure of the innate immunostimulant chemically or enzymatically. The strategy used to modify the polysaccharide

Table 3. ^1H and ^{13}C NMR chemical shifts (ppm) of the acidic fraction recorded in D_2O at 40°C

Glycosyl residue	H-1 C-1	H-2 C-2	H-3 C-3	H-4 C-4	H-5 C-5	H-6 C-6
$\rightarrow 4$ - α -GalpA-(1 \rightarrow)	5.07 99.8	3.76 69.1	3.98 69.8	4.41 78.8	4.73 72.2	- 176.2
$\rightarrow 5$ - α -Araf-(1 \rightarrow)	5.09 108.3	4.13 NA	4.02 NA	4.21 NA	3.84 61.7	- -

NA, not assigned.

Table 4. Methylation analysis of the acidic fraction

Peak ^a	Derivatives	Structural feature	Mol %
1	1,4-di- <i>O</i> -acetyl-2,3,5-tri- <i>O</i> -methyl arabitol	T-Araf	5.7
2	1,5-di- <i>O</i> -acetyl-2,3,4-tri- <i>O</i> -methyl rhamnitol	T-Rhap	1.3
3	1,3,4-tri- <i>O</i> -acetyl-2,5-di- <i>O</i> -methyl arabitol	3-Araf	1.0
4	1,4,5-tri- <i>O</i> -acetyl-2,3-di- <i>O</i> -methyl arabitol	5-Araf	16
5	1,5-di- <i>O</i> -acetyl-2,3,4,6-tetra- <i>O</i> -methyl glucitol	T-Glcp	3.7
6	1,5-di- <i>O</i> -acetyl-2,3,4,6-tetra- <i>O</i> -methyl galactitol	T-Galp	3.6
7	1,3,4,5-tetra- <i>O</i> -acetyl-2-mono- <i>O</i> -methyl arabitol	3,5-Araf	4.4
8	1,2,4,5-tetra- <i>O</i> -acetyl-3-mono- <i>O</i> -methyl rhamnitol	2,4-Rhap	3.2
9	1,4,5-tri- <i>O</i> -acetyl-2,3,6-tri- <i>O</i> -methyl (6,6-dideutero)galactitol ^b	4-GalpA	46
10	1,4,5-tri- <i>O</i> -acetyl-2,3,6-tri- <i>O</i> -methyl galactitol	4-Galp	5.1
11	1,3,5-tri- <i>O</i> -acetyl-2,4,6-tri- <i>O</i> -methyl galactitol	3-Galp	3.7
12	1,5,6-tri- <i>O</i> -acetyl-2,3,4-tri- <i>O</i> -methyl galactitol	6-Galp	1.5
13	1,3,5,6-tetra- <i>O</i> -acetyl-2,4-di- <i>O</i> -methyl galactitol	3,6-Galp	4.5

^aDetected peaks were numbered in Supplementary Figure 1. ^bBefore the methylation reaction, galacturonic acid residue in the acidic fraction was methyl-esterified, and reduced to (6,6-dideutero)galactose using NaBD₄.

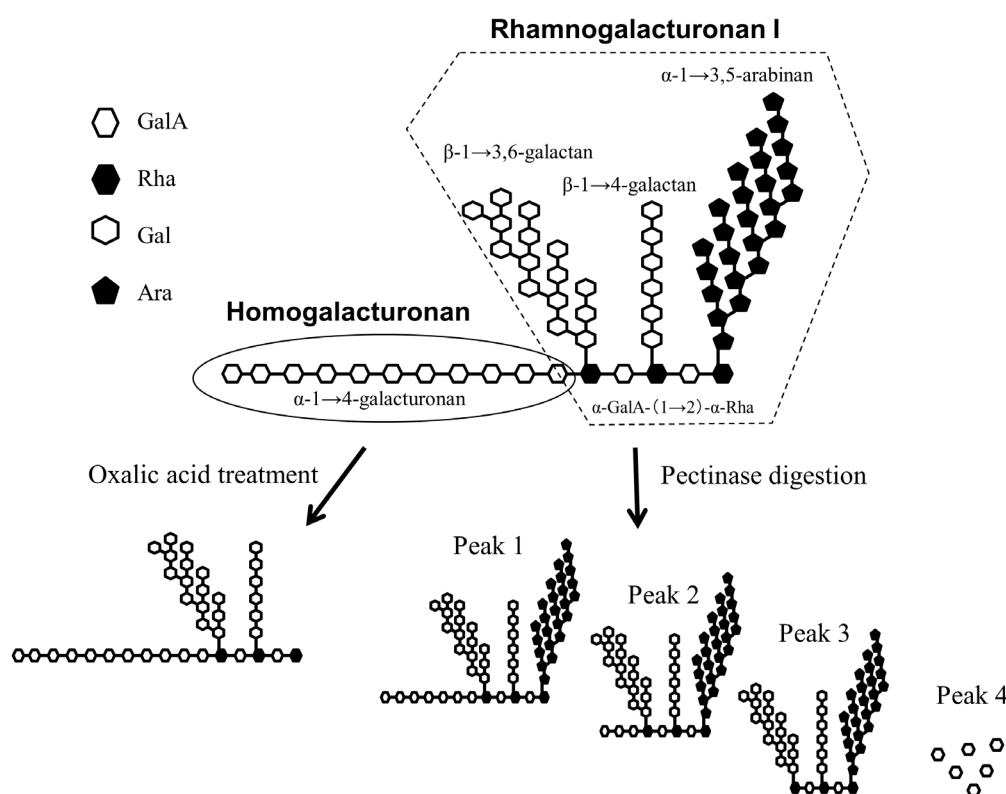


Figure 3. Structural model of the acidic fraction and scheme of the structural modifications. A schematic model of the structure of the acidic fraction and its structural modifications.

structure is shown in Figure 3. α -1,4-Polygalacturonic acid and arabinan are the main structures of the native polysaccharides, and thus we attempted to remove that moiety. Firstly, oxalic acid treatment was performed to remove the arabinan chain from this polysaccharide by specifically hydrolyzing the arabinofuranose bond. NMR analysis of the oxalic acid-treated fraction revealed that the signals of the Ara residue detected in the native polysaccharide (Table 3) were completely abolished (Figure 4). Monosaccharide analysis of this fraction also revealed that the Ara residue in the fraction was drastically reduced compared to the native polysaccharide

(Table 5). The innate immunostimulating activity of the fraction was evaluated using the silkworm muscle contraction assay, and the activity was not affected by oxalic acid treatment (Table 5). These findings suggest that the arabinan structure existing in the AF does not contribute to the innate immunostimulating activity.

Next, pectinase digestion was performed against the native polysaccharide to degrade the α -1,4-polygalacturonic acid structure. The digested sample was fractionated by gel filtration chromatography (Bio-Gel P-4) and carbohydrate-containing fractions were yielded as four peaks numbered from the first eluted one

shown in Figure 5. Monosaccharide analysis of each peak indicated that the molar ratio of the GalA residue contained in peaks 1 and 2 was reduced compared to that of native polysaccharide (Table 5). The GalA residue contained in peak 3 was undetectable. Peak 4 was a monosaccharide-containing fraction, and because the peak only consisted of GalA, it was released by pectinase digestion. Compared with the native polysaccharide, the innate immunostimulating activity was attenuated along with a decrease in the molecular weight by pectinase digestion, and that of peaks 3 and 4 was undetectable. These results suggest that the α -1,4-polygalacturonic acid structure in the AF is necessary for the innate immunostimulating activity.

4. Discussion

In the present study, we screened an innate immunostimulant from hot water extracts of 17 vegetables using the silkworm muscle contraction assay, and found that broccoli extracts had the highest immunostimulant activity among them. Broccoli is an

attractive vegetable for human health, and other bioactive compounds have been extracted, such as sulforaphane, which has anticarcinogenic activities (18). Recently, a polysaccharide having anti-cancer cell proliferation properties was also purified from the broccoli stem (19). Innate immune-stimulating compounds from broccoli, however, have not been reported. White cabbage (*Brassica oleracea* var. *capitata*, cultivar Bartolo), kale (*B. oleracea* var. *Sabellica* cultivar green Moskruset), and red kale (*B. oleracea* var. *Sabellica* cultivar Redbor), related subspecies of broccoli, contain a pectic polysaccharide that activates the complement system, which plays an important role in innate immunity (20). In the present study, hot water extract of cabbage cultivated in Japan (*B. oleracea* var. *capitata*), which is also a related subspecies of broccoli, did not exhibit innate immune-stimulating activity in the silkworm muscle contraction assay. The activities varied according to the vegetable subspecies.

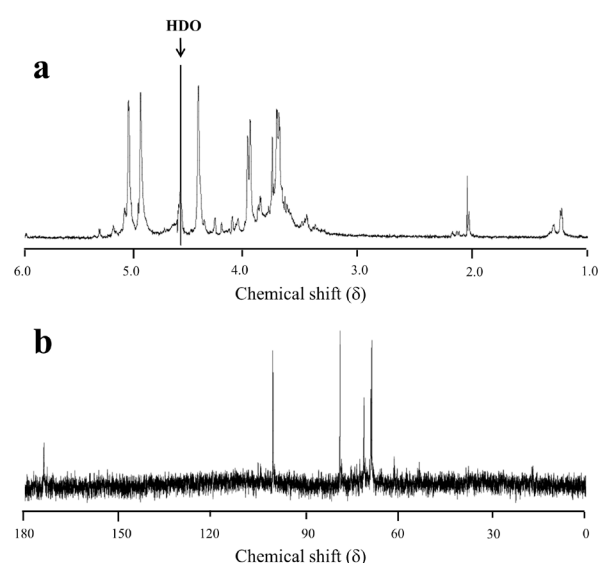


Figure 4. NMR spectra of the oxalic acid-treated acidic fraction. (a), 500 MHz ^1H NMR; (b), 125 MHz ^{13}C NMR spectrum recorded in D_2O at 40°C .

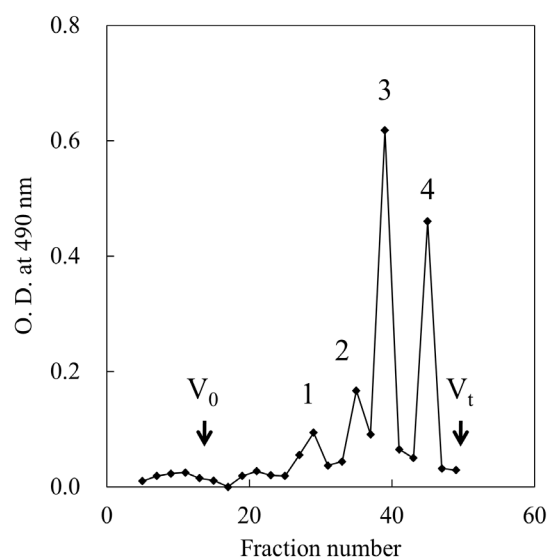


Figure 5. Gel filtration column chromatography of the pectinase-digested acidic fraction. The sample was applied to a Bio-Gel P-4 gel filtration column (1150 mm \times 15 mm ϕ), with 0.2 M acetic acid as an eluate. Blue dextran 2000 was used as a size marker to estimate the void volume (V_0), and V_t indicates the total volume of the gel. Fractions containing saccharide were monitored by the phenol- H_2SO_4 method.

Table 5. Effects of structural modifications on the muscle contraction activity of the acidic fraction

Samples	Sugar composition (mol %)						Activity (units)
	GalA	Gal	Glc	Ara	Xyl	Rha	
Acidic fraction	46	18	3.7	27	ND	4.5	630
Oxalic acid treatment	30	45	5.5	3.2	3.6	12	670 <
Pectinase							
Peak 1	23	22	5.0	28	5.0	18	370
Peak 2	24	24	6.0	17	5.5	24	240
Peak 3	ND	36	5.7	47	ND	12	< 160
Peak 4	100	ND	ND	ND	ND	ND	< 160

Ara, arabinose; Gal, galactose; GalA, galacturonic acid; Glc, glucose; Rha, rhamnose; Xyl, xylose. ND, not detected.

We purified the innate immunostimulant from hot water extract of broccoli, and characterized the chemical structure as a pectic-like polysaccharide, comprising homogalacturonan with an RG-I structure (structural model shown in Figure 3). Pectin is a structurally complex polysaccharide in plant cell walls that comprises mainly homogalacturonan, RG-I, and rhamnogalacturonan II (RG-II), and the distribution of each type of polysaccharide varies by the plant species (14). RG-II has a highly substituted α -1,4-polygalacturonic acid at the C-2 and C-3 positions with various oligosaccharide chains (14). Methylation analysis revealed a GalA residue as only a 4-substituted form in the innate immunostimulant purified from broccoli. This finding suggests that this polysaccharide did not contain the RG-II structure.

Pectin exhibits various types of bioactivity, such as immunomodulating activity, and the active moiety necessary to exert the activities is known for some of the types (21,22). Almost all active moieties of plant pectin having immunostimulating activity have a galactan or arabinan structure (21,22). Because α -1,4-polygalacturonic acid and arabinan were the main structures in the polysaccharide purified in our study, we removed each moiety by chemical and enzymatic treatment, and found that the activity was attenuated by degradation of the α -1,4-polygalacturonic acid structure. To our knowledge, this is the first report that the α -1,4-polygalacturonic acid motif in the pectic-like polysaccharide structure is necessary for the innate immune-stimulating activity. The pectic-like polysaccharide from broccoli may have a novel mode of action to stimulate innate immunity.

Although homogalacturonan is a common structure of plant pectins, it is unclear how the α -1,4-polygalacturonic acid in the broccoli polysaccharide stimulates innate immunity. Previously, we purified a polysaccharide with innate immune-stimulating activity from green tea extracts using the silkworm muscle contraction assay (7). This polysaccharide had a pectic-like structure composed of GalA, Gal, Glc, and Rha in a molar ratio of 22: 4: 5: 1. The main structure of this polysaccharide was α -1,4-polygalacturonic acid, like that of the innate immunostimulant from broccoli. Further studies are necessary to determine the structure-activity relations of the α -1,4-polygalacturonic acid in the silkworm muscle contraction assay. Additional studies are needed to determine whether α -1,4-polygalacturonic acid, which induces silkworm muscle contraction activity, exhibits innate immunostimulating activity in a mammalian system.

Acknowledgements

We acknowledge K. Imamura for technical assistance. This study was supported by a grant from the Genome Pharmaceutical Institute, Ltd.

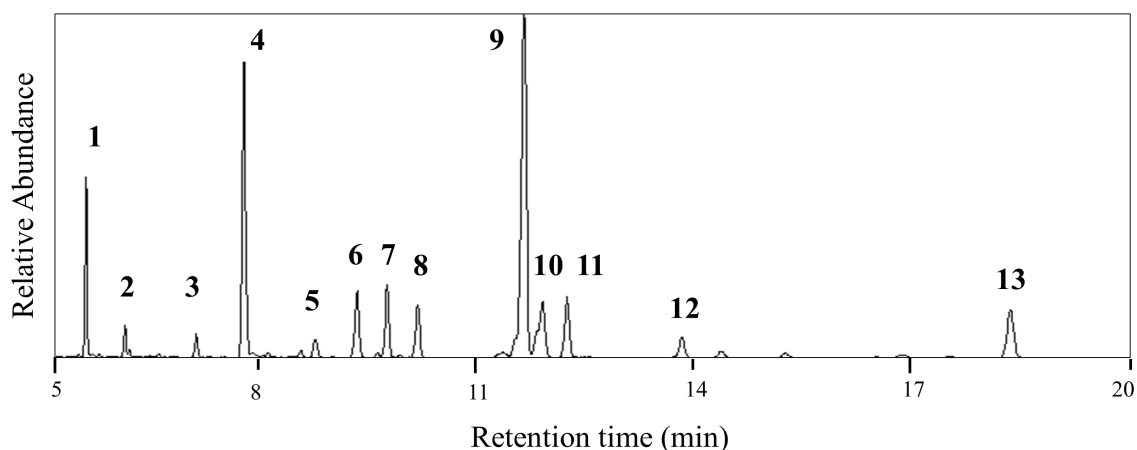
References

- Zong A, Cao H, Wang F. Anticancer polysaccharides from natural resources: A review of recent research. *Carbohydr Polym.* 2012; 90:1395-1410.
- Nwibo DD, Hamamoto H, Matsumoto Y, Kaito C, Sekimizu K. Current use of silkworm larvae (*Bombyx mori*) as an animal model in pharmaco-medical research. *Drug Discov Ther.* 2015; 9:133-135.
- Hamamoto H, Urai M, Ishii K, *et al.* Lysocin E is a new antibiotic that targets menaquinone in the bacterial membrane. *Nat Chem Biol.* 2015; 11:127-133.
- Ishii K, Hamamoto H, Kamimura M, Sekimizu K. Activation of the silkworm cytokine by bacterial and fungal cell wall components via a reactive oxygen species-triggered mechanism. *J Biol Chem.* 2008; 283:2185-2191.
- Ishii K, Hamamoto H, Kamimura M, Nakamura Y, Noda H, Imamura K, Mita K, Sekimizu K. Insect cytokine paralytic peptide (PP) induces cellular and humoral immune responses in the silkworm *Bombyx mori*. *J Biol Chem.* 2010; 285:28635-28642.
- Ishii K, Hamamoto H, Sekimizu K. Studies of host-pathogen interactions and immune-related drug development using the silkworm: Interdisciplinary immunology, microbiology, and pharmacology studies. *Drug Discov Ther.* 2015; 9:238-246.
- Dhital S, Hamamoto H, Urai M, Ishii K, Sekimizu K. Purification of innate immunostimulant from green tea using a silkworm muscle contraction assay. *Drug Discov Ther.* 2011; 5:18-25.
- Fujiyuki T, Hamamoto H, Ishii K, Urai M, Kataoka K, Takeda T, Shibata S, Sekimizu K. Evaluation of innate immune stimulating activity of polysaccharides using a silkworm (*Bombyx mori*) muscle contraction assay. *Drug Discov Ther.* 2012; 6:88-93.
- Sekimizu K, Hamamoto H, Ogata Y. Innate immune activation composition with enhanced plant-derived innate immune activation effect. Patent. 2009; WO2009157409.
- DuBois M, Gilles KA, Hamilton JK, Rebers PA, Smith F. Colorimetric method for determination of sugars and related substances. *Anal Chem.* 1956; 28:350-356.
- Deng C, O'Neill MA, York WS. Selective chemical depolymerization of rhamnogalacturonans. *Carbohydr Res.* 2006; 341:474-484.
- Ciucanu I, Kerek F. A simple and rapid method for the permethylation of carbohydrates. *Carbohydr Res.* 1984; 131:209-217.
- Cartier N, Chambat G, Joseleau JP. An arabinogalactan from the culture medium of *Rubus fruticosus* cells in suspension. *Carbohydr Res.* 1987; 168:275-283.
- Ridley BL, O'Neill MA, Mohnen D. Pectins: Structure, biosynthesis, and oligogalacturonide-related signaling. *Phytochemistry.* 2001; 57:929-967.
- Petersen BO, Meier S, Duus JO, Clausen MH. Structural characterization of homogalacturonan by NMR spectroscopy-assignment of reference compounds. *Carbohydr Res.* 2008; 343:2830-2833.
- Monge ME, Negri RM, Kolender AA, Erra-Balsells R. Structural characterization of native high-methoxylated pectin using nuclear magnetic resonance spectroscopy and ultraviolet matrix-assisted laser desorption/ionization time-of-flight mass spectrometry. Comparative use of 2,5-dihydroxybenzoic acid and nor-harmane as UV-MALDI matrices. *Rapid Commun Mass Spectrom.* 2007;

- 21:2638-2646.
17. Westereng B, Yousif O, Michaelsen TE, Knutsen SH, Samuelsen AB. Pectin isolated from white cabbage – structure and complement-fixing activity. *Mol Nutr Food Res.* 2006; 50:746-755.
 18. Zhang Y, Talalay P, Cho CG, Posner GH. A major inducer of anticarcinogenic protective enzymes from broccoli: Isolation and elucidation of structure. *Proc Natl Acad Sci U S A.* 1992; 89:2399-2403.
 19. Xu L, Cao J, Chen W. Structural characterization of a broccoli polysaccharide and evaluation of anti-cancer cell proliferation effects. *Carbohydr Polym.* 2015; 126:179-184.
 20. Samuelsen AB, Westereng B, Yousif O, Holtekjølen AK, Michaelsen TE, Knutsen SH. Structural features and complement-fixing activity of pectin from three *Brassica oleracea* varieties: White cabbage, kale, and red kale. *Biomacromolecules.* 2007; 8:644-649.
 21. Popov SV, Ovodov YS. Polypotency of the immunomodulatory effect of pectins. *Biochemistry (Mosc).* 2013; 78:823-835.
 22. Aboughe-Angone S, Nguema-Ona E, Boudjeko T, Driouich A. Plant cell wall polysaccharides: Immunomodulators of the immune system and source of natural fibers. *Curr Top Phytochem.* 2006; 10:1-16.

(Received August 14, 2017; Accepted September 10, 2017)

Supplemental Data



Supplementary Figure S1. GLC patterns of partially methylated alditol acetate derivatives from the acidic fraction. 1, 1,4-di-*O*-acetyl-2,3,5-tri-*O*-methyl arabitol; 2, 1,5-di-*O*-acetyl-2,3,4-tri-*O*-methyl rhamnitol; 3, 1,3,4-tri-*O*-acetyl-2,5-di-*O*-methyl arabitol; 4, 1,4,5-tri-*O*-acetyl-2,3-di-*O*-methyl arabitol; 5, 1,5-di-*O*-acetyl-2,3,4,6-tetra-*O*-methyl glucitol; 6, 1,5-di-*O*-acetyl-2,3,4,6-tetra-*O*-methyl galactitol; 7, 1,3,4,5-tetra-*O*-acetyl-2-mono-*O*-methyl arabitol; 8, 1,2,4,5-tetra-*O*-acetyl-3-mono-*O*-methyl rhamnitol; 9, 1,4,5-tri-*O*-acetyl-2,3,6-tri-*O*-methyl (6,6-dideutero)galactitol; 10, 1,4,5-tri-*O*-acetyl-2,3,6-tri-*O*-methyl galactitol; 11, 1,3,5-tri-*O*-acetyl-2,4,6-tri-*O*-methyl galactitol; 12, 1,5,6-tri-*O*-acetyl-2,3,4-tri-*O*-methyl galactitol; and 13, 1,3,5,6-tetra-*O*-acetyl-2,4-di-*O*-methyl galactitol.

Characterization of the chemical structure and innate immune-stimulating activity of an extracellular polysaccharide from *Rhizobium* sp. strain M2 screened using a silkworm muscle contraction assay

Makoto Urai^{1,4,*}, Tomoko Aizawa², Katsutoshi Imamura^{1,5}, Hiroshi Hamamoto^{1,6}, Kazuhisa Sekimizu^{1,3,6}

¹ Graduate School of Pharmaceutical Sciences, The University of Tokyo, Tokyo, Japan;

² Department of Bioscience in Daily Life, College of Bioresource Sciences, Nihon University, Fujisawa, Kanagawa, Japan;

³ Genome Pharmaceuticals Institute Co., Ltd., Tokyo, Japan;

⁴ Department of Chemistry for Life Sciences and Agriculture, Faculty of Life Sciences, Tokyo University of Agriculture, Tokyo, Japan;

⁵ Department of Microbiology and Molecular Genetics, Graduate School of Pharmaceutical Sciences, Chiba University, Chiba, Japan;

⁶ Teikyo University Institute of Medical Mycology, Tokyo, Japan.

Summary

We screened innate immunostimulant-producing bacteria using a silkworm muscle contraction assay, and isolated *Rhizobium* sp. strain M2 from soil. We purified the innate immunostimulant from strain M2, and characterized the chemical structure by nuclear magnetic resonance spectroscopy and chemical analyses. The innate immunostimulant (M2 EPS) comprised glucose, galactose, pyruvic acid, and succinic acid with a molar ratio of 6.8:1.0:0.9:0.4, and had a succinoglycan-like high molecular-weight heteropolysaccharide structure. To determine the structural motif involved in the innate immunostimulating activity, we modified the M2 EPS structure chemically, and found that the activity was increased by removal of the succinic and pyruvic acid substitutions. Strong acid hydrolysis completely inactivated the M2 EPS. Unmasking of the β -1,3/6-glucan structure of the side-chain by deacylation and depyruvylation may enhance the innate immune-stimulating activity of M2 EPS. These findings suggest that the succinoglycan-like polysaccharide purified from strain M2 has innate immune-stimulating activity, and its glycan structure is necessary for the activity.

Keywords: *Rhizobium*, extracellular polysaccharide, structure, innate immune-stimulating activity, silkworm muscle contraction assay

1. Introduction

Innate immunity is an important defense mechanism against microbe infection and tumor development. Natural agents that stimulate innate immunity may contribute to maintain human health. Medicinal

herbs and mushrooms are sources of antitumor and immunomodulating agents based on their empirical drug actions, and many active polysaccharides have been extracted (1). The structures of these active polysaccharides, however, are limited to β -glucans and pectins because they are mainly extracted from the cell walls of fungi and plants, respectively (1). Because polysaccharides extracted from cell walls are generally heterogeneous, the structural motif involved in their immune-stimulating activities is difficult to determine. Chemical synthesis of the highly polymerized glycan structure to imitate the active polysaccharide is also difficult.

Several applications of extracellular polysaccharide (EPS) secreted by bacteria have been proposed,

Released online in J-STAGE as advance publication October 11, 2017.

*Address correspondence to:

Dr. Makoto Urai, Department of Chemistry for Life Sciences and Agriculture, Faculty of Life Sciences, Tokyo University of Agriculture, 1-1-1 Sakuragaoka, Setagaya-ku, Tokyo 156-8502, Japan.

E-mail: mu206177@nodai.ac.jp

including those taking advantage of their antitumor or immunomodulating activities (2). Bacteria produce EPS with diverse structures made up of various kinds of monosaccharides, and are frequently substituted with organic or inorganic substances, such as organic acids, phosphate, and sulfate (2). EPS secreted to an ambient environment by bacteria are usually homogeneous compared to the cell wall polysaccharides extracted from fungi or plants, and their structures are constructed of regularly repeating units (2). This homogeneous and consistent structure may have advantages for determining the structure-activity relations. Wide screening of innate immune stimulants from bacterial EPS using a convenient method to evaluate innate immune-stimulating activities has not been performed.

We previously proposed using silkworm larvae, *Bombyx mori*, as an animal model for the discovery of drug candidates (3). We isolated lysocin E, a bactericidal antibiotic from the soil bacterium *Lysobacter* sp. RH2180-5, using a silkworm model of infection, and characterized its structure and mechanism of action (4). Injection of β -glucans from yeast and peptidoglycans from bacteria into the silkworm *Bombyx mori* induces maturation of the insect cytokine paralytic peptide, which results in muscle contraction of the larvae (5,6). We established an assay using the silkworm based on muscle contraction, which is associated with the activation of innate immunity (7), and isolated a polysaccharide with innate immune-stimulating activity from green tea (8). We also evaluated the activities of natural polysaccharides from various origins using the silkworm muscle contraction assay (9). This assay system does not respond to lipopolysaccharides (LPS) due to the presence of LPS-absorbing proteins in the silkworm hemolymph, which may be highly advantageous for screening innate immune-stimulating compounds from Gram negative bacteria, as contamination of the assay system by LPS during the first screening is negligible.

In the present study, we screened bacteria that produce EPS with innate immunostimulating activity using the silkworm muscle contraction assay system, and isolated *Rhizobium* sp. strain M2 from soil. Furthermore, we purified the EPS from culture of strain M2, and characterized the chemical structure. The structural motif involved in the innate immunostimulating activity is also discussed.

2. Materials and Methods

2.1. Silkworm muscle contraction assay

Eggs of silkworms (*Bombyx mori*, HuYo Tukuba Ne) were purchased from Ehime Sanshu (Ehime, Japan), and larvae were reared on an artificial diet (Silkmate 2S, Nihon Nosan, Yokohama, Japan) at 27°C. A silkworm muscle contraction assay was performed to evaluate innate-immunity activation, as described

previously (5). Samples were dissolved in sterile saline, and 100 μ L of each sample was injected into the body fluid of a specimen. The muscle contraction value was calculated by measuring the maximum length of each specimen before (x cm) and after (y cm) the injection using the formula $(x - y)/x$. One unit of activity was defined as that causing muscle contraction with a value of 0.15. The specific activities of the samples were determined by creating a titration curve with diluted samples.

2.2. Screening of innate immune-stimulant producing bacteria

First, we screened bacteria that form mucoid colonies on a glucose-asparagine (GA) agar plate [containing (l^{-1}): 10 g glucose, 0.5 g L-asparagine, 0.5 g K_2HPO_4 , and 15 g agar (pH 7)] from diluted soil samples collected from various sites in Japan. Isolated mucoid strains were grown on GA agar plates at 30°C under aerobic conditions. After a 5-day incubation, the cells were collected by scraping and suspended in saline. The cell suspensions were vigorously vortexed and centrifuged at 10,000 \times g for 10 min. The supernatant was saved, two volumes of ethanol were added, and the mixture was centrifuged. Precipitates were lyophilized, and the innate immunostimulating activity was evaluated using the silkworm muscle contraction assay.

Taxonomic analysis of the isolated strain was performed as described previously (10). The 16S rRNA gene of the isolated strains (~1,500 bp) was amplified by polymerase chain reaction using universal primers (11). The phylogenetic relationship with closely related species was determined using MEGA version 7 (12) and CLUSTAL_X (13). Evolutionary distances were computed as described previously (14), and the phylogenetic tree was constructed using the neighbor-joining method (15). The reliability of the tree topology was evaluated by bootstrap analysis with 1000 replicates (16).

2.3. Purification of M2 EPS

Strain M2 was grown on GA agar plates at 30°C for 5 days under aerobic conditions, and the cells were collected by scraping and suspended in saline. M2 EPS was extracted from the supernatant of the suspension as described previously (17), except the Sevag method was used instead of phenol-chloroform treatment (18). M2 EPS was further purified by DEAE-Toyopearl 650 M column chromatography as described previously (19). Fractions containing saccharides were monitored using the phenol- H_2SO_4 method (20). Two volumes of ethanol were added to each fraction, and the mixture was centrifuged. The precipitates were dissolved in saline, and the innate immunostimulating activity was evaluated using the silkworm muscle contraction

assay. The fractions contained in the activity peak were combined, dialyzed against MilliQ water, and lyophilized.

To confirm the homogeneity of M2 EPS, gel-filtration column chromatography was performed on a Sephacryl S1000 (850 mm × 15 mm; Amersham Biosciences UK Ltd., Buckinghamshire, UK) column with 1 mM Tris-HCl buffer (pH 8.0) containing 0.1 M NaCl as the eluent (17). Dextran T2000 (Amersham Biosciences UK Ltd., Buckinghamshire, UK) was used as a size marker. Fractions containing saccharide were monitored using the phenol-H₂SO₄ method.

2.4. Monosaccharide analysis

Monosaccharide analysis was performed as described previously (17). Briefly, M2 EPS was hydrolyzed by 4 M trifluoroacetic acid at 100°C for 3 h, and the obtained monosaccharides were labeled with aminobenzoic acid ethyl ester (ABEE) and analyzed by high performance liquid chromatography (HPLC; 1500 HPLC system, Waters, Milford, MA).

2.5. Nuclear magnetic resonance (NMR) experiments

All NMR spectra were recorded at 500 MHz (¹H) and 125 MHz (¹³C) with an ECA 500 instrument (JEOL Ltd. Tokyo, Japan). Chemical shifts were given in δ units, with acetone (δ ¹H 2.23, δ ¹³C 31.1) was used as an internal reference for samples measured in D₂O solutions. Two-dimensional (2D) homonuclear correlation spectroscopy, total correlated spectroscopy, heteronuclear multiple quantum coherence, and heteronuclear multiple bond coherence experiments were used to assign signals. ¹H NMR chemical shifts of overlapping signals were obtained from the center of the cross-peaks in the 2D spectra.

2.6. Methylation analysis

Polysaccharide methylation was performed according to the Ciucanu method using sodium hydroxide and CH₃I (21). The methylated polysaccharide was then hydrolyzed, reduced, and acetylated before analysis by gas chromatography/mass spectroscopy (GLC-MS). The GLC-MS analysis was performed with a QP-2010 plus instrument (Shimadzu, Kyoto, Japan) fitted with a fused silica capillary column (Rtx-5, 30 m × 0.25 mm × 0.25 μm; Restek, Shimadzu).

2.7. Structural modifications of M2 EPS

O-Deacylation and depyruvylation of M2 EPS were performed as described previously (17,22). Acid hydrolysis was performed under the same conditions described above (*Monosaccharide analysis*). The modified structures of M2 EPS were confirmed by

NMR analysis, and the innate immunostimulating activity was evaluated in the silkworm muscle contraction assay.

3. Results

3.1. Isolation of *Rhizobium* sp. strain M2, innate immune stimulant-producing bacteria

First, we screened bacteria from soil that formed mucoid colonies on an agar plate. To prevent contamination of the innate immune stimulant by components of the medium, (e.g., β-glucan from yeast extract), we used a GA agar plate, a chemically defined media. Next, EPS were roughly extracted from the isolated mucoid strains, and the innate immunostimulating activity was evaluated using the silkworm muscle contraction assay. Crude EPS from a strain named M2 exhibited immunostimulating activity (data not shown). The nearly complete 16S rRNA gene sequence (1479 bp) of strain M2 showed high similarities to sequences of other strains of species belonging to the genus *Rhizobium*, and the highest sequence similarities were found with the strain of *R. pusense* (98% similarity). The phylogenetic tree constructed using the neighbor-joining method is shown in Figure 1. *Rhizobium* sp. strain M2 was deposited as NBRC 108899 to the National Institute of Technology and Evaluation, Japan. Next, we purified the active compound from the crude EPS fraction of strain M2.

3.2. Purification of innate immune stimulant from *Rhizobium* sp. strain M2

The innate immune stimulant produced by *Rhizobium* sp. strain M2 was extracted and purified by DEAE-Toyopearl column chromatography, eluted with a linear gradient (0-1 M) of NaCl. This procedure gave a single peak of carbohydrate at ~0.5 M concentration of NaCl detected by the phenol-H₂SO₄ method (Figure 2). The silkworm muscle contraction activity in each fraction was also evaluated, and a single peak of activity was detected in the carbohydrate-eluted fractions. The fractions contained in this peak were combined as the M2 EPS.

M2 EPS was eluted as a symmetric single peak earlier than Dextran T2000 by Sephacryl S1000 gel-filtration chromatography (Figure 3), suggesting an apparent molecular weight greater than 2,000,000. These data indicate that the innate immune stimulant from *Rhizobium* sp. strain M2 was purified to homogeneity as M2 EPS.

M2 EPS induced silkworm muscle contraction in a dose-dependent manner, with a specific activity of 1.4 units/mg (Figure 4). Spectrophotometrically, no absorption was detected at 280 nm or at 255 nm, suggesting that the M2 EPS did not contain proteins or nucleic acids.

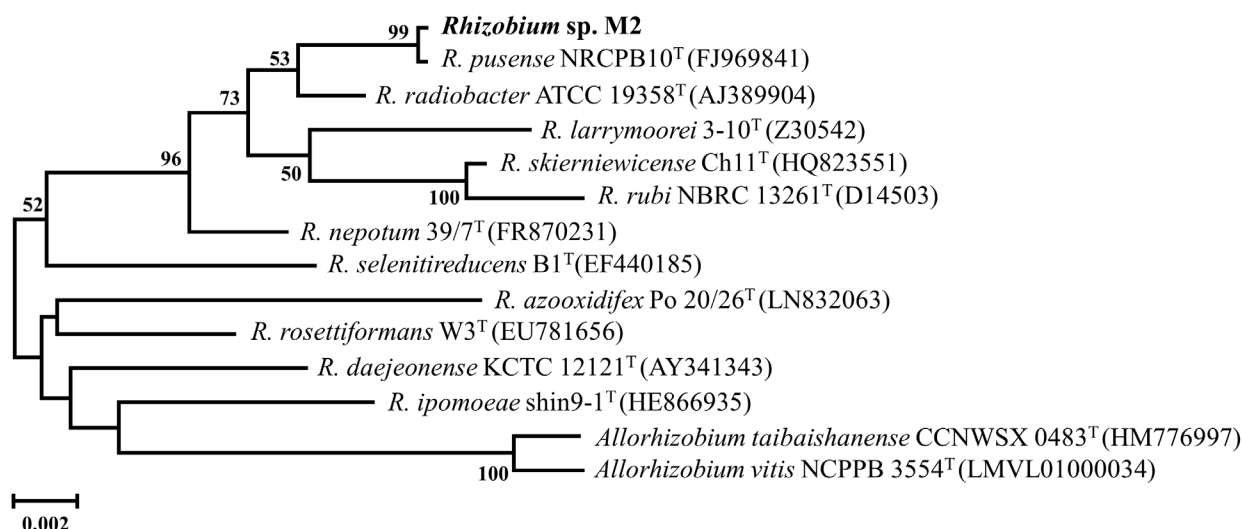


Figure 1. Neighbor-joining tree based on nearly complete 16S rRNA gene sequences, showing the position of the strain M2 among its phylogenetic neighbors. Numbers at branch nodes are percentages of bootstrap support based on 1000 resampling; only values over 50% are given. Bar, 0.002 substitutions per nucleotide position.

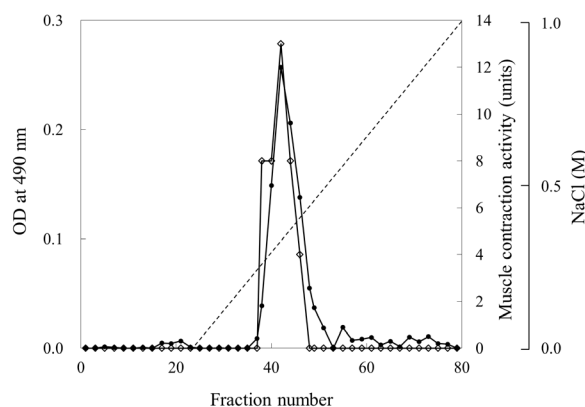


Figure 2. Ion-exchange chromatography of M2 EPS. M2 EPS was dissolved in 10 mM Tris-HCl buffer (pH 8.0), applied to a DEAE-Toyopearl column (100 mm × 25 mm φ), and eluted with a 300-mL linear gradient (0-1 M) of NaCl. Closed circles, OD at 490 nm; opened diamonds, muscle contraction activity.

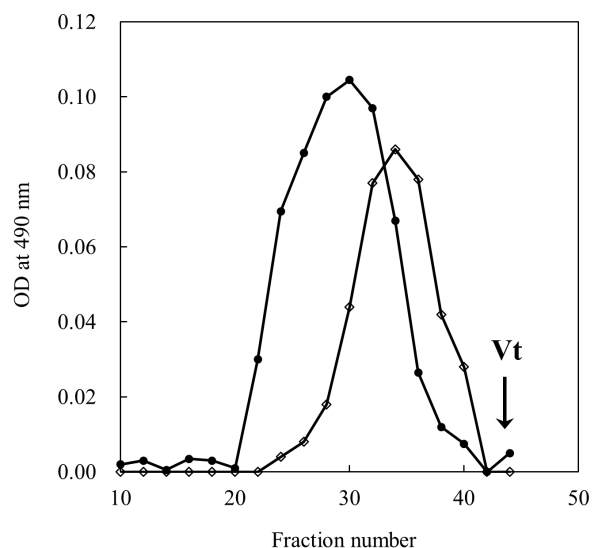


Figure 3. Gel filtration column chromatography of M2 EPS. M2 EPS was applied to a Sephacryl S1000 gel filtration column (1150 mm × 15 mm φ) and 1 mM Tris-HCl (pH 8.0) containing 0.1 M NaCl as an eluate. Blue dextran 2000 was used as a size marker. The arrow indicates the total volume of the gel (V_t). Closed circles, M2 EPS; opened diamonds, Blue dextran 2000.

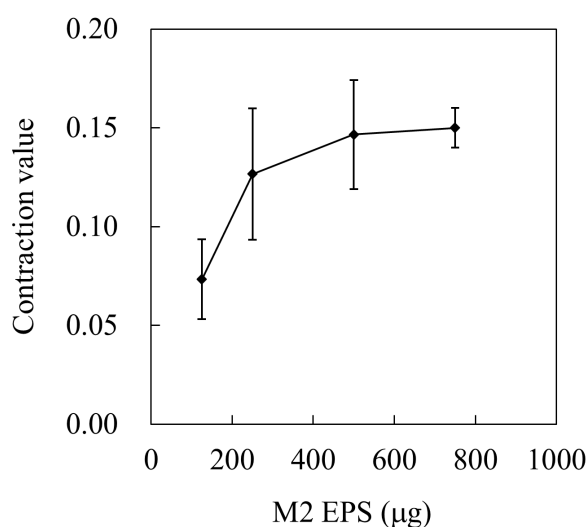


Figure 4. Muscle contraction of silkworm larval specimens by injecting of M2 EPS. The data-points represent the means ± S.D., $n = 3$.

3.3. Structural analysis of M2 EPS

The monosaccharide composition of M2 EPS, determined by trifluoroacetic acid hydrolysis and HPLC analysis, revealed glucose (Glc) and galactose (Gal) in a molar ratio of 6.8:1.0 (Figure 5). ¹H and ¹³C NMR analysis showed that the pattern of signals detected in M2 EPS was characteristic of a polysaccharide, not a protein or lipid (Figure 6). Although the signals detected in anomeric regions of both 1D spectra overlapped (δ 4.54-4.82 for ¹H and δ 101.7-104.4 for ¹³C), all anomeric signals detected were allocated to a

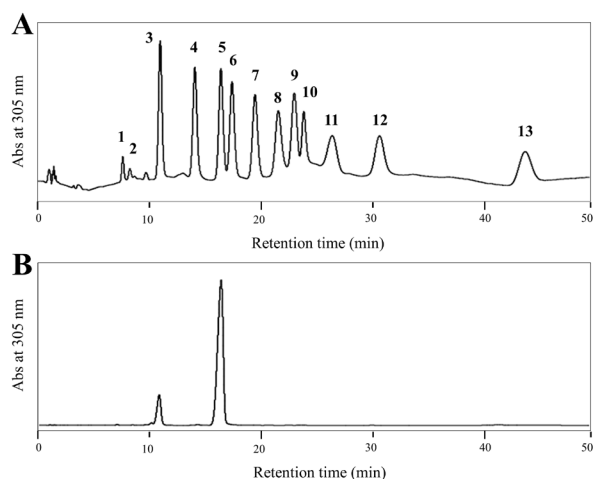


Figure 5. HPLC elution profile of acid hydrolysate of M2 EPS. Panel A, standard monosaccharides; and B, acid hydrolysate of M2 EPS. Standard monosaccharides: **1**, D-glucuronic acid; **2**, D-galacturonic acid; **3**, D-galactose; **4**, D-mannose; **5**, D-glucose; **6**, L-arabinose; **7**, D-ribose; **8**, *N*-acetyl-D-mannosamine; **9**, D-xylose; **10**, *N*-acetyl-D-glucosamine; **11**, L-fucose; **12**, L-rhamnose; and **13**, *N*-acetyl-D-galactosamine.

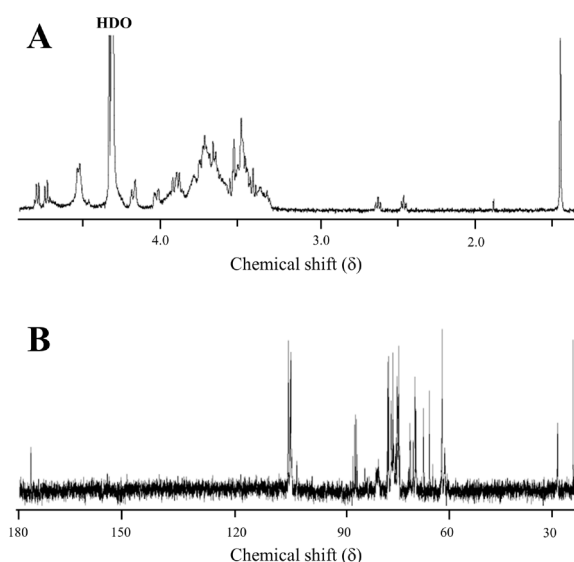


Figure 6. NMR spectra of M2 EPS. A, ^1H NMR; B, ^{13}C NMR spectrum.

Table 1. Methylation analysis of M2 EPS

Peak	Derivatives	Structural feature	Native ^a	Depyruvylated ^a	Succinoglycan ^b
1	1,5-Di- <i>O</i> -acetyl-2,3,4,6-tetra- <i>O</i> -methyl-glucitol	Glc _p -(1→	0.1	0.6	
2	1,3,5-Tri- <i>O</i> -acetyl-2,4,6-tri- <i>O</i> -methyl-glucitol	→3)-Glc _p -(1→	1.5	2.1	2.0
3	1,4,5-Tri- <i>O</i> -acetyl-2,3,6-tri- <i>O</i> -methyl-glucitol	→4)-Glc _p -(1→	1.6	1.6	2.0
4	1,3,5-Tri- <i>O</i> -acetyl-2,4,6-tri- <i>O</i> -methyl-galactitol	→3)-Gal _p -(1→	1.2	1.1	1.0
5	1,5,6-Tri- <i>O</i> -acetyl-2,3,4-tri- <i>O</i> -methyl-glucitol	→6)-Glc _p -(1→	1.0	1.0	1.0
6	1,4,5,6-Tetra- <i>O</i> -acetyl-2,3-di- <i>O</i> -methyl-glucitol	→4,6)-Glc _p -(1→	1.9	1.3	2.0

^aRatio of peak area. ^bTheoretical ratio (24).

β configuration based on the observed chemical shift values (23). Next, we performed methylation analysis to elucidate the details of the connectivity of the sugar residues detected by the monosaccharide analysis. Five major peaks of the partially methylated alditol acetate (PMAA) derivatives were detected from M2 EPS by GLC-MS analysis (Supplementary Figure 1A). The connectivity of the sugar residues was determined based on the retention times and mass fragmentation patterns of the detected peaks (Table 1). M2 EPS mainly comprised \rightarrow 3)-Glc_p-(1 \rightarrow , \rightarrow 4)-Glc_p-(1 \rightarrow , \rightarrow 3)-Gal_p-(1 \rightarrow , \rightarrow 6)-Glc_p-(1 \rightarrow , and \rightarrow 4,6)-Glc_p-(1 \rightarrow in an approximate molar ratio of 2:2:1:1:2. These results indicate that M2 EPS consists of octasaccharide repeating units. The molar ratio of the detected sugar connectivity was in good agreement with the theoretical ratio of PMAA from succinoglycan, a representative polysaccharide produced by genus *Rhizobium* (24).

Signals of the glycan structure detected in the ^1H and ^{13}C NMR spectra of M2 EPS (Figure 6) were almost the same as those previously reported for succinoglycan of *R. meliloti* (25). The glycan chain of succinoglycan is substituted by succinic acid, pyruvic

acid, and acetic acid (25). Succinyl-methylene (δ 2.46 and 2.62 for ^1H and δ 29.9 for ^{13}C) and pyruvate-methyl (δ 1.46 for ^1H and δ 26.1 for ^{13}C) signals were detected in the one-dimensional NMR spectra of M2 EPS (Figure 6). The contents of the succinate and pyruvate residues were 40% and 85%, respectively, as estimated by the ratio of succinyl-methylene and pyruvate-methyl resonances to anomeric protons of the glycan backbone in the ^1H NMR spectra. No methyl signal of an acetyl residue was detected in M2 EPS.

To determine the pyruvylated position of the M2 EPS, we prepared the depyruvylated M2 EPS by mild acid hydrolysis. In the methylation analysis of depyruvylated M2 EPS, the molar ratio of 1,4,5,6-tetra-*O*-acetyl-2,3-di-*O*-methyl-glucitol was decreased, and that of 1,5-di-*O*-acetyl-2,3,4,6-tetra-*O*-methyl-glucitol was increased compared with the native M2 EPS (Supplementary Figure 1, Table 1). These results indicate that the pyruvate residue was bound to both the *O*-4 and *O*-6 positions of terminal glucose residue of side-chain structure. The chemical shift of the pyruvate-methyl carbon (26.1 ppm) indicated that the pyruvate acetal carbon atom had the (*S*) configuration

(26). These findings revealed that M2 EPS consists of branching octasaccharide repeating units substituted by succinate and pyruvate residues shown in Figure 7.

3.4. Effects of structural modifications on the innate immune-stimulating activity of M2 EPS

To determine the structural motif involved in the innate immunostimulating activity of M2 EPS, we modified its structure by chemical treatment. We prepared deacylated (weak alkali hydrolyzed), depyruvylated (weak acid hydrolyzed), deacylated and depyruvylated, and strong acid hydrolyzed M2 EPS. The modified structures of the M2 EPS were confirmed by ¹H NMR analysis (Figure 8), and the succinate and pyruvate residue content was estimated by the ratio of succinyl-methylene and pyruvate-methyl resonances to anomeric protons of the glycan backbone in the spectra (Table 2). Succinate was successfully removed from M2 EPS by the weak alkali hydrolysis, but a small amount of pyruvate remained in the weak acid-hydrolyzed M2 EPS.

The innate immunostimulating activities of chemically modified M2 EPSs were evaluated using the silkworm muscle contraction assay. The activities were increased by removal of the substitution of succinate and pyruvate. Strong acid hydrolysis completely inactivated the M2 EPS.

4. Discussion

In this study, we screened innate immunostimulant-producing bacteria using the silkworm muscle contraction

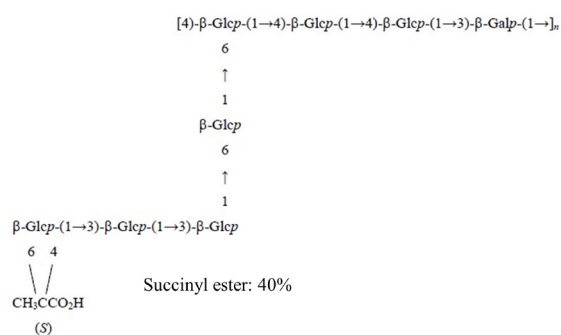


Figure 7. Predicted structure of M2 EPS from *Rhizobium* sp. strain M2

assay, and isolated the bacterial strain M2 from soil. The 16S rRNA gene sequence of strain M2 had the highest similarities with sequences of *R. pusense*. *Rhizobium* is a genus of Gram-negative soil bacteria frequently isolated from plant rhizospheres or root nodules (27). *R. pusense* is a remarkable species as an opportunistic human pathogen in the genus *Agrobacterium/Rhizobium* (28). Many bacterial strains producing EPS belong to this genus (27). Recently, an extracellular β-glucan possessing antitumor activity was purified from the *Rhizobium* sp. N613 (29). To our knowledge, however, this is the first report of the screening of innate immune stimulants from bacterial EPS using a convenient method such as the silkworm muscle contraction assay. Because the silkworm muscle contraction assay does not respond to LPS, the innate immune stimulant produced by strain M2, which is a Gram-negative bacterium, is not LPS.

We purified the innate immunostimulant from the strain M2, and characterized the chemical structure as a succinoglycan like high-molecular weight heteropolysaccharide (structural model is shown in Figure 7). Succinoglycans are acidic heteropolysaccharides produced by a variety of bacteria belonging to the *Rhizobium*, *Agrobacterium*, *Alcaligenes*, and *Pseudomonas* (30). Succinoglycan is important for plant living rhizobia to evade plant immunity (31). A succinoglycan was also isolated from *Agrobacterium*

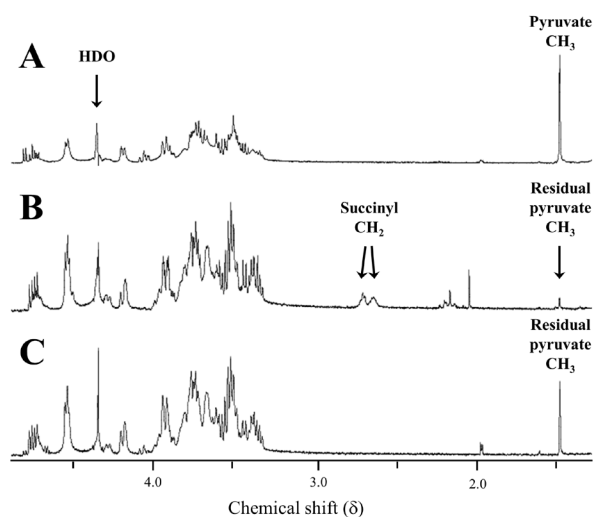


Figure 8. ¹H NMR spectra of chemically modified M2 EPS. A, deacylated; B, depyruvylated; and C, deacylated and depyruvylated M2 EPS.

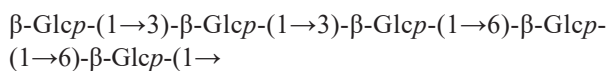
Table 2. Effects of structural modifications on the innate immune-stimulating activity of M2 EPS

Samples	Succinate contents (%) ^a	Pyruvate contents (%) ^a	Specific activity (units/mg)
M2 EPS	40	85	1.4
Deacylated M2 EPS	ND ^b	100	1.6
Depyruvylated M2 EPS	66	7.0	2.6
Deacylated- depyruvylated M2 EPS	ND ^b	32	3.4
Acid hydrolyzed M2 EPS	NA ^c	NA ^c	< 1

^aPercentage of repeating unit substituted by the residue. ^bNot detected. ^cNot analyzed.

radiobacter, a clinical isolate from a patient with cystic fibrosis (24). Innate immunostimulating activity of succinoglycans, however, has not been reported. Further studies are necessary to evaluate whether M2 EPS exerts innate immunostimulating activity in a mammalian system.

To determine the structural motif involved in the innate immunostimulating activity of M2 EPS, we modified its structure by chemical treatment. The activities were increased by the removal of the substitution of succinic and pyruvic acid. Because the deacylation (alkaline hydrolysis) of M2 EPS did not attenuate the innate immune stimulating activity, the active substance is not LPS contaminating the culture of strain M2, reliably. Strong acid hydrolysis completely inactivated the M2 EPS. These results suggest that the acidic residues present in M2 EPS do not participate in the innate immunostimulating activity, and the polysaccharide structure is necessary for the activity. To our knowledge, this is the first report of the glycan chain of succinoglycan possessing innate immune-stimulating activity. A pyruvate residue was bound to both O-4 and O-6 positions of the terminal glucose residue of the side-chain of M2 EPS. Although we could not determine the binding position of the succinate in the M2 EPS, succinate groups bind to glucose residues in the side-chains of succinoglycan from various microbial sources (24,25). The glycan structure of the side-chain of deacylated and depyruvylated M2 EPS is a β -1,3/6-glucan with the following structure:



Previously, the innate immunostimulating activities of β -1,3/6-glucan from various sources were evaluated using the silkworm muscle contraction assay (9), and the activities varied according to the origin. Unmasking of the β -1,3/6-glucan structure of the side chain by deacylation and depyruvylation may enhance the innate immune-stimulating activity of M2 EPS. Detailed analysis of the structure-activity relations of the β -1,3/6-glucan will be an interesting topic for future studies.

Acknowledgements

This study was partly supported by a grant from the Institute for Fermentation (IFO; Osaka, Japan). We thank T. Wakimoto at the Laboratory of Natural Products Chemistry for use of its GLC-MS facilities. We also acknowledge various members of our laboratory for their helpful suggestions, encouragement, and technical assistance.

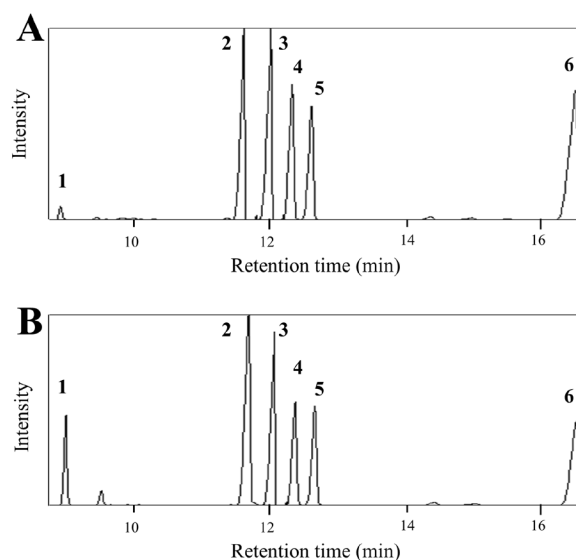
References

- Zong A, Cao H, Wang F. Anticancer polysaccharides from natural resources: A review of recent research. *Carbohydr Polym.* 2012; 90:1395-1410.
- Nwodo UU, Green E, Okoh AI. Bacterial exopolysaccharides: Functionality and prospects. *Int J Mol Sci.* 2012; 13:14002-14015.
- Nwibo DD, Hamamoto H, Matsumoto Y, Kaito C, Sekimizu K. Current use of silkworm larvae (*Bombyx mori*) as an animal model in pharmaco-medical research. *Drug Discov Ther.* 2015; 9:133-135.
- Hamamoto H, Urai M, Ishii K, *et al.* Lysocin E is a new antibiotic that targets menaquinone in the bacterial membrane. *Nat Chem Biol.* 2015; 11:127-133.
- Ishii K, Hamamoto H, Kamimura M, Sekimizu K. Activation of the silkworm cytokine by bacterial and fungal cell wall components *via* a reactive oxygen species-triggered mechanism. *J Biol Chem.* 2008; 283:2185-2191.
- Ishii K, Hamamoto H, Kamimura M, Nakamura Y, Noda H, Imamura K, Mita K, Sekimizu K. Insect cytokine paralytic peptide (PP) induces cellular and humoral immune responses in the silkworm *Bombyx mori*. *J Biol Chem.* 2010; 285:28635-28642.
- Ishii K, Hamamoto H, Sekimizu K. Studies of host-pathogen interactions and immune-related drug development using the silkworm: Interdisciplinary immunology, microbiology, and pharmacology studies. *Drug Discov Ther.* 2015; 9:238-246.
- Dhital S, Hamamoto H, Urai M, Ishii K, Sekimizu K. Purification of innate immunostimulant from green tea using a silkworm muscle contraction assay. *Drug Discov Ther.* 2011; 5:18-25.
- Fujiyuki T, Hamamoto H, Ishii K, Urai M, Kataoka K, Takeda T, Shibata S, Sekimizu K. Evaluation of innate immune stimulating activity of polysaccharides using a silkworm (*Bombyx mori*) muscle contraction assay. *Drug Discov Ther.* 2012; 6:88-93.
- Aizawa T, Urai M, Iwabuchi N, Nakajima M, Sunairi M. *Bacillus trypoxylicola* sp. nov., xylanase-producing alkaliphilic bacteria isolated from the guts of Japanese horned beetle larvae (*Trypoxylus dichotomus septentrionalis*). *Int J Syst Evol Microbiol.* 2010; 60:61-66.
- Tamura T, Hatano K. Phylogenetic analysis of the genus *Actinoplanes* and transfer of *Actinoplanes minutisporangius* Ruan *et al.* 1986 and '*Actinoplanes aurantiacus*' to *Cryptosporangium minutisporangium* comb. nov. and *Cryptosporangium aurantiacum* sp. nov. *Int J Syst Evol Microbiol.* 2001; 51:2119-2125.
- Kumar S, Stecher G, Tamura K. MEGA7: Molecular evolutionary genetics analysis version 7.0 for bigger datasets. *Mol Biol Evol.* 2016; 33:1870-1874.
- Thompson JD, Gibson TJ, Plewniak F, Jeanmougin F, Higgins DG. The CLUSTAL_X windows interface: Flexible strategies for multiple sequence alignment aided by quality analysis tools. *Nucleic Acids Res.* 1997; 25:4876-4882.
- Jukes TH, Cantor CR. Evolution of protein molecules. In: *Mammalian Protein Metabolism* (Munro HN, ed.). Academic Press, New York, 1969; vol. 3, pp. 21-132.
- Saitou N, Nei M. The neighbor-joining method: A new method for reconstructing phylogenetic trees. *Mol Biol Evol.* 1987; 4:406-425.
- Felsenstein J. Confidence limits on phylogenies: An approach using the bootstrap. *Evolution.* 1985; 39:783-791.

17. Urai M, Anzai H, Ogihara J, Iwabuchi N, Harayama S, Sunairi M, Nakajima M. Structural analysis of an extracellular polysaccharide produced by *Rhodococcus rhodochromus* strain S-2. *Carbohydr Res.* 2006; 341:766-775.
18. Staub AM. Removal of proteins. In: *Methods in Carbohydrate Chemistry* (Whistler RL, ed.). Academic Press, New York, 1965; vol.5, pp. 5-6.
19. Urai M, Yoshizaki H, Anzai H, Ogihara J, Iwabuchi N, Harayama S, Sunairi M, Nakajima M. Structural analysis of an acidic, fatty acid ester-bonded extracellular polysaccharide produced by a pristane-assimilating marine bacterium, *Rhodococcus erythropolis* PR4. *Carbohydr Res.* 2007; 342:933-942.
20. DuBois M, Gilles KA, Hamilton JK, Rebers PA, Smith F. Colorimetric method for determination of sugars and related substances. *Anal Chem.* 1956; 28:350-356.
21. Ciucanu I, Kerek F. A simple and rapid method for the permethylation of carbohydrates. *Carbohydr Res.* 1984; 131:209-217.
22. Urai M, Aizawa T, Anzai H, Ogihara J, Iwabuchi N, Neilan B, Couperwhite I, Nakajima M, Sunairi M. Structural analysis of an extracellular polysaccharide produced by a benzene tolerant bacterium, *Rhodococcus* sp. 33. *Carbohydr Res.* 2006; 341:616-623.
23. Bubb WA. NMR spectroscopy in the study of carbohydrates: Characterizing the structural complexity. *Concepts Magn Reson A.* 2003; 19A:1-19.
24. Evans LR, Linker A, Impallomeni G. Structure of succinoglycan from an infectious strain of *Agrobacterium radiobacter*. *Int J Biol Macromol.* 2000; 27:319-326.
25. Matulová M, Toffanin R, Navarini L, Gilli R, Paoletti S, Cesàro A. NMR analysis of succinoglycans from different microbial sources: Partial assignment of their ^1H and ^{13}C NMR spectra and location of the succinate and the acetate groups. *Carbohydr Res.* 1994; 265:167-179.
26. Garegg PJ, Jansson PE, Lindberg B, Lindh F, Lonngren J, Kvarnstrom I, Nimmich W. Configuration of the acetal carbon atom of pyruvic acid acetals in some bacterial polysaccharides. *Carbohydr Res.* 1980; 78:127-132.
27. Skorupska A, Janczarek M, Marczak M, Mazur A, Król J. Rhizobial exopolysaccharides: Genetic control and symbiotic functions. *Microb Cell Fact.* 2006; 5:7.
28. Aujoulat F, Marchandin H, Zorogniotti I, Masnou A, Jumas-Bilak E. *Rhizobium pusense* is the main human pathogen in the genus *Agrobacterium/Rhizobium*. *Clin Microbiol Infect.* 2015; 21:472.e1-5.
29. Zhao L, Chen Y, Ren S, Han Y, Cheng H. Studies on the chemical structure and antitumor activity of an exopolysaccharide from *Rhizobium* sp. N613. *Carbohydr Res.* 2010; 345:637-643.
30. Zevenhuizen L. Succinoglycan and galactoglucan. *Carbohydr Polym.* 1997; 33:139-144.
31. Cheng HP, Walker GC. Succinoglycan is required for initiation and elongation of infection threads during nodulation of alfalfa by *Rhizobium meliloti*. *J Bacteriol.* 1998; 180:5183-5191.

(Received August 14, 2017; Accepted September 17, 2017)

Supplemental Data



Supplementary Figure 1. GLC patterns of partially methylated alditol acetate derivatives from M2 EPS. Panel A, native M2 EPS; and B, depyruvylated M2 EPS. 1, 1,5-Di-*O*-acetyl-2,3,4,6-tetra-*O*-methyl-glucitol; 2, 1,3,5-Tri-*O*-acetyl-2,4,6-tri-*O*-methyl-glucitol; 3, 1,4,5-Tri-*O*-acetyl-2,3,6-tri-*O*-methyl-glucitol; 4, 1,3,5-Tri-*O*-acetyl-2,4,6-tri-*O*-methyl-galactitol; 5, 1,5,6-Tri-*O*-acetyl-2,3,4-tri-*O*-methyl-glucitol; and 6, 1,4,5,6-Tetra-*O*-acetyl-2,3-di-*O*-methyl-glucitol.

Glycyrrhizin inhibits human parainfluenza virus type 2 replication by the inhibition of genome RNA, mRNA and protein syntheses

Kae Sakai-Sugino^{1,§}, Jun Uematsu^{2,*}, Miyuki Kamada¹, Hiroe Taniguchi¹, Saori Suzuki¹, Yumiko Yoshimi¹, Sahoko Kihira¹, Hidetaka Yamamoto³, Mitsuo Kawano⁴, Masato Tsurudome⁴, Myles O'Brien⁵, Makoto Itoh⁶, Hiroshi Komada^{2,†}

¹ Department of Clinical Nutrition, Faculty of Health Science, Suzuka University of Medical Science, Kishioka, Suzuka, Mie, Japan;

² Microbiology and Immunology Section, Department of Clinical Nutrition, Graduate School of Suzuka University of Medical Science, Kishioka, Suzuka, Mie, Japan;

³ Faculty of Pharmaceutical Sciences, Suzuka University of Medical Science, Minamitamagaki, Suzuka, Mie, Japan;

⁴ Department of Microbiology, Mie University Graduate School of Medicine, Edobashi, Tsu, Mie, Japan;

⁵ Graduate School of Mie Prefectural College of Nursing, Yumegaoka, Tsu, Mie, Japan;

⁶ Cokey Systems Co., Ltd., Uegawa, Matsusaka, Mie, Japan.

Summary

The effect of glycyrrhizin on the replication of human parainfluenza virus type 2 (hPIV-2) was examined. Cell fusion induced by hPIV-2 was inhibited by glycyrrhizin, and glycyrrhizin reduced the number of viruses released from the cells. Glycyrrhizin did not change cell morphology at 1 day of culture, but caused some damage at 4 days, as determined by the effect on actin microfilaments. However, it affected the cell viability at 1 day: about 20% of the cells were not alive by 3-(4,5-dimethylthiazol-2-yl)-2,5-diphenyltetrazolium bromide (MTT) assay at 1 day of culture. Real-time polymerase chain reaction (PCR) and PCR showed that virus genome synthesis was largely inhibited. mRNA synthesis was also inhibited by glycyrrhizin. Viral protein synthesis was largely inhibited as observed by an indirect immunofluorescence study. Multinucleated giant cell formation was studied using a recombinant green fluorescence protein (GFP)-expressing hPIV-2 without matrix protein (rhPIV-2ΔMGFP). A few single cells with fluorescence were observed, but the formation of giant cells was completely blocked. Taken together, it was shown that viral genome, mRNA and protein syntheses, including F and HN proteins, were inhibited by glycyrrhizin, and consequently multinucleated giant cell formation was not observed and the infectious virus was not detected in the culture medium.

Keywords: Virus replication, medicinal plant extract, recombinant green fluorescence protein expressing hPIV-2 without matrix protein

Released online in J-STAGE as advance publication October 24, 2017.

*Address correspondence to:

Dr. Jun Uematsu, Microbiology and Immunology Section, Department of Clinical Nutrition, Graduate School of Suzuka University of Medical Science, 1001-1 Kishioka, Suzuka, Mie 510-0293, Japan.
E-mail: uematsu@suzuka-u.ac.jp

§Present address: Department of Life and Environmental Science, Tsu City College, 157 Ishinden Nakano, Tsu, Mie 514-0112, Japan.

†Present address: Department of Microbiology, Mie University Graduate School of Medicine, 2-174 Edobashi, Tsu, Mie 514-8507, Japan.

1. Introduction

Human parainfluenza virus type 2 (hPIV-2) is a member of the genus *Rubulavirus* in the family Paramyxoviridae. hPIV-2 infects the human respiratory tract in infants and children. hPIV causes recurrent infection and there is no vaccine or anti-hPIV drug at present. It possesses a single-stranded, non-segmented, negative stranded RNA genome of 15,654 nucleotides (*I*). The genomic RNA codes 7 structural proteins, nucleoprotein (NP), V, phospho (P), matrix (M), fusion (F), hemagglutinin-neuraminidase (HN) and large (L) proteins, like other

paramyxoviruses. V protein is the fifth structural protein of paramyxovirus (2). The gene order of hPIV-2 is 3'-(leader)-NP-V/P-M-F-HN-L-(trailer)-5' (3).

We have already reported some substances of large molecular weight (MW) that have inhibitory effects on hPIV-2 replication *in vitro*. Fucoidan, sulfated polysaccharides extracted from the brown alga Okinawa mozuku, inhibited hPIV-2 genome and protein syntheses, owing to the inhibition of viral adsorption to the cells (4). Bovine lactoferrin partially inhibited viral genome and protein expression (5). Legume lectins with different sugar binding specificities, concanavalin A, lens culinaris agglutinin and peanut agglutinin, also prevented hPIV-2 adsorption by binding to the specific lectin receptors (6).

Glycyrrhizin is extracted from the roots of *Glycyrrhiza glabra* and it has many biological and pharmacological activities, such as anti-inflammatory and anti-viral effects. Glycyrrhizin is a small molecule with MW 823. Glycyrrhizin inhibits production of pro-inflammatory cytokines (7,8). Anti-viral activities of glycyrrhizin have been reported previously. For instance, glycyrrhizin has inhibitory effects on H5N1 influenza A virus (9), hepatitis C virus (HCV) (10,11), rotavirus (12) and Kaposi's sarcoma-associated herpes virus (13).

In the present investigation, glycyrrhizin was tested for hPIV-2 replication. The number of viruses released from infected cells cultured with glycyrrhizin was determined. The effects of glycyrrhizin on actin microfilaments were analyzed using rhodamine phalloidin. Cell viability was determined by 3-(4,5-dimethylthiazol-2-yl)-2,5-diphenyltetrazolium bromide (MTT) assay. The effect of glycyrrhizin on viral genome synthesis was examined: viral RNA was prepared and analyzed by real-time polymerase chain reaction (PCR) and PCR. The effect of glycyrrhizin on mRNA synthesis was analyzed: cDNA was synthesized using oligo dT primer, and PCR was carried out. Viral protein syntheses were observed by indirect immunofluorescence study using monoclonal antibodies (mAbs) against NP, F and HN proteins of hPIV-2 (14). The effect of glycyrrhizin on hPIV-2-induced multinucleated giant cell formation was analyzed using recombinant green fluorescence protein expressing hPIV-2 without matrix protein (rhPIV-2ΔMGFP) (6,15,16).

2. Materials and Methods

2.1. Glycyrrhizin

Glycyrrhizin (Cokey Systems, Matsusaka, Japan; more than 75% pure) was dissolved at 20 mg/mL in 10 mM phosphate buffered saline, pH 7.2 (PBS). The pH of the solution was about 5, and was adjusted to 7.1-7.2 by 1 M NaOH, and it was sterilized by filtration. Glycyrrhizin was stored at -20°C before use.

2.2. Virus and recombinant virus

The uses of the virus and recombinant virus were approved by the Microbiology Biosafety Committee and Recombinant DNA Biosafety Committee of Suzuka University of Medical Science, respectively.

We used hPIV-2 (Toshiba strain) that causes visible cell fusion. rhPIV-2ΔMGFP was constructed according to the method described previously (6,15,16), and no production of infectious virus particles without addition of M protein gene *in trans* was ascertained (15,16). The virus yield was about 1×10^5 TCID₅₀/mL.

2.3. Cell line and cultivation of cells

LLCMK₂ cells (rhesus monkey kidney cell line) were cultured in a flat-bottomed 24-well plate in 1 mL culture medium. The culture medium was minimum essential medium α (MEMα: Wako, Osaka, Japan), supplemented with 2% fetal calf serum (FCS) and 0.1 mg/mL kanamycin. The cells were cultured at 37°C in a humidified atmosphere with 5% CO₂. After 3 days, the cells became confluent (5×10^5 cells), and the medium was changed to MEMα with 0.5% FCS and 0.1 mg/mL kanamycin. Glycyrrhizin was added to the cells, and after about 5 min, the cells were infected with hPIV-2 (about 1×10^2 TCID₅₀).

2.4. Cytopathogenic assay and MTT assay

Cell fusion was observed under a cell culture light microscope at 4 days post infection. MTT assay was carried out according to the manufacturer's method using CellTiter 96 Aqueous One Solution Cell Proliferation Assay (Promega, Tokyo, Japan) at 1 day and at 4 days post addition of glycyrrhizin.

2.5. RNA preparation, cDNA synthesis and real time PCR

RNA was extracted from the cells (2×10^6 cells) cultured in a flat-bottomed 6-well plate using TRIZOL reagent (Invitrogen, CA, USA) according to the manufacturer's method at 4 days post infection. cDNA was synthesized with 1 μg RNA using Reverse Tra Ace qPCR RT Master Mix (TOYOBO, Osaka, Japan) and NP gene specific primer (nucleotide number 1661-1679: 5'-CAACATTCAATGAATCAGT-3'). Real-time PCR was performed on the ABI PRISM 7700 Sequence Detection System (Life Technologies, Tokyo, Japan) using TaqMan Probe (1932-1956: 5'-FAM-AAGCACCGGATTTCTAACCCGTCCTG-TAMRA-3'), forward primer (1851-1875: 5'-ACACACTCATCCAG ACAATCAAAC-3'), and reverse primer (1958-1980: 5'-TGTGGAGGTTATCTGATCACGAA-3').

2.6. Detection of viral RNA

cDNA was synthesized with 1 μ g RNA using forward primers for NP (nucleotide number 1,081-1,100: 5'-CATGGCCAAGTACATGGCTC-3'), F (5,821-5,840: 5'-CCCTATCCCTGAATCACAAT-3') and HN (7,741-7,760: 5'-ATTCCTGTATATGGTGGTC-3') and superscript II reverse transcriptase (Invitrogen), and PCR was carried out with forward primers for NP (nucleotide number 1,081-1,100), F (5,821-5,840) and HN (7,741-7,760), and reverse primers for NP (1,466-1,489: 5'-CC TCCGAGTATCGATTGGATTGAA-3'), F (6,661-6,681: 5'-TGTCACGAGACGTTACGGACA-3') and HN (8,481-8,500: 5'-GAACTCCCCTAAAAGAGATG-3') genes and Ex Taq (Takara, Shiga, Japan).

2.7. Detection of mRNA

cDNA was synthesized with 1 μ g RNA using oligo dT primer (5'-TTTTTTTTTTTTTTTTTTT-3') and superscript II reverse transcriptase (Invitrogen), and PCR was carried out with forward primers for NP (nucleotide number 1,081-1,100), F (5,821-5,840) and HN (7,741-7,760), and reverse primers for NP (1,466-1,489), F (6,661-6,681) and HN (8,481-8,500) genes and Ex Taq (Takara).

2.8. Immunofluorescence study

Actin was detected using rhodamine phalloidin (Invitrogen) at 1 day and 4 days of cultivation with or without glycyrrhizin. All the following procedures were carried out at 37°C, except for the microscopic observation. The cells were fixed with 3.7% formaldehyde solution in PBS for 10 min, washed with PBS, were further incubated with 0.1% Triton X-100 in PBS for 3 min, and observed under a fluorescence microscope (Olympus, Tokyo, Japan).

To detect virus proteins in the infected cells, the cells were fixed with 3.7% formaldehyde solution in PBS at room temperature for 10 min at 4 days of cultivation. After washing with PBS, the cells were further incubated with 0.1% Triton X-100 in PBS at room temperature for 3 min, washed with PBS, and incubated with mouse mAbs against NP, F and HN proteins of hPIV-2 (14) at room temperature for 30 min. After washing with PBS, the cells were incubated with Alexa 488 conjugated secondary antibody to mouse IgGs (Invitrogen) at room temperature for 30 min, and observed under a fluorescence microscope.

2.9. Observation of multinucleated giant cell

The cells were added with glycyrrhizin and after about 5 min they were infected with rhPIV-2 Δ MGFP (1×10^4 TCID₅₀). After 4 days, the cells were washed with PBS and fixed with 1.2% formaldehyde solution in PBS at room temperature for 10 min, and observed under a fluorescence microscope.

3. Results

3.1. Titration of virus released from the infected cells

The titers of virus released from the cells cultured with and without glycyrrhizin at 4 days post infection were determined. Glycyrrhizin inhibited dose-dependently the virus release from the cells (Figure 1). Without glycyrrhizin, the virus titer was about $(1.9 \pm 0.7) \times 10^6$ TCID₅₀/mL (mean \pm SEM of 3 independent experiments), and with glycyrrhizin (3 mg/mL), it was less than 10 TCID₅₀/mL (results of 3 independent experiments). Glycyrrhizin almost completely inhibited the virus replication and the release of virus from the cells.

In the following experiments, 3 mg/mL of glycyrrhizin was added to the cell culture.

3.2. The effect of glycyrrhizin on actin microfilaments and cell viability

Glycyrrhizin was added to the cells, and actin microfilaments were observed under a fluorescence microscope at 1 day and 4 days of cultivation. Figures 2A and B show actin microfilaments at 1 day and 4 days, respectively. As shown in Figure 2, glycyrrhizin did not disrupt actin microfilaments at 1 day of culture (Figure 2C), but caused some damage at 4 days (Figure 2D). The results indicated that glycyrrhizin did not cause severe morphological change in the cells.

Cell viability was determined by MTT assay at 1 day and 4 days. Figure 3 shows that glycyrrhizin caused some effect on the cell viability. About 20% of the cells were not alive after the addition of glycyrrhizin at 1 day.

3.3. Viral genome RNA and mRNA syntheses

RNA was prepared from the infected cells at 4 days post infection, and the viral genome RNA was analyzed

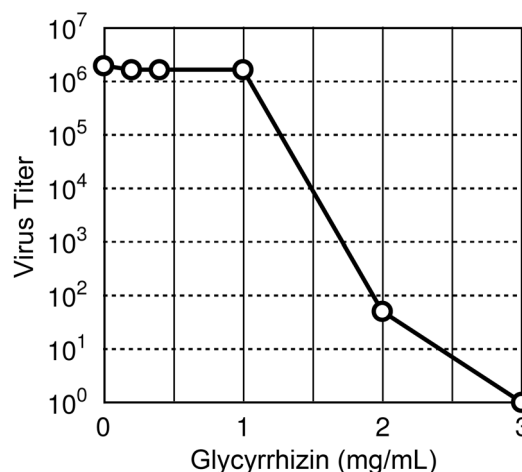


Figure 1. The effect of glycyrrhizin on the virus released from the cells. Glycyrrhizin inhibited the virus release in a dose-dependent manner.

by real-time PCR. The relative copy number in the glycyrrhizin-treated infected cells was about 0.033 compared with the copy number of the infected cells.

Viral genome RNAs of NP, F and HN were analyzed using hPIV-2 specific primers by PCR (Figure 4). The number of base pairs between forward and reverse primers of NP, F and HN genes was about 400, 860 and 760, respectively. Lane 1 (NP), 2 (F) and 3 (HN) were non-infected cells, and no visible bands were observed. In the virus-infected cells, NP (lane 4),

F (lane 5) and HN (lane 6) genes were clearly detected. In the glycyrrhizin-treated infected cells, NP (lane 7), F (lane 8) and HN (lane 9) gene syntheses were almost completely inhibited.

In the following experiment, mRNA synthesis was analyzed. cDNA was synthesized using oligo dT primer, and PCR was carried out using hPIV-2 specific primers. Figure 5 shows that in non-infected cells, no bands were detected, and NP (lane 4), F (lane 5) and HN (lane 6) mRNAs were detected in the virus-infected cells.

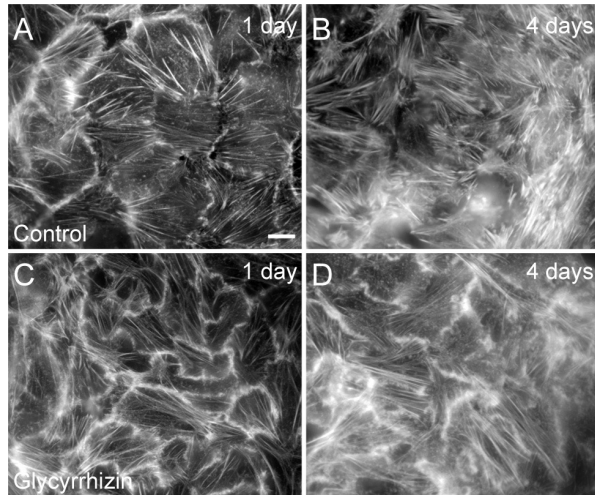


Figure 2. The effect of glycyrrhizin on actin microfilaments at 1 day and 4 days. The cells were cultured with and without glycyrrhizin for 1 day and 4 days, and actin microfilaments were stained with rhodamine phalloidin. Figure 2 shows actin microfilaments of LLCMK, cells cultured without glycyrrhizin for 1 day (A) and 4 days (B), and those of the cells cultured with glycyrrhizin for 1 day (C) and 4 days (D). (bar: 50 μ m). Glycyrrhizin did not cause severe morphological change in the cells.

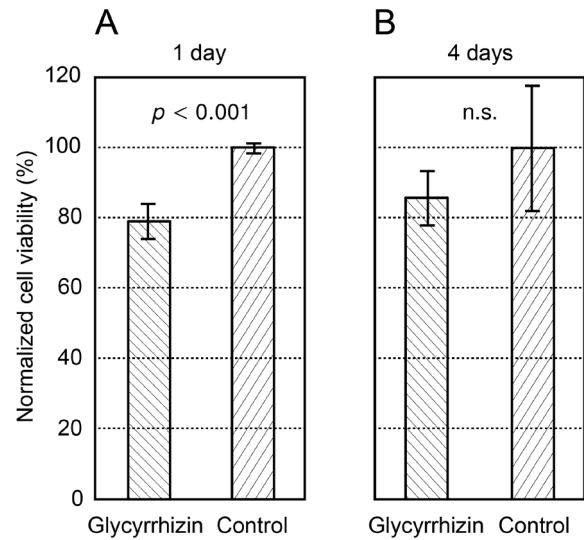


Figure 3. Cell viability determined by MTT assay at 1 day and 4 days. The cells were cultured with and without glycyrrhizin for 1 day (A) and 4 days (B). Glycyrrhizin caused a slight effect on the cell viability at 1 day (A).

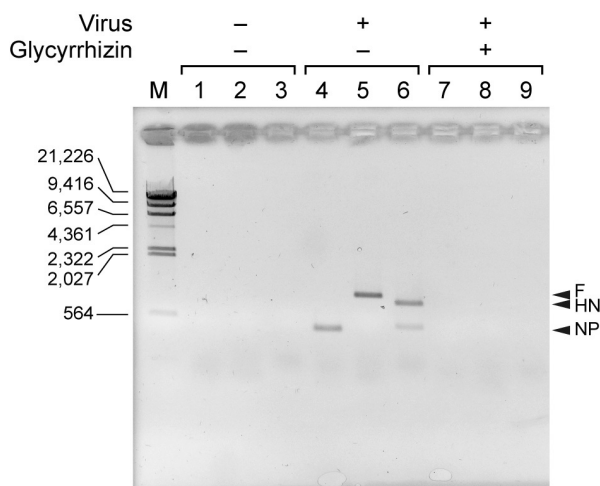


Figure 4. Viral genome RNA synthesis was inhibited by glycyrrhizin. Lane M: marker (base pair), lanes 1 (NP), 2 (F) and 3 (HN): non-infected cells, lanes 4 (NP), 5 (F) and 6 (HN): hPIV-2 infected cells, lanes 7 (NP), 8 (F) and 9 (HN): hPIV-2 infected cells cultured with glycyrrhizin. No visible bands were observed in lanes, 7, 8 and 9. The results were the same as those of real-time PCR, indicating that glycyrrhizin inhibited viral genome synthesis.

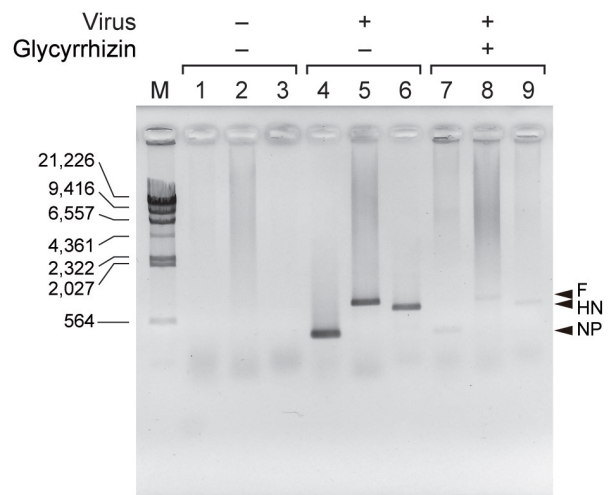


Figure 5. Viral mRNA synthesis was largely inhibited by glycyrrhizin. cDNA was synthesized using oligo dT primer and PCR was carried out using NP, F and HN specific primers. Lane M: marker (base pair), lanes 1 (NP), 2 (F) and 3 (HN): non-infected cells, lanes 4 (NP), 5 (F) and 6 (HN): hPIV-2 infected cells, lanes 7 (NP), 8 (F) and 9 (HN): hPIV-2 infected cells cultured with glycyrrhizin. In lane 7, 8 and 9, slight bands were seen. Glycyrrhizin largely inhibited mRNA synthesis.

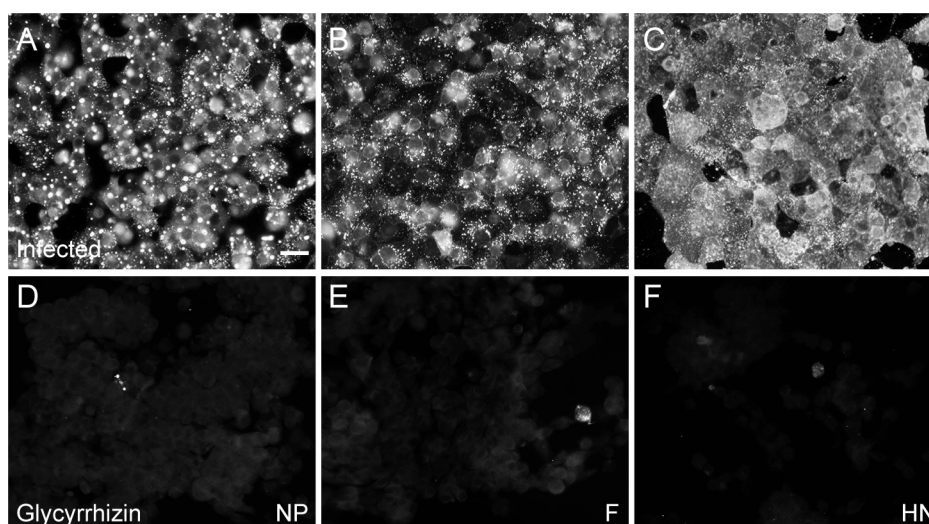


Figure 6. Glycyrrhizin inhibited the expression of NP, F and HN proteins of hPIV-2. The expression of NP (A), F (B) and HN (C) proteins of hPIV-2 infected cells. A small number of cells had fluorescence, indicating that glycyrrhizin largely inhibited the expression of NP (D), F (E) and HN (F) proteins. (bar: 50 μ m).

But mRNAs were only slightly seen in the glycyrrhizin-treated infected cells (NP: lane 7, F: lane 8 and HN: lane 9). These results show that glycyrrhizin largely inhibited the transcription of NP, F and HN genes.

3.4. Viral protein synthesis

Viral protein synthesis was analyzed by indirect immunofluorescence study using mAbs against hPIV-2. Glycyrrhizin was added to the cells, and they were infected with hPIV-2. At 4 days post infection, the cells were fixed, stained with the mAbs and secondary antibody. Figures 6A, B and C show the NP, F and HN protein expression in hPIV-2 infected cells, respectively. Non-infected cells had no fluorescence of the proteins (data not shown). In hPIV-2 infected cells, NP, F and HN proteins were observed in almost all the cells: NP protein was observed in many strong fluorescent dots mainly in the cytoplasm; F and HN proteins were in small dots in the cytoplasm and on the cell surface. In glycyrrhizin-treated infected cells, a few cells had fluorescence, indicating that the syntheses of NP (Figure 6D), F (Figure 6E), and HN (Figure 6F) proteins were almost completely inhibited by glycyrrhizin. As shown in Figure 5, mRNA was only slightly detected in glycyrrhizin-treated infected cells. Therefore, it was suggested that the protein synthesis inhibition by glycyrrhizin was caused by the inhibition of transcription.

3.5. The effect of glycyrrhizin on multinucleated giant cell formation

The above results showed that glycyrrhizin inhibited viral genome RNA synthesis and consequently inhibited mRNA and protein syntheses. In the following experiment, we determined the effect of glycyrrhizin on

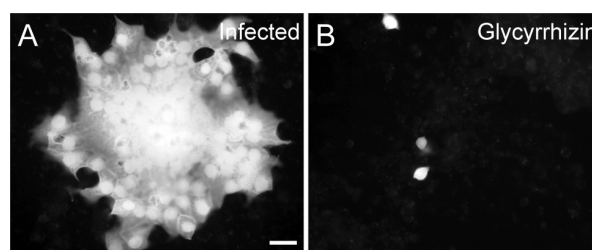


Figure 7. The effect of glycyrrhizin on rhPIV-2 Δ MGFP replication. The cells were infected with rhPIV-2 Δ MGFP and cultured for 4 days (A), the rhPIV-2 Δ MGFP infected cells were cultured with glycyrrhizin for 4 days (B). Figure 7B shows that there are a few fluorescent cells with single nucleus, but there were no multinucleated giant cells, indicating that cell-cell spreading of hPIV-2 was inhibited due to insufficient expression of F and HN proteins. (bar: 50 μ m).

the formation of multinucleated giant cells using rhPIV-2 Δ MGFP (Figure 7). Figure 7A is rhPIV-2 Δ MGFP infected cells at 4 days and there were multinucleated giant cells with strong fluorescence. In non-infected cells, there were no giant cells or fluorescent cells (data not shown). Figure 7B shows that a few fluorescent cells with single nucleus were observed in the infected cells cultured with glycyrrhizin. The results indicate that glycyrrhizin blocked giant cell formation by the inhibition of F and HN protein expressions.

4. Discussion

The present study showed that glycyrrhizin had an inhibitory effect on hPIV-2 replication in LLCMK₂ cells mainly by the inhibition of viral genome RNA and mRNA syntheses.

It was reported that glycyrrhizin has anti-human immunodeficiency virus activity by inhibiting virus replication by interfering with virus to cell binding (17). Glycyrrhizin also exhibited anti-HCV activity

by the inhibition of the expression of HCV core gene when combined with interferon (10). Matsumoto *et al.* (15) also reported that glycyrrhizin inhibited the release of infectious HCV particles due to the inhibition of phospholipase A2. Hardy *et al.* (12) also reported glycyrrhizin primary metabolite 18 β -glycyrrhetic acid reduced rotavirus yield by 99% when added to infected cell culture post virus adsorption, occurring at a step or steps subsequent to virus entry. In addition, glycyrrhizin inhibited respiratory viruses such as respiratory syncytial virus (RSV) mainly by preventing viral attachments (18), and severe acute respiratory syndrome corona virus by affecting many cellular signaling pathways, but the real mechanism is unclear (19). Glycyrrhizin was shown to inhibit H5N1 influenza virus replication and also caused anti-inflammatory responses, indicating that glycyrrhizin is beneficial for treatment of H5N1 virus (9). Wang *et al.* showed that glycyrrhizin directly inactivated coxsackievirus A16, but its inhibitory effect on enterovirus 71 was associated with an event(s) post virus entry (20). However, the effects of glycyrrhizin on parainfluenza virus, which causes respiratory infection, have not been reported. The present investigation is the first report on the inhibitory effect of glycyrrhizin on parainfluenza virus replication.

Glycyrrhizin did not cause morphological change of actin microfilaments at 1 day of culture but caused some damage at 4 days. Cytoskeleton was reported to have an important role in paramyxovirus replication. Actin microfilaments are important in the hPIV-3 life cycle, specifically at the level of viral transport and replication (21). The results indicate that the inhibitory effect of glycyrrhizin on hPIV-2 replication was in part caused by the slight disruption of actin microfilaments at 4 days. MTT assay shows that about 20% of the cells were not alive at 1st day after the addition of glycyrrhizin without virus infection. There is some discrepancy between the actin morphology and cell viability.

Almost no virus was released into the culture medium from glycyrrhizin-treated cells infected with hPIV-2. Viral genome RNA was not detected in the glycyrrhizin-treated infected cells. As the viral genome RNA and mRNA syntheses were inhibited, syntheses of viral proteins were suppressed, consequently cell-cell spreading of hPIV-2 and giant cell formation were inhibited due to insufficient expression of F and HN proteins.

Ribavirin, a drug, which is effective on both DNA and RNA viruses, also inhibits hPIV-2 replication *in vitro* (22). Ribavirin aerosol (20 mg/mL) was effective in the treatment of viral pneumonia caused by hPIV-3 and RSV in severe combined immunodeficiency disease of two boys (23). Thus, the aerosol method may be useful for the treatment of hPIV-2 by glycyrrhizin, because its optimal concentration *in vitro* is high (3 mg/mL).

In summary, the present investigation reported that

glycyrrhizin, one of the important components of herbal medicines, inhibited hPIV-2 replication in LLCMK₂ cells by the inhibition of viral genome RNA, mRNA and protein syntheses, resulting in the inhibition of giant cell formation and viral release from the infected cells into the culture medium. Herbal medicines containing glycyrrhizin or glycyrrhizin may become useful drugs for the treatment of viruses that infect the respiratory tract, such as hPIV and RSV.

Acknowledgements

We are grateful to Prof. Katsuzumi Okumura (Graduate School of Bioresources, Mie University) for guidance and helpful discussion.

References

1. Lamb RA, Parks GP. Paramyxoviridae: The viruses and their replication. In: Fields Virology (Knipe DM, Howley PM, eds.). 5th ed., Lippincott Williams and Wilkins, Philadelphia, USA, 2007; pp. 1449-1496.
2. Peluso RW, Lamb RA, Choppin PW. Polypeptide synthesis in Simian virus 5-infected cells. *J Virol.* 1977; 23:177-187.
3. Kawano M, Okamoto K, Bando H, Kondo K, Tsurudome M, Komada H, Nishio M, Ito Y. Characterizations of the human parainfluenza type 2 virus gene encoding the L protein and the intergenic sequences. *Nucleic Acids Res.* 1991; 19:2739-2746.
4. Taoda N, Shinji E, Nishii K, Nishioka S, Yonezawa Y, Uematsu J, Hattori E, Yamamoto H, Kawano M, Tsurudome M, O'Brien M, Yamashita T, Komada H. Fucoidan inhibits parainfluenza virus type 2 infection to LLCMK₂ cells. *Biomed Res.* 2008; 29:331-334.
5. Yamamoto H, Ura Y, Tanemura M, Koyama A, Takano S, Uematsu J, Kawano M, Tsurudome M, O'Brien M, Komada H. Inhibitory effect of bovine lactoferrin on human parainfluenza type 2 virus infection. *J Health Sci.* 2010; 56:613-617.
6. Uematsu J, Koyama A, Takano S, Ura Y, Tanemura M, Kihira S, Yamamoto H, Kawano M, Tsurudome M, O'Brien M, Komada H. Legume lectins inhibit human parainfluenza virus type 2 infection by interfering with the entry. *Viruses.* 2012; 4:1104-1115.
7. Kim YW, Zao RJ, Park SJ, Lee JR, Cho JJ, Yang CH, Kim SG, Kim SC. Anti-inflammatory effects of liquiritigenin as a consequence of the inhibition of NF- κ B-dependent iNOS and proinflammatory cytokines production. *Br J Pharmacol.* 2008; 154:165-173.
8. Schröfelbauer B, Raffetseder J, Hauner M, Wolkerstorfer A, Ernst W, Szolar OH. Glycyrrhizin, the main active compound in liquorice, attenuates pro-inflammatory responses by interfering with membrane-dependent receptor signaling. *Biochem J.* 2009; 421:473-482.
9. Michaelis M, Geiler J, Naczek P, Sithisarn P, Leutz A, Doerr HW, Cinatl J Jr. Glycyrrhizin exerts antioxidative effects in H5N1 influenza A virus-infected cells and inhibits virus replication and pro-inflammatory gene expression. *Plos One.* 2011; 6:e19705.
10. Ashfaq UA, Masoud MS, Nawaz Z, Riazuddin S. Glycyrrhizin as antiviral agent against hepatitis C virus. *J*

- Transl Med. 2011; 9:112-118.
11. Matsumoto Y, Matsuura T, Aoyagi H, Matsuda M, Hmwe SS, Date T, Watanabe N, Watashi K, Suzuki R, Ichinose S., Waka K., Suzuki T, Miyamura T, Wakita T, Aizaki H. Antiviral activity of Glycyrrhizin against hepatitis C virus *in vitro*. Plos One. 2013; 8:e68992.
 12. Hardy ME, Hendricks JM, Paulson JM, Faunce NR. 18 β -glycyrrhetic acid inhibits rotavirus replication in culture. Virol J. 2012; 9:96-102.
 13. Kang H, Liberman PM. Mechanism of glycyrrhizic acid inhibition of Kaposi's sarcoma-associated herpesvirus: Disruption of CTCF-cohesin-mediated RNA polymerase II pausing and sister chromatid cohesion. J Virol. 2011; 85:11159-11169.
 14. Tsurudome M, Nishio M, Komada H, Bando H, Ito Y. Extensive antigenic diversity among human parainfluenza type 2 virus isolates and immunological relationships among paramyxoviruses revealed by monoclonal antibodies. Virology. 1989; 171:38-48.
 15. Kawano M, Kaito M, Kozuka Y, Komada H, Noda N, Namba K, Tsurudome M, Ito M, Nishio M, Ito Y. Recovery of infectious human parainfluenza type 2 virus from cDNA clones and properties of the defective virus without V-specific cysteine-rich domain. Virology. 2001; 284:99-112.
 16. Kitagawa H, Kawano M, Yamanaka K, Kakeda M, Tsuda K, Inada H, Yoneda M, Sakaguchi T, Nigi A, Nishimura K, Komada H, Tsurudome M, Yasutomi Y, Nosaka T, Mizutani H. Intranasally administered antigen 85B gene vaccine in non-replicating human parainfluenza type 2 virus vector ameliorates mouse atopic dermatitis. Plos One. 2013; 8:e66614.
 17. Ito M, Sato A, Hirabayashi K, Tanabe F, Shigeta S, Baba M, De Clercq E, Nakashima H, Yamamoto N. Mechanism of inhibitory effect of glycyrrhizin on replication of human immunodeficiency virus (HIV). Antiviral Res. 1988; 11:289-298.
 18. Feng YC, Wang KC, Chiang LC, Shieh DE, Yen MH, San Chang J. Water extract of licorice had anti-viral activity against human respiratory syncytial virus in human respiratory tract cell lines. J Ethnopharmacol. 2013; 148:466-473.
 19. Cinatl J Jr, Michaelis M, Hoever G, Preiser W, Doerr HW. Development of antiviral therapy for severe acute respiratory syndrome. Antiviral Res. 2005; 66:81-97.
 20. Wang J, Chen X, Wang W, Zhang Y, Yang Z, Jin Y, Ge HM, Lie E, Yang G. Glycyrrhizic acid as the antiviral component of *Glycyrrhiza uralensis* Fisch. against coxsackievirus A16 and enterovirus 71 of hand foot and mouth disease. J Ethnopharmacol. 2013; 147:114-121.
 21. De BP, Banerjee A. Involvement of actin microfilaments in the transcription/replication of human parainfluenza virus type 3: Possible role of actin in other viruses. Microsc Res Teck. 1999; 47:114-123.
 22. Kihira S, Uematsu J, Kawano M, Itoh A, Ookohchi A, Satoh S, Maeda Y, Sakai K, Yamamoto H, Tsurudome M, O'Brien M, Komada H. Ribavirin inhibits human parainfluenza virus type 2 replication *in vitro*. Microbiol Immunol. 2014; 58:628-635.
 23. Gelfand EW, McCurdy D, Rao CP, Middleton PJ. Ribavirin treatment of viral pneumonitis in severe combined immunodeficiency disease. Lancet. 1983; 24:732-733.

(Received September 15, 2017; Revised October 10, 2017; Accepted October 15, 2017)

Skin permeability of tulobuterol in two transdermal formulations and their followability

Yuichi Takizawa^{1,*}, Takeshi Goto^{2,3}, Shuji Sato^{2,3}, Naoya Ohmori^{2,3}, Kenji Mori³, Yayoi Shimada³, Kuei-Chen³, Takamitsu Miyagi⁴, Fumio Fukai¹

¹ Faculty of Pharmaceutical Sciences, Tokyo University of Science, Chiba, Japan;

² Faculty of Nursing, Josai International University, Chiba, Japan;

³ Kazusa Research Institute for Drug Discovery, Faculty of Pharmaceutical Sciences, Josai International University, Chiba, Japan;

⁴ Faculty of Pharmaceutical Sciences, Aomori University, Aomori, Japan.

Summary

Various generic transdermal formulations of tulobuterol containing rubber and acrylate base polymers are commercially available in Japan. However, none of the formulations have been compared directly with respect to the skin permeability of tulobuterol and to their follow ability. Tulobuterol Tape Sawai of rubber base and Tulobuterol Tape NP of acrylate base were used to conduct the *in vitro* 24-hour skin permeability test of tulobuterol at receiver solution temperatures of 32°C, 37°C, and 40°C. Furthermore, the followability of these tapes were examined by measuring the depth of the pores that were formed in their adhesive layer. Consequently, the maximum flux of tulobuterol was greater for Tulobuterol Tape NP. Arrhenius plot analysis revealed that Tulobuterol Tape Sawai was more sensitive to skin surface temperature compared with Tulobuterol Tape NP. Skin abrasion had a greater effect on the skin permeability of tulobuterol in Tulobuterol Tape Sawai than in Tulobuterol Tape NP. Followability was greater for Tulobuterol Tape NP than for Tulobuterol Tape Sawai. These results suggest that a transdermal formulation of acrylate base is preferable to that with a rubber base when skin surface temperature varies or when the skin is abraded. In clinical settings, therefore, a formulation of acrylate base is preferable to a formulation of rubber base when skin surface temperature varies or when the skin is abraded. The formulation needs to be applied to the skin of less asperity for the achievement of better transdermal absorption of tulobuterol.

Keywords: Tulobuterol, transdermal, rubber base, acrylate base, intact skin, abraded skin

1. Introduction

Various transdermal formulations of tulobuterol, including the pioneer transdermal patch, Hokunalin[®], are commercially available in Japan (Table 1). Hokunalin[®] contains a rubber base polymer, in which only a small portion of tulobuterol is dissolved and most of the drug crystals is suspended in the adhesive layer. Thus, the concentration of tulobuterol dissolved in the layer is thus kept constant by a mechanism called

the "crystal reservoir system (CRS)" that enables the stable release of tulobuterol from the formulation across the skin (1,2). In generic transdermal formulations, on the other hand, tulobuterol is dissolved in two types of base polymers (*i.e.*, rubber and acrylate; Table 1).

Previous studies compared the skin permeability of tulobuterol between the pioneer and generic products (1-3). In an *in vitro* hairless mouse skin permeability test, the difference in permeability between the intact and abraded skin was smaller in the pioneer than generic products, suggesting that the drug release across the skin is well controlled by the CRS and that generic drugs were more prone to be influenced by skin abrasion.

The skin permeability of tulobuterol has not been compared directly among generic products of different base polymers. The rubber base polymers contain

Released online in J-STAGE as advance publication October 11, 2017.

*Address correspondence to:

Yuichi Takizawa, Faculty of Pharmaceutical Sciences, Tokyo University of Science, 2641, Yamazaki, Noda, Chiba 278-8510, Japan.

E-mail: sephyroot1979@gmail.com

Table 1. Characteristics of the transdermal formulations of tulobuterol commercially available in Japan

Approval year	Manufacturer	Product name	Base polymer
1998	Abbott Japan Co., Ltd.	Hokunalin®	PIB
2006	Sawai Pharmaceutical Co., Ltd.	Tulobuterol Tape Sawai	SIS
	Nichi-Iko Pharmaceutical Co., Ltd.	Tulobuterol Tape Nichi-Iko	
	Yutoku Pharmaceutical Ind. Co., Ltd.	Tulobuten Tape	
	Hisamitsu Pharmaceutical Co., Inc.	Tulobuterol Tape HMT	Acrylate
	Towa Pharmaceutical Co., Ltd.	Sekinarin Tape	
	Takata Pharmaceutical Co., Ltd.	Tulobuterol Tape Takata	
2007	Ohara Pharmaceutical Co., Ltd.	Tulobuterol Tape Ohara	SIS
	Teikoku Seiyaku Co., Ltd.	Tulobuterol Tape Teikoku	
	Medisa Shinyaku Inc.	Tulobuterol Tape MED	
2008	Shiono Chemical Co., Ltd.	Tulobuterol Tape SN	SIS
2009	Nipro Corporation	Tulobuterol Tape NP	Acrylate

PIB, polyisobutylene; SIS, styrene-isoprene-styrene.

nonpolar functional groups, while acrylate base polymers contain polar functional groups (e.g., amido). The polar functional groups of acrylate base polymers interact with the polar functional groups (e.g., hydroxyl groups) of drugs, resulting in retention of drugs in base polymers (4,5). Hence, the skin permeability of tulobuterol that has the hydroxyl group may be affected by the polarity of base polymers.

Morimoto *et al.* conducted the release test of drugs containing the amido, carboxyl, or ester group into the 40% aqueous solution of polyethyleneglycol (PEG) at 37°C; they calculated the distribution coefficients (logD), glass-transition temperature (T_g), and wavelength of the hydroxyl group and reported the amido group, amino group, carboxyl group, and ester group in decreasing order of the interactions of the function groups with base polymers (4,5).

Kato *et al.* prepared the transdermal formulations of tulobuterol containing gum, silicon, or acrylate polymers to examine the 24-hour releasability of the drug across rabbit skin (1). Consequently, they reported gum base, silicon base, and acrylate base in decreasing order of drug releasability. These findings led us to hypothesize that drug releasability would be controlled by base polymers, and we conducted an *in vitro* hairless mouse skin permeability test to confirm our hypothesis.

Transdermal formulations, also called pressure-sensitive agents (PSAs), acquire adhesion between the skin and their adhesive layer by applying a slight pressure when attached to the skin. Transdermal formulations are endowed with the function of PSAs by selecting base polymers with a low T_g to exert adhesion or by adding a tackifier at skin surface temperature (6,7).

Tojo *et al.* reported lower elasticity and greater peeling strength in association with the lower T_g of acrylate base polymers (3). Furthermore, Zhao *et al.* added isopropyl myristate to the acrylate adhesive to decrease T_g and degree of elasticity (G') and to increase tack adhesiveness (8).

Another important index of base polymers for the transdermal formulations is followability that enables

close contact between the formulation and the skin surface (6). In the present study, we examined the skin permeability of tulobuterol in and the followability of two tulobuterol tapes.

2. Materials and Methods

2.1. Materials, animals, and devices

Tulobuterol Tape Sawai (2 mg; 32 × 32 mm, Sawai Pharmaceutical Co., Ltd., Osaka, Japan) and Tulobuterol Tape NP (2 mg; 32 × 32 mm, Nipro Corporation, Osaka, Japan) were purchased from the market.

Male Hos:HR-1 hairless mice aged 7-8 weeks (17-25 g in body weight) were purchased from Japan SLC Co., Inc. (Shizuoka, Japan). Animals were handled in accordance with the rules established by the Institutional Animal Care and Use Committee at Josai International University.

In an *in vitro* 24-hour hairless mouse skin permeability test of tulobuterol, a vertical diffusion cell (LGA-1084-CL, Laboratory Glass Apparatus, Berkeley, CA) was used to diffuse tulobuterol across the resected hairless mouse skin and an autosampler (FOXY200, Nikkaki Bios Co., Ltd., Tokyo, Japan) to collect the sample solution.

2.2. *In vitro* 24-hour hairless mouse skin permeability test of tulobuterol

The skin was resected from mice after cervical dislocation. The resected skin was inverted to remove subcutaneous fat, followed by standing of the dermis placed downward onto the filter paper that was impregnated with saline.

Tulobuterol Tape Sawai and Tulobuterol Tape NP were punched out into 15 round pieces of 24 mm in diameter, and the protective liner was peeled off and then attached to the resected skin. Test material was set onto the vertical diffusion cell, and the upper and lower rims of the cell were fixed with a metallic pinch clamp. The

interior of the cell was filled with the receiver solution (40% PEG 400 [NOF Corporation, Tokyo, Japan]) to remove air bubbles, followed by passage through the cell at a rate of 10 mL/h. Aliquots of the solution were collected every 2 h up to 24 h. Subsequently, 500 μ L of the internal reference solution (760 μ g/mL celecoxib, Edmond Pharma, Paderno Dugnano, Italy) were mixed with 400 μ L of the sample solution, and an ultra-performance liquid chromatograph (Nihon Waters Co., Ltd., Tokyo, Japan) with a ODS C18 column (2.1 \times 50 mm; detection wavelength: 215 nm; column temperature at measurement: 40°C; and injection volume of sample: 5 μ L) was used to measure the tulobuterol concentration. Tulobuterol (Shiono Chemical Co., Ltd., Tokyo, Japan) was used as reference standard and celecoxib as internal standard. The flow rate for the mobile phase (0.5% phosphoric acid [Wako Pure Chemical Industries Ltd., Osaka, Japan], 0.01 M sodium dodecyl sulfate [Wako Pure Chemical Industries], and 55% acetonitrile [Wako Pure Chemical Industries]) was 5.0 mL/min (3). In consideration of clinical application, the temperature of the receiver solution was varied from the skin surface temperature, 32°C to the temperature at the time of taking a sauna or bath, 40°C (9).

The flux was calculated based on the ratio of tulobuterol in the reference standard solution to that in the internal standard, and the *Flux* (μ g/cm²/h) and maximum flux values (J_{max}) were calculated according to the following equation (10):

$$Flux = (VdC/dt)/A$$

where, C: drug concentration in the sample, t: measurement time (hr), V: volume (mL) of the receiver in the sample, and A: effective diffusion area (cm²).

2.3. Preparation of the abraded skin and measurement of water content in the skin surface

The resected skin was placed onto an aluminum tray, followed by the stripping of the stratum corneum (SC) 7 times with Scotch Brand BookTape 845 (3M Japan Co., Ltd., Tokyo, Japan) as described previously (9). A water content meter (Corneometer[®] CM 825; Courage + Khazaka Electronic GmbH, Cologne, Germany) was used to measure water content in the skin surface. The probe was cleaned with absorbent cotton impregnated with ethanol before application onto the skin surface. Water content in the skin surface was measured six times to calculate the mean value.

2.4. Followability test of 2 transdermal formulations

At a room temperature of 25°C, a sandpaper (Fuji Star #120, Sankyo Rikagaku Co., Ltd., Saitama, Japan) was cut into 2 sheets (3 \times 4 cm in size), and each sheet was placed on a table, with the grinding surface upward.

Subsequently, the adhesive surface of the sample was applied to the grinding surface of the sandpaper, a sheet of paper towel (Kim Towel[®], Nippon Paper Crexia Co., Ltd., Tokyo, Japan) was put onto each sample, and a 1-kg cylinder weight was then placed onto the sample for 1 min. Subsequently, the weight, the paper towel, and the sandpaper were removed, and a laser microscope (LS-5040, Keyence Co., Ltd., Osaka, Japan) was used to measure the depth of the pores that were formed in the adhesive layer of the examined tapes.

2.5. Statistical analysis

Welch's *t*-test was conducted to test differences in flux between the intact and abraded skin in the skin permeability test of tulobuterol and differences in pore depth before and after treatment in the followability test by using Microsoft Excel for windows (Microsoft, Tokyo, Japan). A value of *p* < 0.05 was considered statistically significant. All values are expressed as mean \pm SE.

3. Results

3.1. Skin permeability of tulobuterol at 3 temperatures

Tulobuterol Tape Sawai and Tulobuterol Tape NP have rubber and acrylate base polymers, respectively. Time-course changes in the *Flux* of tulobuterol from both formulations at 32°C, 37°C, and 40°C are shown in Figure 1. At all temperatures, the J_{max} values were higher in Tulobuterol Tape NP than in Tulobuterol Tape Sawai. Both formulations showed an increase in J_{max} in association with temperature elevations (Figure 1). Tulobuterol Tape Sawai exhibited a greater rate of increase than did Tulobuterol Tape NP (Table 2). Namely, the J_{max} of Tulobuterol Tape Sawai increased 1.19- and 1.29-fold at 37°C and 40°C, respectively,

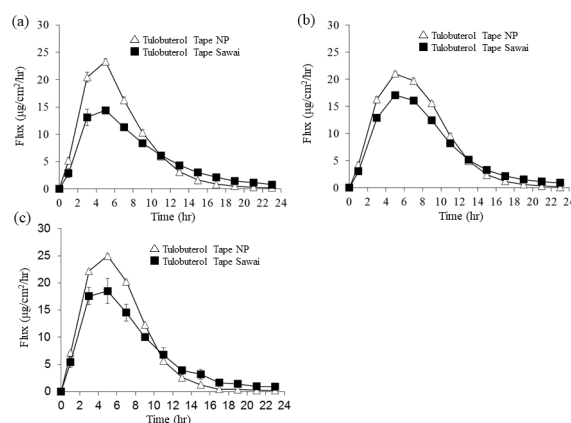


Figure 1. Time-course changes in *J* at various receiver solution temperatures. The *Flux* of tulobuterol released from Tulobuterol Tape Sawai and Tulobuterol Tape NP was determined at 32°C (a), 37°C (b), and 40°C (c). Values are expressed as mean \pm SE (*n* = 3). SE, standard error.

Table 2. J_{max} values of tulobuterol in tulobuterol Tape Sawai and tulobuterol Tape NP in an *in vitro*, 24-hour hairless mouse skin permeability test

Items	J_{max} ($\mu\text{g}/\text{cm}^2/\text{h}$), Tulobuterol Tape Sawai ($n = 3$)	J_{max} ($\mu\text{g}/\text{cm}^2/\text{h}$), Tulobuterol Tape NP ($n = 3$)
Temperature		
32°C	14.37 \pm 0.29	23.34 \pm 0.52
37°C (vs. 32°C)	17.10 \pm 0.19 (1.19 fold)	21.07 \pm 0.33 (0.90 fold)
40°C (vs. 32°C)	18.50 \pm 2.28 (1.29 fold)	24.99 \pm 0.33 (1.07 fold)
Skin		
Intact skin	10.73 \pm 0.99	22.44 \pm 0.76
Abraded skin (vs. intact skin)	15.66 \pm 0.40 (1.46 fold)	28.94 \pm 0.11 (1.29 fold)

Values are expressed as mean \pm SE. SE, standard error. J_{max} , maximum value of flux.

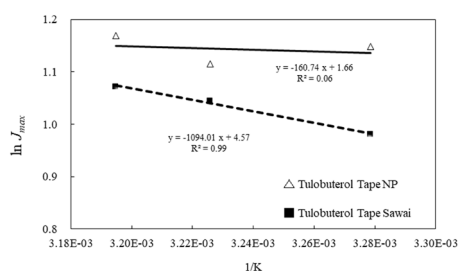


Figure 2. Arrhenius plot analysis on the skin permeability of tulobuterol. The natural logarithms of J_{max} of the skin permeability of tulobuterol in Tulobuterol Tape Sawai and Tulobuterol Tape NP were plotted against the inverse of skin surface temperature to depict linear approximations of skin permeability. \ln , skin permeation; J_{max} , maximum flux; K, skin surface temperature.

against at 32°C. On the other hand, the J_{max} of Tulobuterol Tape NP increased 0.09- and 1.07-fold at 37°C and 40°C, respectively, against at 32°C. Arrhenius plot analysis disclosed a steeper slope by linear approximations for Tulobuterol Tape Sawai compared to Tulobuterol Tape NP (Figure 2), suggesting that the former is more prone to be influenced by skin surface temperature.

3.2. Skin permeability of tulobuterol across the intact and abraded skin

The J values of tulobuterol in the intact and abraded skin at 32°C were compared between Tulobuterol Tape Sawai and Tulobuterol Tape NP (Figure 3). Namely, the J_{max} of tulobuterol in Tulobuterol Tape Sawai increased 1.46-fold in the abraded skin against the intact skin, while that of Tulobuterol Tape NP increased 1.29-fold (Table 2).

Water content of the skin was measured because of its importance for skin permeability. The water contents of the intact ($n = 6$) and abraded ($n = 6$) skin were 26.83 \pm 10.72 a.u. and 75.5 \pm 8.5 a.u., respectively. A statistically significant difference ($p < 0.05$) was found between these two types of skin, indicating that the water content of the abraded skin had increased as a consequence of SC stripping. In the test using Tulobuterol Tape Sawai, a statistically significant difference ($p < 0.05$) was found in the water contents of

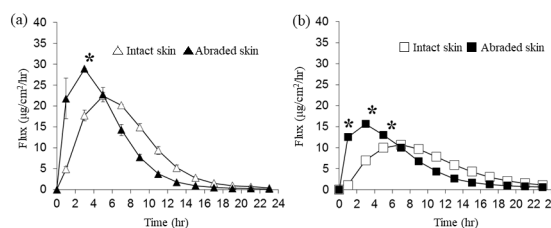


Figure 3. Time-course changes in flux with intact and abraded skin. The flux of tulobuterol from Tulobuterol Tape NP (a) and Tulobuterol Tape Sawai (b) was determined at 32°C in intact or abraded skin. Values are expressed as mean \pm SE ($n = 3$). $p < 0.05$ (Welch's *t*-test). SE, standard error.

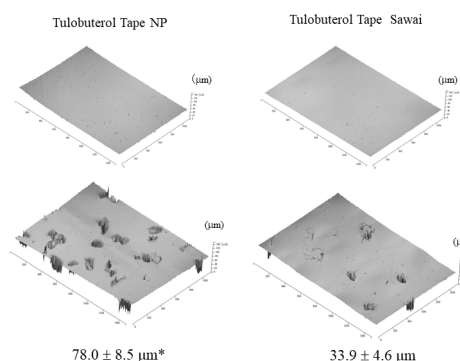


Figure 4. Followability test. Tulobuterol Tape Sawai and Tulobuterol Tape NP were placed on sandpapers. 1 min later, the sandpaper was removed to measure the depth of 6 pores with a laser microscope. Values are expressed as mean \pm SE ($n = 6$). $p < 0.05$ (Welch's *t*-test). SE, standard error.

the intact and abraded skin (32.3 \pm 13.1 a.u. and 77.5 \pm 10.1 a.u., respectively). In the test using Tulobuterol Tape NP, a statistically significant difference ($p < 0.05$) was also found in the water contents of the intact and abraded skin (26.5 \pm 8.6 a.u. and 75.2 \pm 11.9 a.u., respectively).

3.3. Followability test of 2 transdermal formulations

A statistically significant difference ($p < 0.05$) was found in the depths of the pores that had been formed in the adhesive layer of Tulobuterol Tape Sawai and Tulobuterol Tape NP (33.9 \pm 4.6 μm and 78.0 \pm 8.5 μm , respectively). This result suggests that followability is greater for Tulobuterol Tape NP than for Tulobuterol Tape Sawai (Figure 4).

4. Discussion

Tulobuterol containing the hydroxyl group in its molecule interacts with the polar function group of the acrylate base polymer with the amido group, while Tulobuterol Tape Sawai with a rubber base that does not contain the polar function groups exhibits no such interaction. Kato *et al.* conducted a 24-hour rabbit skin releasability test of the transdermal formulations of tulobuterol of gum, silicon, and acrylate bases and reported gum base, silicon base, and acrylate base in decreasing order of drug releasability (1). Furthermore, Kokubo *et al.* prepared the transdermal formulations of dipropylphthalate, ketoprofen, ampicillin, and lidocaine that contained acrylate, gum, and silicon base polymers to examine drug releasability (11). Consequently, they reported no effect of gum and silicon base polymers on drug releasability and a decrease in drug releasability in the transdermal formulations of acrylate base due to the interactions of carboxyl group-containing drugs and acrylate base polymers. Therefore, the skin permeability of tulobuterol was predicted to be greater in Tulobuterol Tape Sawai. Surprisingly, however, the skin permeability of tulobuterol was greater for Tulobuterol Tape NP than for Tulobuterol Tape Sawai; the result was probably attributable to the greater followability of Tulobuterol Tape NP compared with Tulobuterol Tape Sawai.

The skin permeability of tulobuterol in both Tulobuterol Tape Sawai and Tulobuterol Tape NP increased in association with elevations in receiver solution temperature. Similar results were obtained in an *in vitro* skin permeability test of nonsteroidal anti-inflammatory drugs in the transdermal formulations of rubber base (12). Drug solubility into the skin increased exponentially in association with elevations in receiver solution temperatures, resulting in higher skin permeability at higher temperatures (12,13). We speculate that a similar mechanism is responsible for higher skin permeability at higher receiver solution temperatures in the present study. Arrhenius plots analysis suggested that Tulobuterol Tape Sawai is more sensitive to changes in skin surface temperature compared to Tulobuterol Tape NP. The interaction of the polar functional groups of acrylate base polymers with tulobuterol probably reduces the skin permeability of tulobuterol at 37°C and 40°C where the skin permeability of tulobuterol is increased.

The skin is composed of the epidermis containing the stratum corneum (SC) and dermis. The SC is a biobarrier that prevents water evaporation and the penetration of foreign matter from the exterior into the body and also functions as a biomembrane that controls drug diffusion into the skin (14-17). Both Tulobuterol Tape Sawai and Tulobuterol Tape NP showed a higher J_{max} in abraded skin than in intact skin. We consider that these findings are attributable to the fact that the

thinner SC of the abraded skin lost its function as the drug release-controlling membrane. Furthermore, the increase rate of J_{max} in the abraded skin was higher for Tulobuterol Tape Sawai than for Tulobuterol Tape NP. Again, we speculate that the interaction of the polar functional groups of the acrylate base with tulobuterol inhibits the skin permeability of tulobuterol which is enhanced by skin abrasion.

The followability of Tulobuterol Tape NP was greater compared with Tulobuterol Tape Sawai, suggesting that the former is more flexible than the latter. The skin surface has asperity. The transdermal formulations of drugs that do not follow the asperity produce a less effective area of contact between the adhesive surface and the skin and cause concerns about a decrease in the skin absorbability of the drugs.

Miyazaki *et al.* used the transdermal formulations of acrylate base with different storage elastic moduli to examine the relationships between the followability of the formulations and the severity of SC detachment (6). Consequently, they reported the better followability to skin surface asperity with respect to the transdermal formulations of adhesive bases that had lower storage elastic moduli and that these formulations homogeneously detached the SC. Tojo *et al.* reported lower storage elastic moduli and greater peeling strengths in acrylate base polymers with lower Tg values (7). Thus, in general, base polymers with a lower Tg value and/or a lower storage elastic modulus exhibit greater followability at skin surface temperature (6-8).

Tulobuterol Tape Sawai has styrene-isoprene-styrene (SIS) block copolymers that contain polyisoprene as a soft segment and polystyrene as a hard segment. On the other hand, Tulobuterol Tape NP has acrylate 2-ethylhexyl as a soft segment and diacetone-acrylamide, acetoacetoxyethyl methacrylate, and methyl methacrylate copolymers as a hard segment (18-20). SIS block copolymers, which contain polystyrene, have a higher Tg compared with diacetone-acrylamide, acetoacetoxyethyl methacrylate, and methyl methacrylate copolymers; therefore, Tulobuterol Tape Sawai would have a higher Tg compared with Tulobuterol Tape NP, resulting in lower followability.

In conclusion, a formulation of acrylate base is clinically preferable to a formulation of rubber base when skin surface temperature varies or when the skin is abraded. The formulation needs to be applied to the skin of less asperity for the achievement of better transdermal absorption of tulobuterol.

Acknowledgements

The authors thank Satoshi Sakima, MD, for his critical review of the manuscript and are grateful to Josai International University for the provision of study material and physical space for this study.

References

1. Kato H, Nagata O, Yamazaki M, Suzuki T, Nakano Y. Development of transdermal formulation of tulobuterol for the treatment of bronchial asthma. *Yakugaku Zasshi*. 2002; 122:57-69. (in Japanese)
2. Yoshihara S, Fukuda H, Abe T, Arisaka O. Comparative study of skin permeation profile between brand and generic tulobuterol patches. *Biol Pharm Bull*. 2010; 33:1763-1765.
3. Tojo K, Hikima T. Bioequivalence of marketed transdermal delivery systems for tulobuterol. *Biol Pharm Bull*. 2007; 30:1576-1579.
4. Morimoto Y, Kokubo T, Sugibayashi K. Diffusion of drugs in acrylic-type pressure-sensitive adhesive matrix. II. Influence of interaction. *J Control Release*. 1992; 18:113-121.
5. Furuishi T, Io T, Fukami T, Suzuki T, Tomono K. Formulation and *in vitro* evaluation of pentazocine transdermal delivery system. *Biol Pharm Bull*. 2008; 31:1439-1443.
6. Miyazaki K, Tatsuno T, Miyata S. Mechanism of the stratum corneum stripping of acrylic pressure sensitive adhesives with different storage elastic modulus. *J Adhes S J*. 2011; 47:465-470. (in Japanese)
7. Tojo K. Polymers for transdermal drug delivery systems. *Membrane*. 1994; 19:75-80. (in Japanese)
8. Zhao C, Quan P, Liu C, Li Q, Fang L. Effect of isopropyl myristate on the viscoelasticity and drug release of a drug-in-adhesive transdermal patch containing blonanserin. *Acta Pharm Sin B*. 2016; 6:623-628.
9. Prodduturi S, Sadrieh N, Wokovich AM, Doub WH, Westenberger BJ, Buhse L. Transdermal delivery of fentanyl from matrix and reservoir systems: Effect of heat and compromised skin. *J Pharm Sci*. 2010; 99:2357-2366.
10. Roy SD, Gutierrez M, Flynn GL, Cleary GW. Controlled transdermal delivery of fentanyl: Characterizations of pressure-sensitive adhesives for matrix patch design. *J Pharm Sci*. 1996; 85:491-495.
11. Kokubo T, Sugibayashi K, Morimoto Y. Interactions between drug and pressure-sensitive adhesives in transdermal therapeutic systems. *Pharm Res*. 1994; 11:104-107.
12. Tominaga K, Tojo K. Effect of environmental temperature on transdermal drug penetration. *Biol Pharm Bull*. 2010; 33:1983-1987.
13. Takizawa Y, Fukai F, Goto T, Sato S, Ohmori N, Mori K, Shimada Y, Chiang K, Miyagi T, Tane E, Chiba S. The 24-hour *in vitro* hairless rat skin permeability study of the 1-day fentanyl transdermal formulations marketed in Japan – Fentos[®] Tape and OneDuro[®] Patch. *J Drug Deliv Res*. 2015; 4:1-15.
14. Hadgraft J. Skin, the final frontier. *Int J Pharm*. 2001; 224:1-18.
15. Sandler A. Transdermal fentanyl: Acute analgesic clinical studies. *J Pain Symptom Manage*. 1992; 7:S27-35.
16. Wertz PW. Lipids and barrier function of the skin. *Acta Derm Venereol Suppl*. 2000; 208:7-11.
17. De jager MW, Gooris GS, Dolbnya IP, Ponc M, Bouwstra JA. Modelling the stratum corneum lipid organization with synthetic lipid mixture: The importance of synthetic ceramide composition. *Biochim Biophys Acta*. 2004; 1664:132-140.
18. Sawai Pharmaceutical Co., Ltd. Package insert of Tulobuterol Tape Sawai. <http://database.japic.or.jp/pdf/newPINS/00051883.pdf> (accessed September 6, 2017). (in Japanese)
19. NIPRO. Package insert of Tulobuterol Tape NP. <http://database.japic.or.jp/pdf/newPINS/00058046.pdf> (accessed September 6, 2017). (in Japanese)
20. Oshima S, Hazama Y, Hosoya O, Nagashima K, Tanaka T, Sano M, Ohta S, Yasuno S, Juni K. Investigation of fentanyl patch to evaluate its usability and adhesiveness. *Jpn J Pharm Palliat Care Sci*. 2012; 5:7-13. (in Japanese)

(Received September 20, 2017; Revised September 23, 2017; Accepted September 24, 2017)

Two-spotted cricket as an animal infection model of human pathogenic fungi

Yuto Kochi¹, Yasuhiko Matsumoto², Kazuhisa Sekimizu², Chikara Kaito^{1,*}

¹Laboratory of Microbiology, Graduate School of Pharmaceutical Sciences, The University of Tokyo, Bunkyo-ku, Tokyo, Japan;

²Institute of Medical Mycology, Teikyo University, Tokyo, Japan.

Summary

Invertebrate infection models that can be evaluated at human body temperature are limited. In this study, we utilized the two-spotted cricket, a heat-tolerant insect, as an animal infection model of human pathogenic fungi. Injection of human pathogenic fungi, including *Candida albicans*, *Candida glabrata*, and *Cryptococcus neoformans* killed crickets within 48 h at both 27°C and 37°C. The median lethal dose values (LD₅₀ values) of *C. albicans* and *C. glabrata* against crickets were decreased at 37°C compared to that at 27°C, whereas the LD₅₀ value of *C. neoformans* was not different between 27°C and 37°C. Heat-killed cells of the three different fungi also killed crickets, but the LD₅₀ value of the heat-killed cells was higher than 5-fold that of live fungal cells in the respective species. *C. neoformans* gene-knockout strains of *ena1*, *gpa1*, and *pka1*, which are required for virulence in mammals, had greater LD₅₀ values than the parent strain in crickets. These findings suggest that the two-spotted cricket is a valuable infection model of human pathogenic fungi that can be used to evaluate fungal virulence at variable temperatures, including 37°C, and that the killing abilities of *C. albicans* and *C. glabrata* against animals are increased at 37°C.

Keywords: Cricket, animal infection model, temperature, virulence, human pathogenic fungi

1. Introduction

Human pathogenic fungi such as *Candida albicans*, *Candida glabrata*, and *Cryptococcus neoformans* cause superficial infections in the skin and oral cavity as well as deep infections in organs such as the lung and brain. Immunocompromised patients, such as those with AIDS and cancer, are especially susceptible to lethal fungal infection (1-4). Because fungi are eukaryotes, limited numbers of antifungal drugs are available and thus novel antifungal drugs are desired. To develop new antifungal drugs, it is important to understand the molecular mechanisms of fungal infectious processes using an animal infection model and to identify new drug targets. Many mammalian pathogens including fungi are assumed to detect an increase in the environmental

temperature as information regarding the host environment (5). At 37°C, the human body temperature, *C. albicans* modulates its nucleosome structure with temperature-induced transcription factors to accomplish physiologic alterations that enhance virulence, such as hyphae formation (6,7). To clarify the significance of such temperature-dependent processes for fungal infectious processes, it is essential to utilize animal infection models at both low and high temperatures.

Animal models of infection that can withstand both low and high temperatures, however, are scarce. Mammals such as mice and rabbits have been used to evaluate fungal virulence properties in various organs, including the skin (8), lung (9), stomach (10), oral cavity (11), urethral tube (12), and vagina (13). Mammals are homeothermic animals, however, and cannot be used to evaluate fungal virulence at low temperatures. Many non-mammalian animals have been used as animal models of fungal infection to overcome the ethical and cost-related issues associated with mammalian model animals (14,15); a vertebrate model such as zebra fish (16), and invertebrate models such as nematode (*Caenorhabditis elegans*) (17), fruit fly (*Drosophila melanogaster*) (18), silkworm (*Bombyx mori*) (19,20), and the greater

Released online in J-STAGE as advance publication October 29, 2017.

*Address correspondence to:

Dr. Chikara Kaito, Laboratory of Microbiology, Graduate School of Pharmaceutical Sciences, The University of Tokyo, 3-1, 7-chome, Hongo, Bunkyo-ku, Tokyo 113-0033, Japan.
E-mail: kaito@mol.f.u-tokyo.ac.jp

wax moth larva (*Galleria mellonella*) (21,22). The heterothermic characteristics of zebra fish were used to evaluate fungal virulence at a high temperature of 33°C (23,24). The applicability of this model at 37°C, however, is not known. The nematode *C. elegans* and the fruit fly *D. melanogaster* cannot survive at 37°C. Silkworms and the greater wax moth larva can be used as animal infection models at 37°C (25-27), but their infection sensitivities to fungi are drastically increased at 37°C compared to that at a lower temperature (19,28-31). The increased infection sensitivity of these insects at 37°C is considered to be due to damage to the immune system at a high temperature (32-34).

We focused on the two-spotted cricket, *Gryllus bimaculatus*, an Orthopteran insect that is distributed across tropical and subtropical regions in the world, to investigate the effects of temperature on the infectious processes of human pathogens. The two-spotted cricket develops from nymph to adult at a wide range of temperatures, from 19°C to 37°C (35,36). We previously reported that the two-spotted cricket is infected and killed by human pathogenic bacteria, including *Staphylococcus aureus*, *Pseudomonas aeruginosa*, and *Listeria monocytogenes* (37). The infection sensitivity of the two-spotted cricket to *S. aureus* and *P. aeruginosa* does not differ between 27°C and 37°C, but the infection sensitivity to *L. monocytogenes* is higher at 37°C than at 27°C (37). Thus, the two-spotted cricket does not generally increase the infection sensitivity to pathogens at 37°C, and is an animal infection model that can be used to evaluate the effect of temperature on infectious processes without perturbing host system to identify the temperature-dependent virulence mechanisms of specific pathogens. In addition, the two-spotted cricket is available at a low price throughout the world, because crickets are cultured as food for amphibians and reptiles. The body size of the cricket is appropriate for injecting accurate amounts of samples and to quantitatively evaluate the virulence properties of pathogens by determining the median lethal dose (LD₅₀) value (37). In this study, we examined the virulence properties of human pathogenic fungi, including *C. albicans*, *C. glabrata*, and *C. neoformans*, using the cricket infection model at 27°C and 37°C. The findings revealed that the two-spotted cricket can be used as an animal infection model of human pathogenic fungi, and that *C. albicans* and *C. glabrata* exhibit increased killing abilities against crickets at a high temperature.

2. Materials and Methods

2.1. Crickets

Two-spotted crickets in the final nymph stage were purchased from Tsukiyono Farm (Tone-gun, Gunma, Japan) and raised to adults by feeding them water and food at 27°C, as previously reported (38,39). Briefly,

Table 1. Fungal strains used in this study

Strain	Genotypes and Characteristics	Ref.
<i>Candida albicans</i> ATCC10231	Serotype A	(56)
<i>Candida glabrata</i> CBS138	ATCC2001	(57)
<i>Cryptococcus neoformans</i> H99	Serotype A, clinical isolate	(58)
Δcna	H99, <i>cna1::ade2, mata</i>	(43)
$\Delta gpa1$	H99, <i>gpa1::ade2, mata</i>	(45)
$\Delta pka1$	H99, <i>pka1::ade2, mata</i>	(47)

100 crickets were kept in a plastic cage (W320 × L170 × H210) with food 'Koorogi-food' (Tsukiyono-Farm), wet paper towel, and paper egg trays. Adult crickets within 1 week after eclosion were used for the infection experiments.

2.2. Fungal strains and culture conditions

Fungal strains, including *C. albicans*, *C. glabrata*, *C. neoformans*, and the gene-knockout strains of *C. neoformans*, which were stocked at -80°C, were streaked on YPD agar plates and cultured overnight at 30°C. A single colony of each strain was inoculated into 30 ml of YPD liquid medium in a 225-mL conical tube (cat. no. 352075, BD Falcon, Bedford, MA) and aerobically cultured overnight by shaking at 150 rpm (BR-3000LF, TAITEC co., Ltd., Koshigaya, Saitama, Japan) at 30°C. The details of the fungal strains used in this study are listed in Table 1.

2.3. Infection experiments using crickets

Overnight fungal cultures were centrifuged at 5,000 g for 6 min and the precipitated cells were suspended in saline. The fungal cell solution was serially diluted with saline. Crickets were injected with 50 µL of fungal solution *via* an intra-hemolymph route from the ventral abdominal region using a 1-mL syringe equipped with a 30 gauge-needle, as previously reported (37). The injected crickets ($n = 5$ /group) were maintained in a disposable cylindrical dish (Φ129 × H97 mm, MINERON KASEI Co., Ltd., Higashi-Osaka, Osaka, Japan) with food and wet Kimwipes (NIPPON PAPER CRECIA Co., Ltd., Chiyoda-ku, Tokyo, Japan) in dark conditions at 27°C or 37°C. Cricket survival was monitored after the injection. The fungal solution used for the infection experiment was 10⁵-fold diluted with saline, spread onto YPD agar plates, and incubated overnight at 30°C. The appearing colonies were counted and the number of live fungal cells injected into the crickets was calculated. The LD₅₀ values of fungal strains against the crickets were determined by logistic regression from the dose-survival plots. All the survival data are listed in Table S1 (<http://www.ddtjournal.com/action/getSupplementalData.php?ID=16>).

2.4. Preparation of heat-killed fungal cells

Overnight fungal cultures were centrifuged at 5,000 g for 6 min, and the precipitated cells were suspended in 1 mL of saline and transferred to a 2-mL Eppendorf tube. A small part of the fungal solution was 10^5 -fold diluted with saline, spread onto YPD agar plates, and incubated overnight at 30°C to measure the number of fungal cells. The fungal solution in a 2-mL Eppendorf tube was autoclaved at 121°C for 20 min, serially diluted with saline, and used for the infection experiments.

2.5. Measurement of fungal doubling time

Single colonies of *C. albicans*, *C. glabrata*, or *C. neoformans* were inoculated into 10 mL of YPD liquid medium in a 50-mL conical tube (Cat. No. 352070, BD-Falcon) and aerobically cultured overnight at 30°C by shaking at 150 rpm. A 100- μ L aliquot of the overnight culture was inoculated into 10 mL of YPD liquid medium in a 50-mL conical tube and aerobically cultured by shaking at 150 rpm at 27°C or 37°C. The OD₆₀₀ values were measured over time using a spectrophotometer (UV-1280, SHIMADZU Co., Kyoto, Japan). To measure the condensed cell culture, the culture was appropriately

diluted with saline. The doubling time was calculated from the exponential growth phase by linear regression, as previously reported (40,41).

2.6. Statistical analysis

Cricket survival at different fungal doses were plotted on an X-Y graph and the dose-response survival curves were determined by logistic regression. To compare the two dose-survival curves, a likelihood ratio test was performed using R ver. 3.2.3 (42). The LD₅₀ value and the standard error were determined using 'Mass' in R.

3. Results

3.1. Cricket killing by human pathogenic fungi

To determine whether human pathogenic fungi kill the two-spotted crickets, we injected *C. albicans*, *C. glabrata*, and *C. neoformans* into crickets via the intra-hemolymph route and maintained the crickets at 27°C or 37°C. At both temperatures, a high number of *C. albicans* cells killed crickets within 18 h after the injection, whereas a low number of *C. albicans* cells killed crickets 40 h after injection (Figure 1A). A similar tendency was

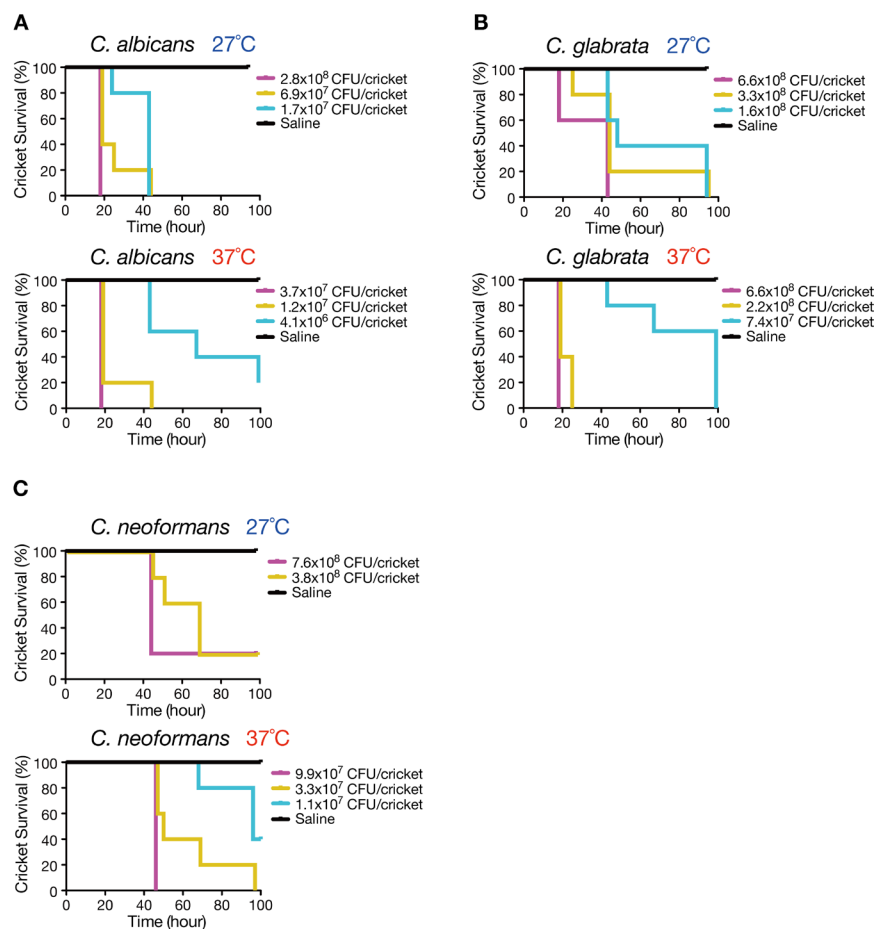


Figure 1. Killing of crickets after injecting human pathogenic fungi. Crickets ($n = 5$ /group) were injected with saline or various doses of *C. albicans* (A), *C. glabrata* (B), or *C. neoformans* (C), and were maintained at 27°C or 37°C. The time-course of cricket survival was monitored.

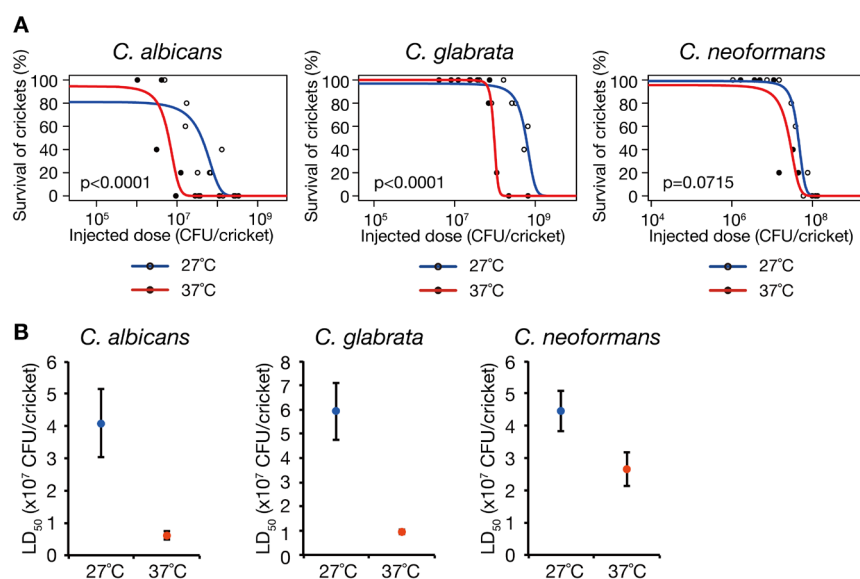


Figure 2. Effect of temperature on cricket sensitivity against fungal infection. (A) The dose-response survival curve of crickets injected with *C. albicans*, *C. glabrata*, or *C. neoformans* was examined at 27°C or 37°C. Serial dilutions of the fungal solution were injected into crickets ($n = 5/\text{dose}$) and survival was monitored at 24 h (*C. albicans* and *C. glabrata*) or 48 h (*C. neoformans*) after the injection. Results from independent experiments (*C. albicans* [27°C], three times; *C. albicans* [37°C], two times; *C. glabrata* [27°C], three times; *C. glabrata* [37°C], three times; *C. neoformans* [27°C], three times; *C. neoformans* [37°C], two times) were pooled and the survival curve was determined by logistic regression. The p -values determined by using likelihood ratio tests between the survival curves at 27°C and 37°C are presented in the graphs. All survival data are presented in Table S1 (Supporting Information) and no crickets injected with saline died in any of the experiments. (B) The LD₅₀ values of *C. albicans*, *C. glabrata*, or *C. neoformans* at 27°C or 37°C were determined by logistic regression in (A). Error bars indicate standard errors.

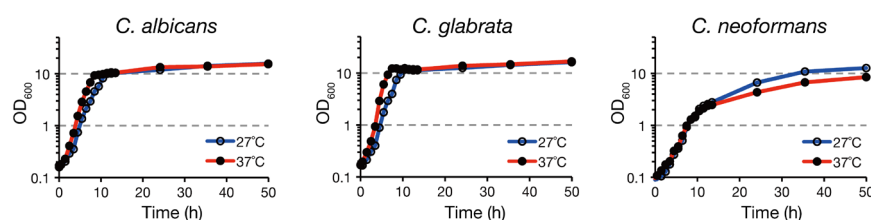


Figure 3. Effect of temperature on fungal growth curve. Overnight cultures of *C. albicans*, *C. glabrata*, or *C. neoformans* were inoculated into 100-fold amounts of fresh YPD medium and aerobically cultured at 27°C or 37°C. OD₆₀₀ was measured during the time-course.

observed in the injection of *C. glabrata* cells (Figure 1B). *C. neoformans* killed crickets 43 h after injection (Figure 1C). In all experiments, injection of saline did not kill the crickets (Figures 1A-1C). These results suggest that *C. albicans*, *C. glabrata*, and *C. neoformans* kill crickets.

3.2. Comparison of cricket killing ability by fungi between 27°C and 37°C

Because the two-spotted cricket does not universally increase infection sensitivity to pathogens (37), the two-spotted cricket is useful for evaluating the temperature effect on the infection properties of pathogens. We examined whether *C. albicans*, *C. glabrata*, and *C. neoformans* increase their killing activities against crickets at a higher temperature. Crickets were injected with fungi, maintained at 27°C or 37°C, and survival was measured. The dose-response survival curve of *C. albicans* differed between 27°C and 37°C (Figure 2A), and the LD₅₀ value at 37°C was less than one-fifth that at

27°C (Figure 2B). The dose-response survival curve of *C. glabrata* was different between 27°C and 37°C (Figure 2A), and the LD₅₀ value at 37°C was less than one-fifth that at 27°C (Figure 2B). In contrast, the dose-response survival curve of *C. neoformans* did not differ between 27°C and 37°C (Figure 2A). These results suggest that *C. albicans* and *C. glabrata* have increased killing ability against crickets at 37°C compared to 27°C.

3.3. Comparison of fungal growth between 27°C and 37°C

We hypothesized that one reason for the increased virulence of *C. albicans* and *C. glabrata* at a high temperature is an increased growth rate at high temperature. To address this point, we measured the growth curves of *C. albicans*, *C. glabrata*, and *C. neoformans* at 27°C and 37°C, and determined the doubling times. All fungal strains showed logarithmic growth from 2 h to 6 h after inoculation (Figure 3). The

doubling times of *C. albicans* and *C. glabrata* were shorter at 37°C than at 27°C (Table 2). In contrast, the doubling time of *C. neoformans* was not shorter at 37°C than at 27°C (Table 2). These results suggest that the growth rates of *C. albicans* and *C. glabrata* increase at 37°C compared to at 27°C.

3.4. Killing activity of heat-killed fungal cells against crickets

To address whether the cricket killing ability by fungi is caused by live fungal cells, we examined the killing activities of heat-killed fungal cells against crickets. *C. albicans*, *C. glabrata*, and *C. neoformans* cells were autoclaved and injected into crickets. In all fungal species, the dose-response survival curve was different between the live fungal cells and the heat-killed fungal cells (Figure 4A). The LD₅₀ value of heat-killed fungal cells was higher than 5-fold that of live fungal cells in

each species (Figure 4B). These results suggest that live fungal cells have higher killing activity against crickets than dead fungal cells.

3.5. Killing activities of *C. neoformans* gene-knockout strains against crickets

To determine the applicability of the cricket model for evaluation of fungal virulence factors, we examined whether the *C. neoformans* gene-knockout strains of *cnal*, *gpa1*, and *pkal*, which are virulence factors in mammals, exhibit decreased killing activities against crickets. *cnal* encodes a subunit of calcineurin, a protein phosphatase involved in the signaling pathway (43,44). *gpa1* and *pkal* are involved in capsule formation and melanin synthesis via a calcineurin-independent pathway (45-47). Crickets were injected with the gene-knockout strains and the dose-response survival curve at 37°C was determined. The survival curve differed between the parent strain and the respective gene-knockout strain (Figure 5A). The LD₅₀ values of the *cnal*-, *gpa1*-, and *pkal*-knockout strains were higher than 2-fold that of the parent strains (Figure 5B). These results suggest that the cricket-fungus infection model is effective for evaluating fungal virulence factors.

Table 2. Doubling times of fungal strains

Temperature	<i>C. albicans</i>	<i>C. glabrata</i>	<i>C. neoformans</i>
27°C	1.56 ± 0.09	1.34 ± 0.16	1.80 ± 0.04
37°C	1.05 ± 0.04	0.802 ± 0.020	2.16 ± 0.22
P value	0.0099	0.0259	0.0776

Doubling time (h) was calculated from fungal growth curves at 27°C or 37°C. Data are the means ± standard errors from three independent experiments. Student's *t*-test *p* values between 27°C and 37°C are presented.

4. Discussion

This study revealed that human pathogenic fungi,

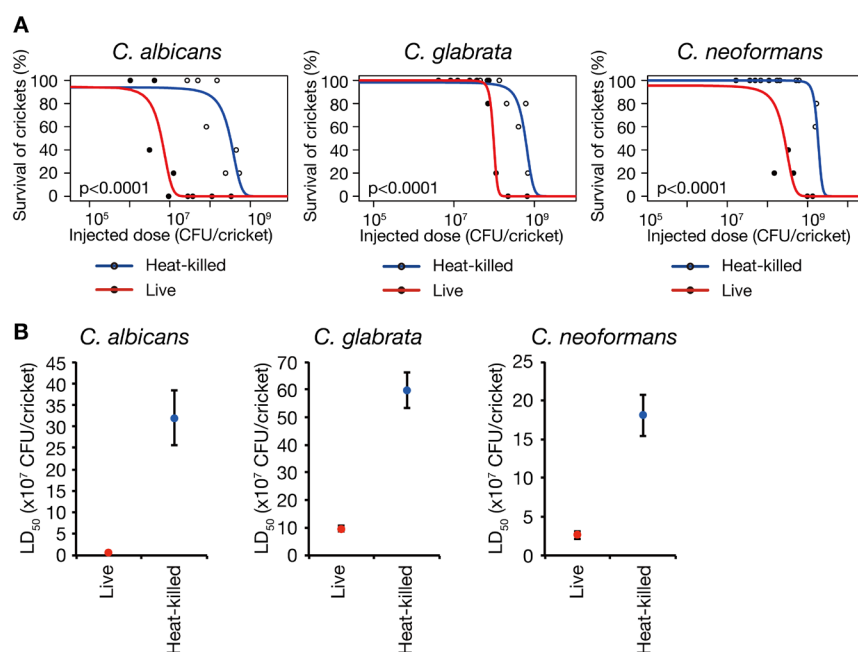


Figure 4. Killing effects of heat-killed fungal cells against crickets. (A) The dose-response survival curve of crickets injected with heat-killed cells of *C. albicans*, *C. glabrata*, or *C. neoformans* was examined at 37°C. Serial dilutions of heat-killed fungal solutions were injected into crickets (*n* = 5/dose) and survival was monitored at 24 h (*C. albicans* and *C. glabrata*) or 48 h (*C. neoformans*) after the injection. Results from three independent experiments were pooled and the survival curve was determined by logistic regression. Results of live fungal cells (closed symbols and red line) are the same as in Figure 2A. The *p*-values determined by using likelihood ratio tests between the survival curves of dead fungal cells and of live fungal cells are presented in the graphs. All survival data are presented in Table S1 (Supporting Information), and no crickets injected with saline died in any of the experiments. (B) The LD₅₀ values of heat-killed fungal cells were determined by logistic regression in (A). The LD₅₀ values of live fungal cells were the same as those in Figure 2B. Error bars indicate standard errors.

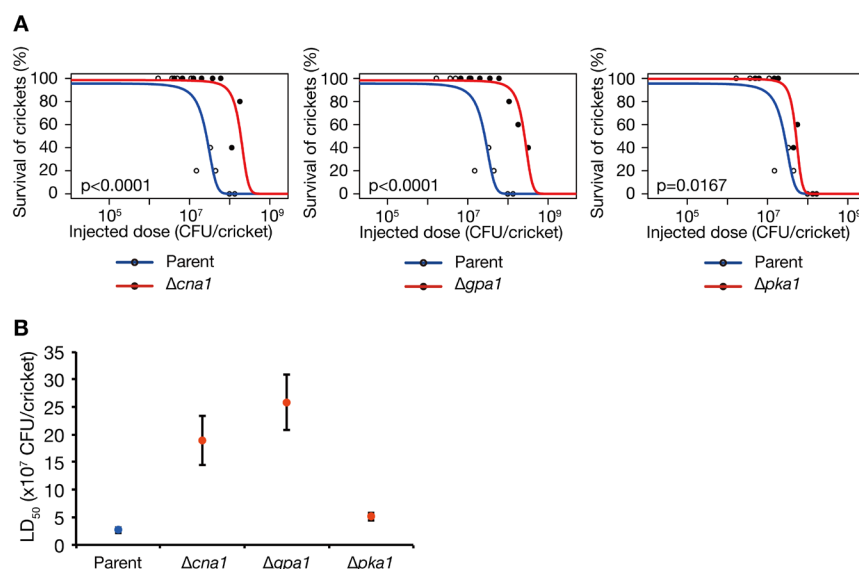


Figure 5. Evaluation of *C. neoformans* virulence factors in the cricket infection model. (A) The dose-response survival curves of crickets ($n = 5/\text{dose}$) injected with *C. neoformans* gene knockout strains of *cna1*, *gpa1*, and *pka1* were determined at 37°C. Survival was monitored at 48 h after fungal injection. Results from two independent experiments were pooled and the survival curve was determined by logistic regression. All survival data are presented in Table S1 (Supporting Information) and no crickets injected with saline died in any of the experiments. The p -values determined using likelihood ratio tests between the parent strain and the gene-knockout strain are presented in the graphs. The survival curve of crickets infected with the parent strain of *C. neoformans* was the same as in Figure 2A (*C. neoformans*, 37°C). **(B)** The LD₅₀ values of *C. neoformans* gene knockout strains of *cna1*, *gpa1*, and *pka1* were determined by logistic regression in (A) and compared with the parent strain. The LD₅₀ value of the parent strain was the same as that in Figure 2B (*C. neoformans*, 37°C). Error bars indicate standard errors.

including *C. albicans*, *C. glabrata*, and *C. neoformans*, kill the two-spotted cricket. The killing activity of the fungi was drastically decreased by heat inactivation of the fungal cells, indicating that live fungal cells contribute to kill crickets. Furthermore, we evaluated fungal virulence against crickets at both 27°C and 37°C, and revealed that the killing activities of *C. albicans* and *C. glabrata* were increased at 37°C compared to that at 27°C, but the killing activity of *C. neoformans* was not different between the two temperatures. This study also demonstrated that the *C. neoformans* gene-knockout strains of virulence factors attenuated the killing activities against crickets. Based on these results, we propose that the two-spotted cricket is a useful animal infection model of human pathogenic fungi, and is effective for clarifying the temperature-dependent virulence system of fungal pathogens.

To our knowledge, this study is the first to reveal that *C. albicans* and *C. glabrata* exhibit a temperature-dependent increase in killing activity against animals. This finding was obtained because we utilized the two-spotted cricket, a heterothermic animal, which can grow at both 27°C and 37°C. We found that the growth rate of these two fungi increases at 37°C, compared to that at 27°C, and assumed it to be a possible reason for the increased killing activities at 37°C. In addition to the growth rate, increasing the temperature leads to many physiologic alterations of fungi. *C. albicans* forms hyphae at high temperature, and a gene-knockout strain that is unable to form hyphae exhibits attenuated virulence

(48,49). *C. glabrata* alters cell surface polysaccharides and shows different cell surface hydrophobicity at 37°C compared to that at a lower temperature (50,51). *C. neoformans* upregulates nucleotide metabolism and capsule formation at a high temperature, enabling growth at a high temperature (52,53). Because *C. neoformans* did not exhibit increased killing activity against crickets at 37°C, the physiologic alteration that is present in the two *Candida* species but is absent in *C. neoformans* may contribute to the temperature-dependent killing activity against crickets. These points should be investigated in future studies by evaluating the virulence properties of fungal genetic mutants for each physiologic process in the cricket infection model to clarify the temperature-dependent virulence system of these fungi.

Heat-killed fungal cells showed killing activity against crickets, although the killing activity of the heat-killed fungal cells was drastically lower than that of live fungal cells. It is plausible that live fungal cells proliferate in the cricket body and the proliferated fungal cells kill crickets in the same manner as the heat-killed cells. In silkworms, β -glucan, a component of the fungal cell wall, excessively activates the humoral immune system, which kills silkworms (54,55). To optimize the utility of the two-spotted cricket as an animal infection model of human pathogenic fungi, further studies are needed to investigate the immune response of crickets against fungal cells and to reveal the molecular mechanism underlying infection-induced death in crickets.

Acknowledgements

This work was supported by Grants-in-Aid for Scientific Research [grant number 16K15274].

References

- Cassone A, Cauda R. Candida and candidiasis in HIV-infected patients: Where commensalism, opportunistic behavior and frank pathogenicity lose their borders. *AIDS*. 2012; 26:1457-1472.
- Silva S, Negri M, Henriques M, Oliveira R, Williams DW, Azeredo J. *Candida glabrata*, *Candida parapsilosis* and *Candida tropicalis*: Biology, epidemiology, pathogenicity and antifungal resistance. *FEMS Microbiol Rev*. 2012; 36:288-305.
- Ramirez-Garcia A, Rementeria A, Aguirre-Urizar JM, Moragues MD, Antoran A, Pellon A, Abad-Diaz-de-Cerio A, Hernando FL. *Candida albicans* and cancer: Can this yeast induce cancer development or progression? *Crit Rev Microbiol*. 2016; 42:181-193.
- Wingard JR. Infections due to resistant *Candida* species in patients with cancer who are receiving chemotherapy. *Clin Infect Dis*. 1994; 19 (Suppl 1):S49-53.
- Shapiro RS, Cowen LE. Thermal control of microbial development and virulence: Molecular mechanisms of microbial temperature sensing. *MBio*. 2012; 3. pii: e00238-12.
- Leach MD, Farrer RA, Tan K, Miao Z, Walker LA, Cuomo CA, Wheeler RT, Brown AJ, Wong KH, Cowen LE. Hsf1 and Hsp90 orchestrate temperature-dependent global transcriptional remodelling and chromatin architecture in *Candida albicans*. *Nat Commun*. 2016; 7:11704.
- Shapiro RS, Uppuluri P, Zaas AK, Collins C, Senn H, Perfect JR, Heitman J, Cowen LE. Hsp90 orchestrates temperature-dependent *Candida albicans* morphogenesis via Ras1-PKA signaling. *Curr Biol*. 2009; 19:621-629.
- De Cremer K, Delattin N, De Brucker K, Peeters A, Kucharikova S, Gerits E, Verstraeten N, Michiels J, Van Dijck P, Cammue BP, Thevissen K. Oral administration of the broad-spectrum antibiofilm compound toremifene inhibits *Candida albicans* and *Staphylococcus aureus* biofilm formation *in vivo*. *Antimicrob Agents Chemother*. 2014; 58:7606-7610.
- Murdock BJ, Teitz-Tennenbaum S, Chen GH, Dils AJ, Malachowski AN, Curtis JL, Olszewski MA, Osterholzer JJ. Early or late IL-10 blockade enhances Th1 and Th17 effector responses and promotes fungal clearance in mice with cryptococcal lung infection. *J Immunol*. 2014; 193:4107-4116.
- Maekawa T, Ishijima AS, Ida M, Izumo T, Ono Y, Shibata H, Abe S. Prophylactic effect of *Lactobacillus pentosus* strain S-PT84 on *Candida* infection and gastric inflammation in a murine gastrointestinal candidiasis model. *Med Mycol J*. 2016; 57:E81-E92.
- Altmeier S, Toska A, Sparber F, Teijeira A, Halin C, LeibundGut-Landmann S. IL-1 coordinates the neutrophil response to *C. albicans* in the oral mucosa. *PLoS Pathog*. 2016; 12:e1005882.
- Stock SJ, Patey O, Thilaganathan B, White S, Furfaro LL, Payne MS, Spiller OB, Noe A, Watts R, Carter S, Ireland DJ, Jobe AH, Newnham JP, Kemp MW. Intrauterine *Candida albicans* infection causes systemic fetal candidiasis with progressive cardiac dysfunction in a sheep model of early pregnancy. *Reprod Sci*. 2016. pii: 1933719116649697.
- Nash EE, Peters BM, Lilly EA, Noverr MC, Fidel PL, Jr. A murine model of *Candida glabrata* vaginitis shows no evidence of an inflammatory immunopathogenic response. *PLoS One*. 2016; 11:e0147969.
- Baumans V. Use of animals in experimental research: An ethical dilemma? *Gene Ther*. 2004; 11 (Suppl 1):S64-66.
- Kaito C, Yoshikai H, Sekimizu K. Utilization of a silkworm model for understanding host-pathogen interactions. *Invert Surviv J*. 2012; 9:163-168.
- Tenor JL, Oehlers SH, Yang JL, Tobin DM, Perfect JR. Live Imaging of host-parasite interactions in a zebrafish infection model reveals cryptococcal determinants of virulence and central nervous system invasion. *MBio*. 2015; 6:e01425-01415.
- Mylonakis E, Ausubel FM, Perfect JR, Heitman J, Calderwood SB. Killing of *Caenorhabditis elegans* by *Cryptococcus neoformans* as a model of yeast pathogenesis. *Proc Natl Acad Sci U S A*. 2002; 99:15675-15680.
- Glittenberg MT, Silas S, MacCallum DM, Gow NA, Ligoxygakis P. Wild-type *Drosophila melanogaster* as an alternative model system for investigating the pathogenicity of *Candida albicans*. *Dis Model Mech*. 2011; 4:504-514.
- Matsumoto Y, Miyazaki S, Fukunaga DH, Shimizu K, Kawamoto S, Sekimizu K. Quantitative evaluation of cryptococcal pathogenesis and antifungal drugs using a silkworm infection model with *Cryptococcus neoformans*. *J Appl Microbiol*. 2012; 112:138-146.
- Hamamoto H, Kurokawa K, Kaito C, Kamura K, Manitra Razanajatovo I, Kusuhara H, Santa T, Sekimizu K. Quantitative evaluation of the therapeutic effects of antibiotics using silkworms infected with human pathogenic microorganisms. *Antimicrob Agents Chemother*. 2004; 48:774-779.
- Trevijano-Contador N, Herrero-Fernandez I, Garcia-Barbazan I, Scorzoni L, Rueda C, Rossi SA, Garcia-Rodas R, Zaragoza O. *Cryptococcus neoformans* induces antimicrobial responses and behaves as a facultative intracellular pathogen in the non mammalian model *Galleria mellonella*. *Virulence*. 2015; 6:66-74.
- Frenkel M, Mandelblat M, Alastruey-Izquierdo A, Mendlovic S, Semis R, Segal E. Pathogenicity of *Candida albicans* isolates from bloodstream and mucosal candidiasis assessed in mice and *Galleria mellonella*. *J Mycol Med*. 2016; 26:1-8.
- Brudal E, Ulanova LS, E OL, Rishovd AL, Griffiths G, Winther-Larsen HC. Establishment of three *Francisella* infections in zebrafish embryos at different temperatures. *Infect Immun*. 2014; 82:2180-2194.
- Mallick EM, Bergeron AC, Jones SK, Jr., Newman ZR, Brothers KM, Creton R, Wheeler RT, Bennett RJ. Phenotypic plasticity regulates *Candida albicans* interactions and virulence in the vertebrate host. *Front Microbiol*. 2016; 7:780.
- Miyashita A, Iyoda S, Ishii K, Hamamoto H, Sekimizu K, Kaito C. Lipopolysaccharide O-antigen of enterohemorrhagic *Escherichia coli* O157:H7 is required for killing both insects and mammals. *FEMS Microbiol Lett*. 2012; 333:59-68.
- Kaito C, Usui K, Kyuma T, Sekimizu K. Isolation of mammalian pathogenic bacteria using silkworms. *Drug*

- Discov Ther. 2011; 5:66-70.
27. Thomaz L, Garcia-Rodas R, Guimaraes AJ, Taborda CP, Zaragoza O, Nosanchuk JD. *Galleria mellonella* as a model host to study *Paracoccidioides lutzii* and *Histoplasma capsulatum*. *Virulence*. 2013; 4:139-146.
 28. Garcia-Solache MA, Izquierdo-Garcia D, Smith C, Bergman A, Casadevall A. Fungal virulence in a lepidopteran model is an emergent property with deterministic features. *MBio*. 2013; 4:e00100-00113.
 29. Mylonakis E, Moreno R, El Khoury JB, Idnurm A, Heitman J, Calderwood SB, Ausubel FM, Diener A. *Galleria mellonella* as a model system to study *Cryptococcus neoformans* pathogenesis. *Infect Immun*. 2005; 73:3842-3850.
 30. Desbois AP, Coote PJ. Wax moth larva (*Galleria mellonella*): An *in vivo* model for assessing the efficacy of antistaphylococcal agents. *J Antimicrob Chemother*. 2011; 66:1785-1790.
 31. Peleg AY, Jara S, Monga D, Eliopoulos GM, Moellering RC, Jr., Mylonakis E. *Galleria mellonella* as a model system to study *Acinetobacter baumannii* pathogenesis and therapeutics. *Antimicrob Agents Chemother*. 2009; 53:2605-2609.
 32. Kiuchi T, Aoki F, Nagata M. Effects of high temperature on the hemocyte cell cycle in silkworm larvae. *J Insect Physiol*. 2008; 54:454-461.
 33. Eguchi D, Iwabuchi K. A new cell line from the wax moth *Galleria mellonella* Linne (Lepidoptera: Pyralidae). *In Vitro Cell Dev Biol Anim*. 2006; 42:1-3.
 34. Browne N, Surlis C, Kavanagh K. Thermal and physical stresses induce a short-term immune priming effect in *Galleria mellonella* larvae. *J Insect Physiol*. 2014; 63:21-26.
 35. Rivnay E, Ziv M. A contribution to the biology of *Gryllus bimaculatus* Deg. in Israel. *Bull Entomol Res*. 1963; 54:37-47.
 36. Merkel G. The effects of temperature and food quality on the larval development of *Gryllus bimaculatus* (Orthoptera, Gryllidae). *Oecologia*. 1977; 30:129-140.
 37. Kochi Y, Miyashita A, Tsuchiya K, Mitsuyama M, Sekimizu K, Kaito C. A human pathogenic bacterial infection model using the two-spotted cricket, *Gryllus bimaculatus*. *FEMS Microbiol Lett*. 2016; 363. pii: fnw163.
 38. Miyashita A, Kizaki H, Sekimizu K, Kaito C. Body-enlarging effect of royal jelly in a non-holometabolous insect species, *Gryllus bimaculatus*. *Biol Open*. 2016; 5:770-776.
 39. Miyashita A, Kizaki H, Sekimizu K, Kaito C. No effect of body size on the frequency of calling and courtship song in the two-spotted cricket, *Gryllus bimaculatus*. *PLoS One*. 2016; 11:e0146999.
 40. Kyuma T, Kizaki H, Ryuno H, Sekimizu K, Kaito C. 16S rRNA methyltransferase KsgA contributes to oxidative stress resistance and virulence in *Staphylococcus aureus*. *Biochimie*. 2015; 119:166-174.
 41. Kyuma T, Kimura S, Hanada Y, Suzuki T, Sekimizu K, Kaito C. Ribosomal RNA methyltransferases contribute to *Staphylococcus aureus* virulence. *FEBS J*. 2015; 282:2570-2584.
 42. Team RDC R: A language and environment for statistical computing. R Foundation for Statistical Computing. 2011.
 43. Odom A, Muir S, Lim E, Toffaletti DL, Perfect J, Heitman J. Calcineurin is required for virulence of *Cryptococcus neoformans*. *EMBO J*. 1997; 16:2576-2589.
 44. Steinbach WJ, Reedy JL, Cramer RA, Jr., Perfect JR, Heitman J. Harnessing calcineurin as a novel anti-infective agent against invasive fungal infections. *Nat Rev Microbiol*. 2007; 5:418-430.
 45. Alspaugh JA, Perfect JR, Heitman J. *Cryptococcus neoformans* mating and virulence are regulated by the G-protein alpha subunit GPA1 and cAMP. *Genes Dev*. 1997; 11:3206-3217.
 46. Kozubowski L, Lee SC, Heitman J. Signalling pathways in the pathogenesis of *Cryptococcus*. *Cell Microbiol*. 2009; 11:370-380.
 47. D'Souza CA, Alspaugh JA, Yue C, Harashima T, Cox GM, Perfect JR, Heitman J. Cyclic AMP-dependent protein kinase controls virulence of the fungal pathogen *Cryptococcus neoformans*. *Mol Cell Biol*. 2001; 21:3179-3191.
 48. Shapiro RS, Cowen L. Coupling temperature sensing and development: Hsp90 regulates morphogenetic signalling in *Candida albicans*. *Virulence*. 2010; 1:45-48.
 49. Hwang CS, Oh JH, Huh WK, Yim HS, Kang SO. Ssn6, an important factor of morphological conversion and virulence in *Candida albicans*. *Mol Microbiol*. 2003; 47:1029-1043.
 50. Okawa Y, Goto K. Disappearance of antigenic factor 6 in *Candida glabrata* IFO 0622 strain cells cultured at high temperature. *Biol Pharm Bull*. 2006; 29:187-189.
 51. Luo G, Samaranayake LP. *Candida glabrata*, an emerging fungal pathogen, exhibits superior relative cell surface hydrophobicity and adhesion to denture acrylic surfaces compared with *Candida albicans*. *APMIS*. 2002; 110:601-610.
 52. de Gontijo FA, Pascon RC, Fernandes L, Machado J, Jr., Alspaugh JA, Vallim MA. The role of the de novo pyrimidine biosynthetic pathway in *Cryptococcus neoformans* high temperature growth and virulence. *Fungal Genet Biol*. 2014; 70:12-23.
 53. Yang DH, Jung KW, Bang S, Lee JW, Song MH, Floyd-Averette A, Festa RA, Ianiri G, Idnurm A, Thiele DJ, Heitman J, Bahn YS. Rewiring of signaling networks modulating thermotolerance in the human pathogen *Cryptococcus neoformans*. *Genetics*. 2017; 205:201-219.
 54. Ishii K, Hamamoto H, Kamimura M, Sekimizu K. Activation of the silkworm cytokine by bacterial and fungal cell wall components via a reactive oxygen species-triggered mechanism. *J Biol Chem*. 2008; 283:2185-2191.
 55. Ishii K, Hamamoto H, Imamura K, Adachi T, Shoji M, Nakayama K, Sekimizu K. *Porphyromonas gingivalis* peptidoglycans induce excessive activation of the innate immune system in silkworm larvae. *J Biol Chem*. 2010; 285:33338-33347.
 56. Lingappa BT, Prasad M, Lingappa Y, Hunt DF, Biemann K. Phenethyl alcohol and tryptophol: Autoantibiotics produced by the fungus *Candida albicans*. *Science*. 1969; 163:192-194.
 57. Dujon B. Yeasts illustrate the molecular mechanisms of eukaryotic genome evolution. *Trends Genet*. 2006; 22:375-387.
 58. Toffaletti DL, Rude TH, Johnston SA, Durack DT, Perfect JR. Gene transfer in *Cryptococcus neoformans* by use of biolistic delivery of DNA. *J Bacteriol*. 1993; 175:1405-1411.

(Received October 5, 2017; Revised October 16, 2017; Accepted October 21, 2017)

Isolation of antibiotic-producing *Pseudomonas* species with low-temperature cultivation of temperate soil

Shuhei Mitsutomi¹, Kazuhisa Sekimizu², Chikara Kaito^{1,*}

¹Laboratory of Microbiology, Graduate School of Pharmaceutical Sciences, The University of Tokyo, Tokyo, Japan;

²Institute of Medical Mycology, Teikyo University, Tokyo, Japan.

Summary

We performed low-temperature cultivation of soil samples in Tokyo, Japan, and isolated 30 bacterial strains that formed colonies at 4°C. All the culture supernatants of these bacteria exhibited antibacterial activity against *Escherichia coli*. The 16S rDNA sequences of 29 strains showed similarity to that of the *Pseudomonas* genus, whereas the 16S rDNA sequence of one strain showed similarity to that of the *Janthinobacterium* genus. We classified the 29 strains into 10 groups according to the 16S rDNA sequence similarities, and performed two phylogenetic analyses using the 16S rDNA and *rpoD* gene sequences. Four groups formed a unique branch within *Pseudomonas* species in both phylogenetic analyses. Four other groups were closely related to the *Pseudomonas* species, but the most closely related species differed between the two phylogenetic tree analyses. These results suggest that low-temperature cultivation of temperate soil is effective for isolating new bacterial sources for producing antibiotics.

Keywords: Low-temperature cultivation, *Pseudomonas* species, phylogenetic analyses, soil bacteria

1. Introduction

Many antibiotics have been identified from bacterial culture supernatants. Unfortunately, however, the discovery rates of novel antibiotics from bacterial sources have been steadily decreasing over the years (1). Thus, new sources are needed for the development of novel antibiotics.

An estimated 99% of all bacterial species on earth are uncultured (2). These uncultured bacteria are expected to produce secondary metabolites distinct from those of known bacteria and are promising sources of new antibiotics (3). Thus, many methods have been investigated for culturing these bacteria or for isolating new genetic sources without culturing bacteria. A recent study identified a novel antibiotic from uncultured bacteria that is effective against drug-resistant bacteria (4).

Low temperature cultivation is a useful method of

culturing bacteria from cold areas, because bacteria in cold areas can grow at low temperature. Such psychrophilic microorganisms have been targeted as new biologic resources for antibiotics, protein expression systems, or environmental pollution control (5,6). In contrast, bacteria in temperate regions are normally cultivated at 20-30°C, because many bacteria in these regions have optimal temperature growth at this range. The temperature of temperate soil falls to around 0°C in the winter with a year-round mean temperature below 20°C. In the present study, we performed low temperature cultivation of temperate soil bacteria to search for new bacterial sources for novel antibiotics.

2. Materials and Methods

2.1. Isolation of environmental strains

Soil samples were collected from the ground at the University of Tokyo (35° 71' 20.56" N 139° 76' 2775" E) in February 2016 and March 2016. Approximately 5 g of soil was suspended in 50 mL of sterilized saline. One hundred microliters of the suspended solution was spread on a Luria-Bertani (LB) plate and incubated at 4°C for 7 to 10 days.

Released online in J-STAGE as advance publication October 29, 2017.

*Address correspondence to:

Dr. Chikara Kaito, Laboratory of Microbiology, Graduate School of Pharmaceutical Sciences, The University of Tokyo, 3-1, 7-chome, Hongo, Bunkyo-ku, Tokyo 113-0033, Japan.

E-mail: kaito@mol.f.u-tokyo.ac.jp

2.2. Bacteria or fungi

Escherichia coli JM109 was cultured in LB medium at 37°C, *Staphylococcus aureus* RN4220 was cultured in tryptic soy broth medium at 37°C, and *Candida albicans* ATCC10231 was cultured in YPD medium at 37°C.

2.3. Assay of antimicrobial activities of the supernatants of the isolates

The isolates were cultured for 1 week at 4°C on a rotary shaker at 150 rpm. The cultures were centrifuged at 20,400g for 5 min and the supernatants were filtered with 0.44-µm filters and stored at 4°C until the assay was performed. Overnight cultures of the microbes (*Escherichia coli* JM109, *Staphylococcus aureus* RN4220, and *Candida albicans* ATCC10231) were diluted 100-fold with Muller-Hinton broth. A 100-µL aliquot of the supernatant was serially diluted, mixed with 100 µL of the microbial solution in 96-well round bottom plates, and then incubated at 37°C overnight. The microbial growth in each well was observed by visual inspection. The maximum dilution that inhibited microbial growth was defined as the growth inhibitory activity.

2.4. Extraction of genomic DNA

Genomic DNA (gDNA) of the bacteria was extracted as described previously (7) with minor modification. Bacterial cells were collected from 2 mL liquid culture by centrifugation at 20,400g for 5 min. The bacteria were lysed in 200 µL extraction buffer (0.05 M Tris-HCl [pH 8.0], 0.05 M NaCl, 0.05 M EDTA, 0.5% sodium dodecyl sulfate), 25 mg acid-washed glass beads, and 200 µL PCI (phenol: chloroform: isoamyl alcohol = 25:24:1, v/v) by vortex for 5 min. Four hundred microliters of TE buffer (0.01 M Tris-HCl, 1 mM EDTA, pH8.0) and 200 µL of PCI was added to the sample, and the sample was centrifuged at 20,400g for 5 min. Forty microliters of 3 M sodium acetate (pH 7.0) and 400 µL of 2-propanol were added to the centrifuged supernatant (400 µL). After incubating at room temperature for 5 min, the samples were centrifuged at 20,400g for 10 min. The precipitate was washed with 70% ethanol and solved in 50 µL TE. The gDNA solutions were preserved at 4°C.

2.5. 16s rRNA gene phylogeny reconstruction

The 16s rRNA genes of isolates were amplified by polymerase chain reaction (PCR) from the extracted gDNA with four universal primers: E9F, E939R, E334F, and E1541R (8). After analysis of the products by electrophoresis on 1% agarose gels, the amplified PCR products were purified by phenol-chloroform extraction and ethanol precipitation. The purified PCR products were sequenced with an ABI PRISM 3730

Genetic Analyzer (Applied Biosystems) following the manufacturer's instructions. The sequences were compared with those of the type strains of bacterial species recorded in the EzTaxon database (9). The sequences of the isolates were aligned with the sequences of similar strains of the genus *Pseudomonas* using the ClustalW software (10). Based on the 16s rRNA gene sequences, phylogenetic trees were reconstructed using the maximum-likelihood (11) and neighbor-joining (12) methods with the MEGA7 package (13). The 16s rRNA gene sequences of the bacterial isolates in this study were registered in Genbank (LC230063-LC230092).

2.6. rpoD gene phylogeny reconstruction

The *rpoD* genes of isolates were amplified by PCR from gDNA extracted with two primers, PsEG30F and PsEG790R (14). The amplified *rpoD* gene was sequenced as described above. The obtained *rpoD* sequences were compared with those from the GenBank database in BLAST (15). The phylogenetic trees were constructed using the *rpoD* sequences that showed high similarity in the BLAST search, as described above. The *rpoD* sequences of the bacterial isolates in this study were registered in Genbank (LC230053-LC230062).

2.7. Growth assay at different temperatures

The isolates were cultured overnight at 17°C in LB medium. A 150-µL aliquot of the overnight cultures was inoculated into 5 mL of fresh LB broth. The cultures were incubated at four different temperatures (4, 17, 30, 37°C) on a rotary shaker at 150 rpm. The optical densities at 600 nm (OD₆₀₀) were measured at four time-points (0, 3, 6, and 24 h). The experiment was repeated three times. The OD₆₀₀ values at each time-point were averaged and plotted with the standard errors of the mean.

3. Results

Five grams of soil samples were obtained in Tokyo, Japan, which is a temperate region. The samples were suspended in sterilized saline, spread on Luria-Bertani agar plates, and cultured at 4°C for 7 to 10 days. Thirty microbial strains that formed colonies were isolated.

To investigate whether the 30 isolated strains are potential sources of antibiotics, we examined the antimicrobial activities of the culture supernatants of these strains. All supernatants of the isolated strains inhibited the growth of *E. coli* (Table 1). A supernatant of one strain (P-11) weakly inhibited the growth of *S. aureus*, but the supernatants of the others did not inhibit *S. aureus* growth (Table 1). None of the supernatants inhibited the growth of *C. albicans* (Table 1). These

Table 1. Antimicrobial activities of the culture supernatants of the 30 isolated strains

Strain ¹	Growth inhibitory activity ²		
	<i>E. coli</i>	<i>S. aureus</i>	<i>C. albicans</i>
P-1	2	ND	ND
P-2	2	ND	ND
P-3	2	ND	ND
P-4	2	ND	ND
P-5	2	ND	ND
P-6	2	ND	ND
P-7	4	ND	ND
P-8	4	ND	ND
P-9	4	ND	ND
P-10	4	ND	ND
P-11	16	2	ND
P-12	4	ND	ND
P-13	8	ND	ND
P-14	2	ND	ND
P-15	2	ND	ND
P-16	2	ND	ND
P-17	2	ND	ND
P-18	2	ND	ND
P-19	2	ND	ND
P-20	2	ND	ND
P-21	2	ND	ND
P-22	16	ND	ND
P-23	16	ND	ND
P-24	32	ND	ND
P-25	2	ND	ND
P-26	2	ND	ND
P-27	4	ND	ND
P-28	4	ND	ND
P-29	2	ND	ND
P-30	2	ND	ND

¹"Strain" indicates the ID of the isolated strains. ²"growth inhibitory activity" indicates the growth inhibitory activities of the supernatants of the isolates against microbes (*E. coli*, *S. aureus*, and *C. albicans*). The growth inhibitory activity was defined as the maximum dilution of the supernatants that inhibited the growth of the pathogens. ND means that the two-fold diluted culture supernatants did not inhibit microbial growth.

results suggest that all of the isolated strains secrete antimicrobial substances against *E. coli*.

To investigate the novelty of the isolated microorganisms, we analyzed the taxonomies of the isolates. We performed phylogenetic analyses with the *16s rRNA* gene sequences, which are widely used to classify bacteria (16,17). The full length of each of the *16s rRNA* genes was amplified with PCR and sequenced. Microbial species that have *16s rRNA* gene sequences highly similar to those of the isolated strains were searched using the EzTaxon-e database (9) (Table 2). One strain (P-20) had high similarity to the *Janthinobacterium* genus, and the other 29 strains had high similarity to the *Pseudomonas* genus. According to the closest match species, we classified the 29 strains into 10 groups as follows: *Pseudomonas helmanticensis* (18), *Pseudomonas moorei* (19), *Pseudomonas koreensis* (20), *Pseudomonas mohnii* (19), *Pseudomonas vancouverensis* (21), *Pseudomonas baetica* (22), *Pseudomonas frederiksbergensis* (23), *Pseudomonas congelans* (24), *Pseudomonas mandelii* (25), or *Pseudomonas*

mediterranea (26) (Table 2). We selected 10 strains (P-1, P-7, P-12, P-13, P-14, P-16, P-22, P-23, P-25, and P-26) as representative strains of each group for further phylogenetic analysis (Table 2).

A phylogenetic tree based on the *16S rRNA* sequences was constructed between the *Pseudomonas*-type strains and the 10 representative strains using the maximum likelihood method (11) (Figure 1). P-22, P-23, P-25, and P-26 formed a cluster that is clearly distinct from the *Pseudomonas* genus type strains. P-13 branched off from *P. mohnii* (19) and *P. umsongensis* (20). P-7 and P-14 branched off from a cluster including *P. moorei* (19), *P. vancouverensis* (21), and *P. jessenii* (25). P-1 and P-16, respectively, branched off from a cluster including *P. granadensis* (27) and *P. helmanticensis* (18). P-12 branched off from *P. batumici* (28). A phylogenetic tree constructed by the neighbor-joining method (12) also confirmed the distinct cluster of P-22, P-23, P-25, and P-26 and the branches of P-13, P-14, P-12, and P-1, but not those of P-7 and P-16 (Figure 2).

The *16s rRNA* sequences are widely used in the phylogenetic analyses of bacteria including *Pseudomonads* (16,17,29,30), but phylogenetic analysis based on the *16s rRNA* sequences does not have sufficient resolution to distinguish different species of the *Pseudomonas* genus. Thus, other housekeeping genes, including *gyrB*, *rpoB*, and *rpoD* are used for phylogenetic analyses of *Pseudomonas* species (14,31-37). Because analysis using the *rpoD* gene has the highest resolution (14), we used the *rpoD* gene for additional phylogenetic analyses. The *rpoD* gene was amplified by PCR and sequenced. Microbial species with similar *rpoD* sequences to those of the 10 representative strains were searched in the BLAST database (15). Eight representative strains other than P-7 and P-13 showed similarities lower than 96% to the *rpoD* sequences of known species (Table 3). A phylogenetic tree based on the *rpoD* sequences was constructed between *Pseudomonas*-type strains and the 10 representative strains using the maximum likelihood method (Figure 3). P-7 branched off from *P. umsongensis* and P-13 branched off from *P. jessenii*. P-14 formed a distinct branch with P-7, P-13, *P. umsongensis*, and *P. jessenii*. P-12 and P-16, respectively, branched off from *P. koreensis* and *P. helmanticensis*. P-22, P-23, P-25, and P-26 formed a distinct cluster. P-1 formed a distinct branch from *P. proteolytica*. The phylogenetic tree branches, except those of P-1, P-14, and P-16, were also observed in the phylogenetic tree constructed using the neighbor-joining method (Figure 4). The phylogenetic tree branches of P-1, P-14, and P-16 were slightly different between the maximum likelihood method and the neighbor-joining method, but both methods indicated that P-1 was related to *P. aeruginosa* and *P. proteolytica*, P-14 was related to *P. umsongensis*, *P. putida*, and *P. vancouverensis*, and P-16 was related to *P. marginalis* and *P. helmanticensis*.

Phylogenetic trees based on the *16S rRNA*

Table 2. Closest matched species estimated from 16S rRNA gene sequences

Strain ¹	Closest Match ²	Accession Number ³	Similarity (%) ⁴	Completeness (%) ⁵
P-1*	<i>P. helmanticensis</i>	HG940537	99.4	100
P-2	<i>P. helmanticensis</i>	HG940537	99.4	100
P-3	<i>P. helmanticensis</i>	HG940538	99.6	100
P-4	<i>P. helmanticensis</i>	HG940539	99.4	100
P-5	<i>P. helmanticensis</i>	HG940539	99.6	100
P-6	<i>P. helmanticensis</i>	HG940539	99.6	100
P-15	<i>P. helmanticensis</i>	HG940537	99.7	100
P-7*	<i>P. moorei</i>	AM293566	99.7	100
P-8	<i>P. moorei</i>	AM293565	99.9	100
P-9	<i>P. mohnii</i>	AM293567	100	100
P-10	<i>P. mohnii</i>	AM293567	99.7	100
P-12*	<i>P. koreensis</i>	AF468452	99.6	99.7
P-30	<i>P. koreensis</i>	AF468452	99.7	99.7
P-13*	<i>P. mohnii</i>	AM293567	99.6	100
P-11	<i>P. vancouverensis</i>	AJ011507	99.9	100
P-14*	<i>P. vancouverensis</i>	AJ011507	99.7	100
P-16*	<i>P. baetica</i>	FM201274	99.4	99.1
P-21	<i>P. baetica</i>	FM201274	99.6	99.1
P-20*	<i>J. swalbardensis</i>	DQ355146	99.7	96.8
P-22*	<i>P. frederiksbergensis</i>	AJ249382	98.8	100
P-27	<i>P. frederiksbergensis</i>	AJ249383	98.6	100
P-28	<i>P. frederiksbergensis</i>	AJ249383	98.6	100
P-29	<i>P. frederiksbergensis</i>	AJ249383	98.7	100
P-23*	<i>P. congelans</i>	AJ492828	98.6	100
P-24	<i>P. congelans</i>	AJ492828	98.5	100
P-17	<i>P. mandelii</i>	AF058286	98.7	100
P-18	<i>P. mandelii</i>	AF058286	98.7	100
P-19	<i>P. mandelii</i>	AF058286	98.7	100
P-25*	<i>P. mandelii</i>	AF058286	98.7	100
P-26*	<i>P. mediterranea</i>	AUPB01000004	98.9	100

¹"Strain" indicates the ID of the isolated strains. ²"Closest match" indicates the species with which the 16S rRNA gene sequences of the isolated strain were most similar. ³"Accession Number" indicates the accession number of the sequence of the most similar species in Genbank. ⁴"Similarity" indicates the similarity of the sequences of the isolated strain and the closest matched species. ⁵"Completeness" indicates the ratio of the length of the query sequence to the full-length sequence. 11 groups are segmented by horizontal lines, and asterisks indicate the representative strain in each group.

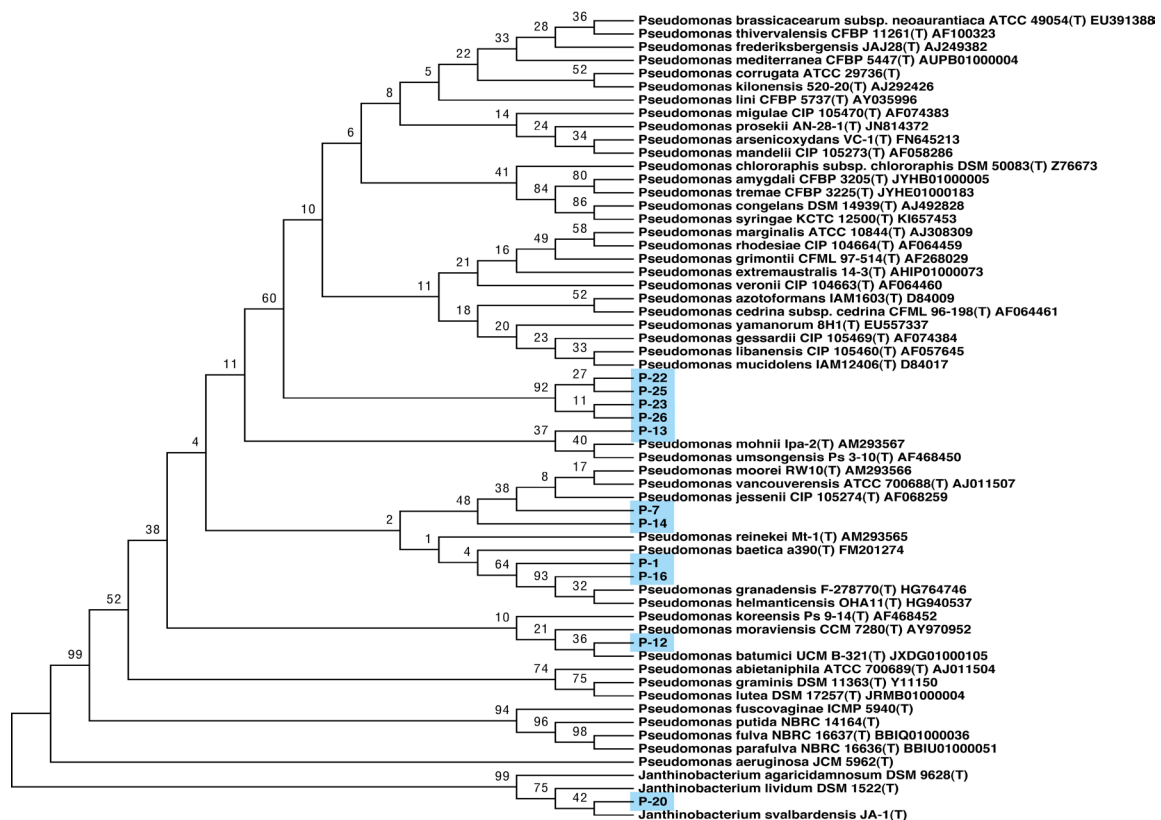


Figure 1. 16S rRNA-based phylogenetic tree by the maximum likelihood method. The evolutionary history was inferred with the maximum likelihood method. The bootstrap values (1,000 replicates) are shown above the branches. Only the topology is shown.

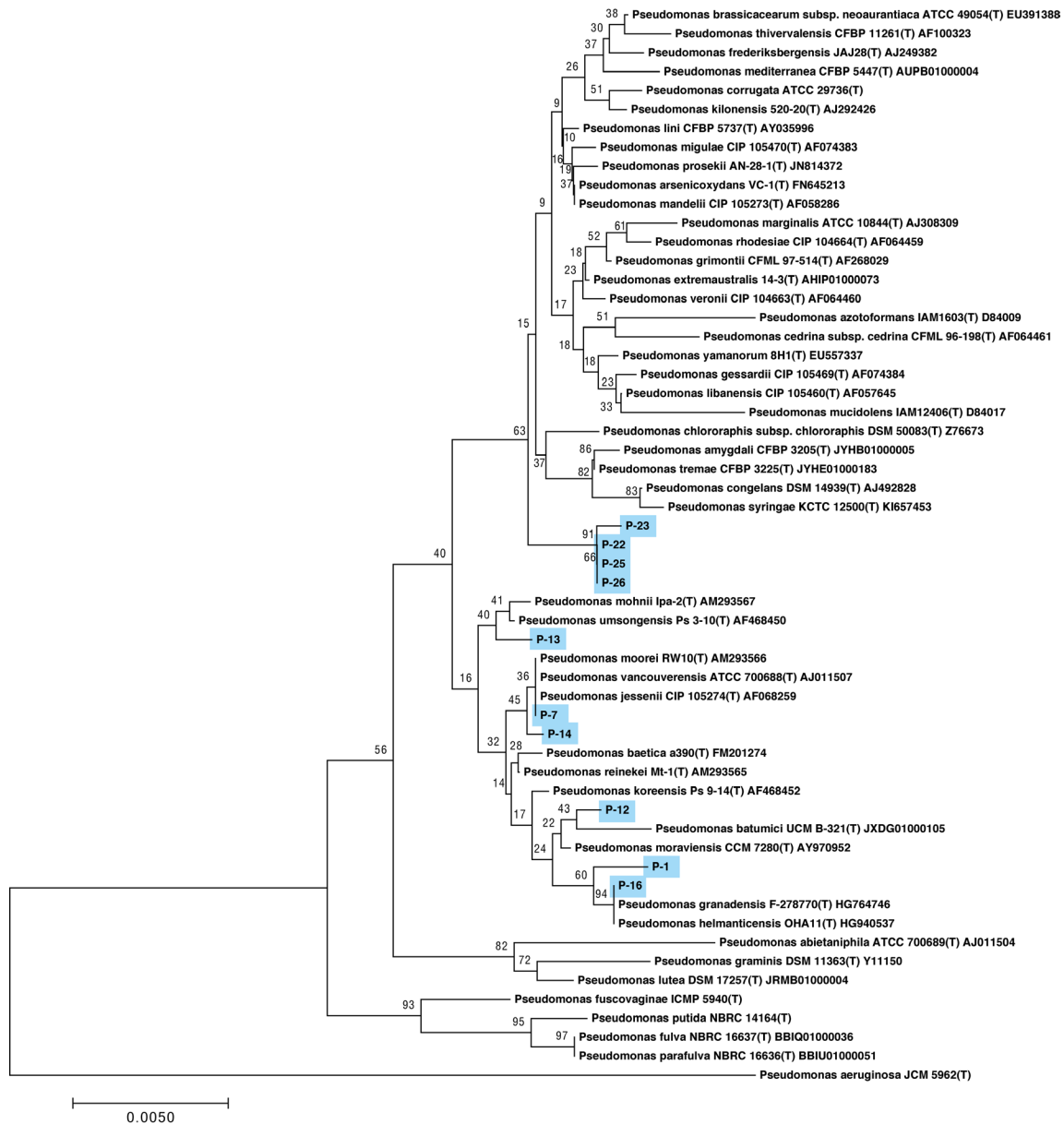


Figure 2. 16S rRNA-based phylogenetic tree by the neighbor-joining method. The evolutionary history was inferred with the neighbor-joining method. The bootstrap values (1,000 replicates) are shown above the branches. The evolutionary distances are in the units of the number of base substitutions per site.

Table 3. Closest matched species estimated from the *rpoD* gene sequences

Strain ¹	Closest Match ²	Accession Number ³	Identity (%) ⁴	Query Cover (%) ⁵
P-1	<i>P. marginalis</i>	AB039544.1	95	100
P-7	<i>P. putida</i>	D86031.1	98	99
P-12	<i>P. fluorescens</i>	CP000094.2	96	99
P-13	<i>P. jessenii</i>	FN678364.1	97	99
P-14	<i>P. reinekei</i>	FN678362.1	94	99
P-16	<i>P. marginalis</i>	AB039544.1	95	100
P-22	<i>P. mandelii</i>	CP005960.1	93	100
P-23	<i>P. mandelii</i>	CP005960.1	93	99
P-25	<i>P. mandelii</i>	CP005960.1	93	100
P-26	<i>P. mandelii</i>	CP005960.1	93	100

¹"Strain" indicates the ID of the isolated strains. ²"Closest Match" indicates bacterial species with the highest similarity to the *rpoD* gene sequences of the isolated strains. ³"Accession Number" indicates the accession numbers of the *rpoD* gene sequences of the closest matched species in Genbank. ⁴"Identity" indicates the similarity of the *rpoD* gene sequences of the isolated strains and closest matched species. ⁵"Query Cover" indicates the ratio of the sequences of the isolated strains aligned to the those of the closest matched species.

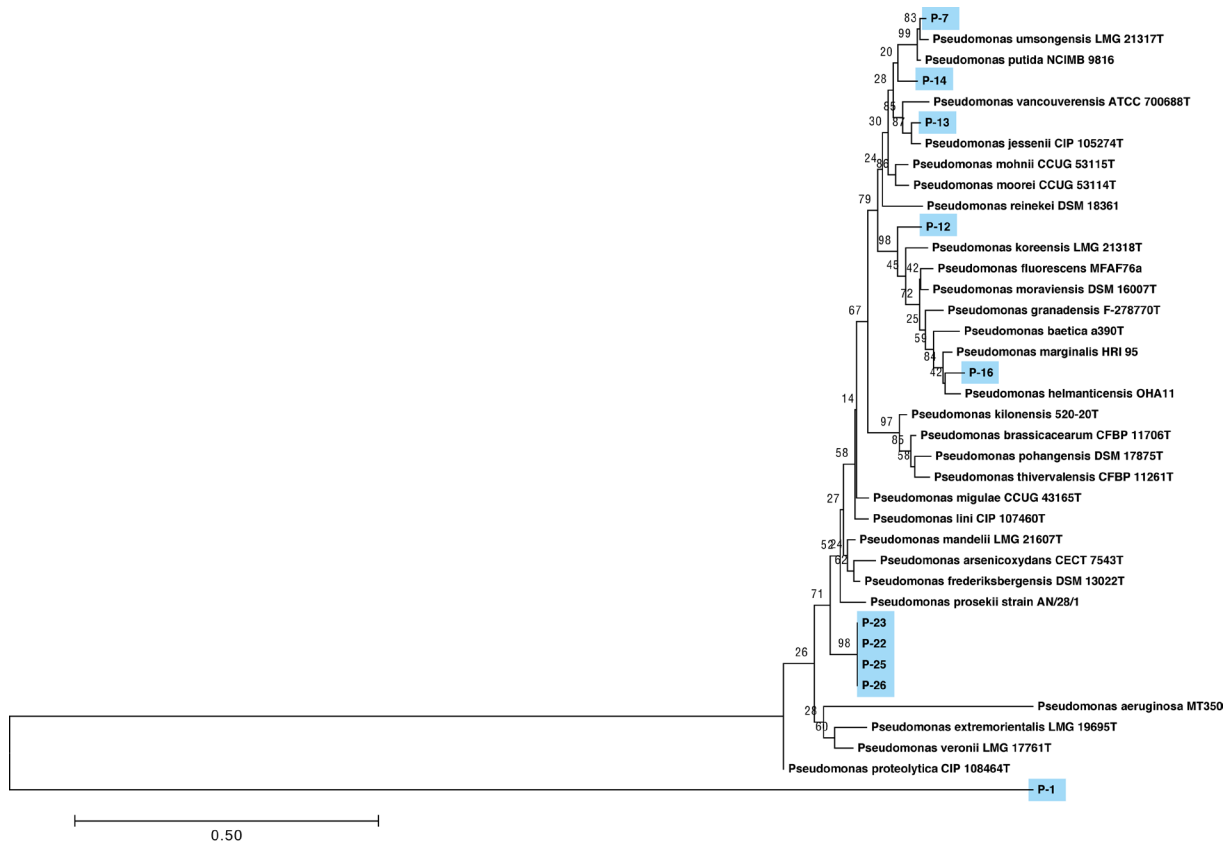


Figure 3. The *rpoD* gene-based phylogenetic tree by the maximum likelihood method. The evolutionary history was inferred with the maximum likelihood method. The bootstrap values (1,000 replicates) are shown above the branches. The branch lengths are measured in the number of substitutions per site.

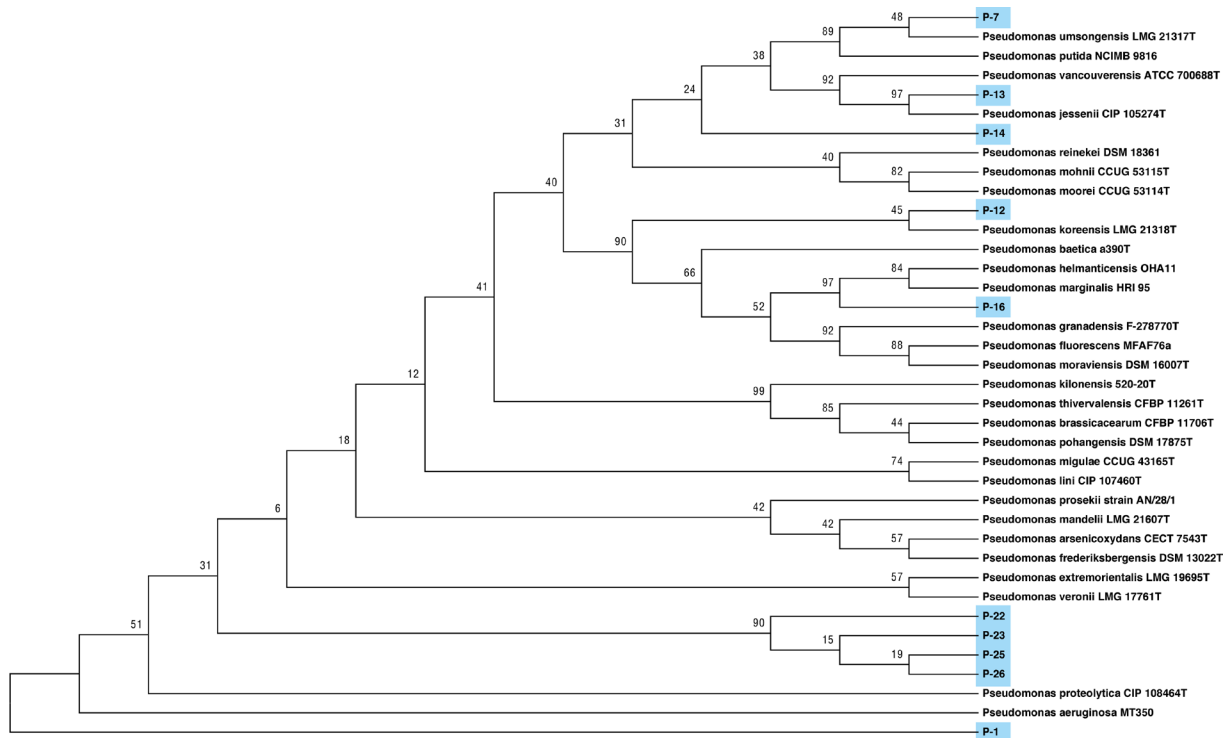


Figure 4. The *rpoD* gene-based phylogenetic tree by the neighbor-joining method. The evolutionary history was inferred with the neighbor-joining method. The bootstrap values (1,000 replicates) are shown above the branches.

Table 4. Comparison of the closest matched species between *16s rRNA*- or *rpoD*-based phylogenies

Strain ¹	Closest Match ²	
	<i>16s rRNA</i>	<i>rpoD</i>
P-1	<i>P. helmanticensis</i> , <i>P. granadensis</i> , P-16	<i>P. aeruginosa</i> , <i>P. proteolytica</i>
P-7	<i>P. moorei</i> , <i>P. vancouverensis</i> , <i>P. jessenii</i>	<i>P. umsongensis</i>
P-12	<i>P. batumici</i>	<i>P. koreensis</i>
P-13	<i>P. mohnii</i> , <i>P. umsongensis</i>	<i>P. jessenii</i>
P-14	<i>P. vancouverensis</i> , <i>P. moorei</i> , <i>P. jessenii</i> , P-7	<i>P. vancouverensis</i> , <i>P. umsongensis</i> , <i>P. putida</i>
P-16	<i>P. helmanticensis</i> , <i>P. granadensis</i>	<i>P. helmanticensis</i> , <i>P. marginalis</i>
P-22	P-23, P-25, P-26	P-23, P-25, P-26

¹"Strain" indicates the ID of the isolated strains. ²"Closest match" indicates the closest match species estimated from the sequences of conserved genes.

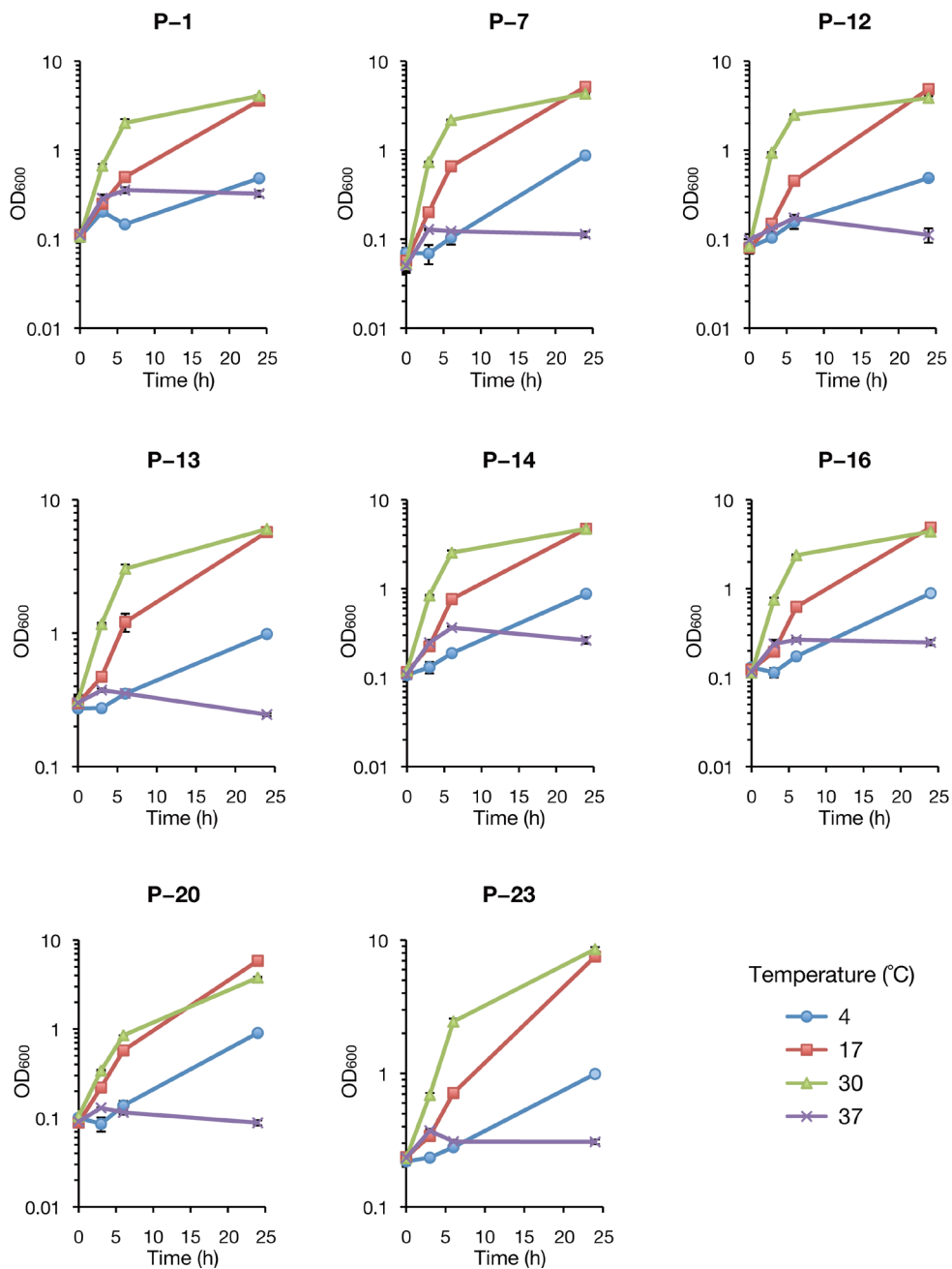


Figure 5. Growth curves of the isolated bacterial strains at different temperatures. The growth curves of the isolated strains were examined at several temperatures (4, 17, 30, or 37°C). The vertical axis represents the optical densities (OD_{600}) and the horizontal axis represents incubation time. The experiment was independently performed three times. Mean values with standard errors of the mean are shown.

sequences and *rpoD* gene sequences estimated the closest matched species of each representative strain (Table 4). Both analyses consistently estimated that P-22, P-23, P-25, and P-26 were related to each other, and formed a cluster distant from *Pseudomonas*-type strains. Also, both analyses estimated that P-14 was related to *P. Vancouverensis*, and P-16 was related to *P. helmanticensis* (Table 4). The closest match species of P-1, P-7, P-12, and P-13, however, were not consistent between the analyses using *16S rRNA* sequences and the *rpoD* sequences.

Psychrophilic bacteria are defined as bacteria that grow optimally at or below 15°C, and psychrotolerant bacteria are defined as bacteria that can grow below 15°C, but have a higher optimal temperature (5). To determine whether the isolated strains were psychrophilic or psychrotolerant bacteria, growth curves of seven representative strains (P-1, P-7, P-12, P-13, P-14, P-16, and P-23), which were related to the *Pseudomonas* genus, and P-20, which was related to the *Janthinobacterium* genus, were measured at several temperatures (4, 17, 30, or 37°C; Figure 5). The optical densities of the culture medium of all strains increased over time at 4, 17, and 30°C. At 37°C, the optical densities increased from 0 to 3 h, but did not increase from 6 to 24 h. The rank order of optical density at 6 h was 30°C > 17°C > 37°C > 4°C. These results suggest that the optimal growth temperature of the isolates was between 17°C and 37°C and these bacteria are psychrotolerant.

4. Discussion

In the present study, we isolated bacteria from temperate soil by culturing at a low temperature and performed phylogenetic analyses of 10 representative isolates using the two housekeeping genes: *16S rRNA* and *rpoD*. Both analyses estimated that four representative isolates (P-22, P-23, P-25, P-26) formed a distinct cluster from *Pseudomonas*-type strains. The two phylogenetic analyses differed with respect to the related species for four other representative isolates (P-1, P-7, P-12, P-13). These results suggest that the bacterial strains isolated in this study are novel *Pseudomonas* species. All of the isolated bacteria exhibited antimicrobial activity against *E. coli*. Thus, we propose that low temperature incubation of temperate soil is an effective method of isolating novel bacterial sources of antibiotics.

In this study, most isolated strains belonged to the genus *Pseudomonas*. The genus *Pseudomonas* comprises 218 species of Gram-negative gamma proteobacteria. Members of the genus *Pseudomonas* are isolated from many environments including land, freshwater, and seawater. Its high stress-resistance capability is one reason for its wide range of habitats. Optimal temperatures of the genus *Pseudomonas* are around 25-30°C, but many of them can grow at low temperature, around 5°C (38). These characteristics are consistent

with those of the *Pseudomonas* strains isolated in this study, which grew at 4°C and had a growth-optimal temperature of around 30°C.

The supernatants of the isolated *Pseudomonas* strains showed antibiotic activities against *E. coli*. The supernatants, except that of P-11, did not inhibit the growth of *S. aureus*, and none of them inhibited the growth of *C. albicans*. Several antimicrobial drugs have been discovered from *Pseudomonads*; two beta-lactams including sulfazecin and isosulfazecin (39) effective against both *S. aureus* and *E. coli*, and many anti-fungal chemicals (40,41). Because the antimicrobial activities of the isolates in this study are more effective against *E. coli* than *S. aureus* and *C. albicans*, the antimicrobial compounds are expected to differ from the known antibiotics obtained from other *Pseudomonas* species.

Acknowledgements

This work was supported by Grants-in-Aid for Scientific Research [grant number 16K15274 and 15H05783].

References

- Lewis K. Antibiotics: Recover the lost art of drug discovery. *Nature*. 2012; 485:439-440.
- Pham VHT, Kim J. Cultivation of unculturable soil bacteria. *Trends Biotechnol*. 2012; 30:475-484.
- Lewis K, Epstein S, D'Onofrio A, Ling LL. Uncultured microorganisms as a source of secondary metabolites. *J Antibiot (Tokyo)*. 2010; 63:468-476.
- Ling LL, Schneider T, Peoples AJ, *et al*. A new antibiotic kills pathogens without detectable resistance. *Nature*. 2015; 517:455-459.
- Cavicchioli R, Siddiqui KS, Andrews D, Sowers KR. Low-temperature extremophiles and their applications. *Curr Opin Biotechnol*. 2002; 13:253-261.
- Margesin R, Feller G. Biotechnological applications of psychrophiles. *Environ Technol*. 2010; 31:835-844.
- Miyashita A, Hirai Y, Sekimizu K, Kaito C. Antibiotic-producing bacteria from stag beetle mycangia. *Drug Discov Ther*. 2015; 9:33-37.
- Baker GC, Smith JJ, Cowan DA. Review and re-analysis of domain-specific 16S primers. *J Microbiol Methods*. 2003; 55:541-555.
- Kim OS, Cho YJ, Lee K, Yoon SH, Kim M, Na H, Park SC, Jeon YS, Lee JH, Yi H, Won S, Chun J. Introducing EzTaxon-e: A prokaryotic *16S rRNA* gene sequence database with phylotypes that represent uncultured species. *Int J Syst Evol Microbiol*. 2012; 62:716-721.
- Thompson JD, Higgins DG, Gibson TJ. CLUSTAL W: Improving the sensitivity of progressive multiple sequence alignment through sequence weighting, position-specific gap penalties and weight matrix choice. *Nucleic Acids Res*. 1994; 22:4673-4680.
- Felsenstein J. Evolutionary trees from DNA sequences: A maximum likelihood approach. *J Mol Evol*. 1981; 17:368-376.
- Saitou N, Nei M. The neighbour-joining method: A new method for reconstructing phylogenetic trees. *Mol Biol*

- Evo. 1987; 4:406-425.
13. Kumar S, Stecher G, Tamura K. MEGA7: Molecular Evolutionary Genetics Analysis version 7.0 for bigger datasets. *Mol Biol Evol.* 2016; 33:msw054.
 14. Mulet M, Lalucat J, García-Valdés E. DNA sequence-based analysis of the *Pseudomonas* species. *Environ Microbiol.* 2010; 12:1513-1530.
 15. Altschul SF, Gish W, Miller W, Myers EW, Lipman DJ. Basic local alignment search tool. *J Mol Biol.* 1990; 215:403-410.
 16. Rossello-Mora R, Amann R. The species concept for prokaryotes. *FEMS Microbiol Rev.* 2001; 25:39-67.
 17. Tindall BJ, Rosselló-Móra R, Busse HJ, Ludwig W, Kämpfer P. Notes on the characterization of prokaryote strains for taxonomic purposes. *Int J Syst Evol Microbiol.* 2010; 60:249-266.
 18. Ramírez-Bahena MH, Cuesta MJ, Flores-Félix JD, Mulas R, Rivas R, Castro-Pinto J, Brañas J, Mulas D, González-Andrés F, Velázquez E, Peix A. *Pseudomonas helmanticensis* sp. nov., isolated from forest soil. *Int J Syst Evol Microbiol.* 2014; 64:2338-2345.
 19. Cámara B, Strömpl C, Verborg S, Spröer C, Pieper DH, Tindall BJ. *Pseudomonas reinekei* sp. nov., *Pseudomonas moorei* sp. nov. and *Pseudomonas mohnii* sp. nov., novel species capable of degrading chlorosalicylates or isopimaric acid. *Int J Syst Evol Microbiol.* 2007; 57:923-931.
 20. Kwon SW, Kim JS, Park IC, Yoon SH, Park DH, Lim CK, Go SJ. *Pseudomonas koreensis* sp. nov., *Pseudomonas umsongensis* sp. nov. and *Pseudomonas jinjuensis* sp. nov., novel species from farm soils in Korea. *Int J Syst Evol Microbiol.* 2003; 53:21-27.
 21. Gupta G, Prakash V. Isolation and identification of a novel, cold active lipase producing psychrophilic bacterium *Pseudomonas vancouverensis*. *Trends Biosci.* 2014; 7:3708-3711.
 22. López JR, Diéguez AL, Doce A, de la Roca E, de la Herran R, Navas JI, Toranzo AE, Romalde JL. *Pseudomonas baetica* sp. nov., a fish pathogen isolated from wedge sole, *Dicologlossa cuneata* (Moreau). *Int J Syst Evol Microbiol.* 2012; 62:874-882.
 23. Andersen SM, Johnsen K, Sørensen J, Nielsen P, Jacobsen CS. *Pseudomonas frederiksbergensis* sp. nov., isolated from soil at a coal gasification site. *Int J Syst Evol Microbiol.* 2000; 50:1957-1964.
 24. Behrendt U, Ulrich A, Schumann P. Fluorescent pseudomonads associated with the phyllosphere of grasses; *Pseudomonas trivialis* sp. nov., *Pseudomonas poae* sp. nov. and *Pseudomonas congelans* sp. nov. *Int J Syst Evol Microbiol.* 2003; 53:1461-1469.
 25. Verhille S, Baida N, Dabboussi F, Izard D, Leclerc H. Taxonomic study of bacteria isolated from natural mineral waters: Proposal of *Pseudomonas jessenii* sp. nov. and *Pseudomonas mandelii* sp. nov. *Syst Appl Microbiol.* 1999; 22:45-58.
 26. Catara V, Sutra L, Morineau A, Achouak W, Christen R, Gardan L. Phenotypic and genomic evidence for the revision of *Pseudomonas corrugata* and proposal of *Pseudomonas mediterranea* sp. nov. *Int J Syst Evol Microbiol.* 2002; 52:1749-1758.
 27. Pascual J, Garcia-Lopez M, Bills GF, Genilloud O. *Pseudomonas granadensis* sp. nov., a new bacterial species isolated from the Tejada, Almirajara and Alhama Natural Park, Granada, Spain. *Int J Syst Evol Microbiol.* 2014; 65:625-632.
 28. Kiprianova EA, Klochko VV, Zelena LB, Churkina LN, Avdeeva LV. *Pseudomonas batumici* sp. nov., the antibiotic-producing bacteria isolated from soil of the Caucasus Black Sea coast. *Mikrobiol Z.* 2011; 73:3-8.
 29. Moore ERB, Mau M, Arnscheidt AK, Bottger EC, Hutson RA, Collins MD, van de Per Y, de Wachter R, Timmis KN. The determination and comparison of the *16S rRNA* gene sequences of species of the genus *Pseudomonas* (sensu stricto) and estimation of the natural intrageneric relationships. *Syst Appl Microbiol.* 1996; 19:478-492.
 30. Anzai Y, Kim H, Park J, Wakabayashi H, Oyaizu H, The P. Phylogenetic affiliation of the pseudomonads based on *16S rRNA* sequence become a dumping ground for incompletely characterized polarly flagellated, of 128 valid and invalid *Pseudomonas* species, which included almost valid species of the genus *Pseudomonas*. *Int J Syst Evol Microbiol.* 2000; 50:1563-1589.
 31. Yamamoto S, Kasai H, Arnold DL, Jackson RW, Vivian A, Harayama S. Phylogeny of the genus *Pseudomonas*: Intrageneric structure reconstructed from the nucleotide sequences of *gvrB* and *rpoD* genes. *Microbiology.* 2000; 146:2385-2394.
 32. Hilario E, Buckley TR, Young JM. Improved resolution on the phylogenetic relationships among *Pseudomonas* by the combined analysis of *atp D*, *car A*, *rec A* and *16S rDNA*. *Antonie Van Leeuwenhoek.* 2004; 86:51-64.
 33. Ait Tayeb L, Ageron E, Grimont F, Grimont PAD. Molecular phylogeny of the genus *Pseudomonas* based on *rpoB* sequences and application for the identification of isolates. *Res Microbiol.* 2005; 156:763-773.
 34. Mulet M, Bennasar A, Lalucat J, García-Valdés E. An *rpoD*-based PCR procedure for the identification of *Pseudomonas* species and for their detection in environmental samples. *Mol Cell Probes.* 2009; 23:140-147.
 35. Mulet M, Gomila M, Lemaitre B, Lalucat J, García-Valdés E. Taxonomic characterisation of *Pseudomonas* strain L48 and formal proposal of *Pseudomonas entomophila* sp. nov. *Syst Appl Microbiol.* 2012; 35:145-149.
 36. Ramos E, Ramírez-Bahena MH, Valverde A, Velázquez E, Zúñiga D, Velezmoro C, Peix A. *Pseudomonas punonensis* sp. nov., isolated from straw. *Int J Syst Evol Microbiol.* 2013; 63:1834-1839.
 37. Toro M, Ramírez-Bahena MH, José Cuesta M, Velázquez E, Peix A. *Pseudomonas guariconensis* sp. nov., isolated from rhizospheric soil. *Int J Syst Evol Microbiol.* 2013; 63:4413-4420.
 38. Moreno R, Rojo F. Features of pseudomonads growing at low temperatures: Another facet of their versatility. *Environ Microbiol Rep.* 2014; 6:417-426.
 39. Imada A, Kitano K, Kintaka K, Muroi M, Asai M. Sulfazecin and isosulfazecin, novel beta-lactam antibiotics of bacterial origin. *Nature.* 1981; 289:590-591.
 40. Weller D. Biological control of soilborne plant pathogens in the rhizosphere with bacteria. *Ann Rev Phytopathol.* 1988; 26:379-407.
 41. O'Sullivan DJ, O'Gara F. Traits of fluorescent *Pseudomonas* spp. involved in suppression of plant root pathogens. *Microbiol Rev.* 1992; 56:662-676.

(Received October 7, 2017; Accepted October 22, 2017)

Effect of methyl p-hydroxybenzoate on the culture of mammalian cell

Hidenori Tani^{1,*}, Jun-ichi Takeshita², Hiroshi Aoki¹, Kaoru Nakamura¹, Ryosuke Abe³, Akinobu Toyoda³, Yasunori Endo⁴, Sadaaki Miyamoto⁴, Masashi Gamo², Masaki Torimura¹, Hiroaki Sato¹

¹ Environmental Management Research Institute, National Institute of Advanced Industrial Science and Technology (AIST), Tsukuba, Ibaraki, Japan;

² Research Institute of Science for Safety and Sustainability, National Institute of Advanced Industrial Science and Technology (AIST), Tsukuba, Ibaraki, Japan;

³ College of Engineering Systems, School of Science and Engineering, University of Tsukuba, Tsukuba, Ibaraki, Japan;

⁴ Department of Risk Engineering, Faculty of Systems and Information Engineering, University of Tsukuba, Tsukuba, Ibaraki, Japan.

Summary

Several chemicals, such as methyl p-hydroxybenzoate (MHB), have been widely used as preservatives in the water baths of CO₂ incubators used for mammalian cell culture, and they are not considered to produce any biological effects. However, no detailed analyses of the effects of these compounds on cultured cells have been reported. In this study, we thus examined whether MHB in the incubator water bath affects cell viability or genome-wide gene expression in mouse embryonic stem cells under control conditions [using only dimethyl sulfoxide (DMSO) in the culture medium] and under chemical-treated conditions using benzene and chloroform; conditions that simulate a cell-based toxicity assay. We found that (i) MHB significantly altered cell growth rate, and (ii) MHB affected gene expression levels related to pathways that modulate cell growth and basic molecular processes, not only under control conditions but also the chemical-treated conditions. Furthermore, Gene Ontology term analyses revealed that the effects of MHB cannot be accounted for by subtracting the gene expression pattern in the control conditions from that in the chemical-treated conditions. Thus, we suggest that the use of MHB or other preservatives in a CO₂ incubator water bath is reconsidered in terms of potential confounding effects on cultured cells.

Keywords: Methyl p-hydroxybenzoate, mouse embryonic stem cells, deep sequencing; incubator, toxicological assessment

1. Introduction

In regular laboratory practice, mammalian cells are cultured in a CO₂ incubator using chemical compounds such as methyl p-hydroxybenzoate (MHB), sodium dehydroacetic acid, sodium dodecyl sulfate, ethylenediaminetetraacetic acid, sodium azide, or copper sulfate in the incubator water bath as a preservative to

prevent bacterial or mycoplasma contamination. These chemicals are not considered to produce any biological effects on the cultured cells. For example, MHB, which is widely used for this purpose, was reported to be mostly non-toxic by both oral and parenteral routes, and non-irritating and non-sensitizing to normal skin at acute toxicity levels in animal experiments (1). However, no detailed analyses of *in vitro* cell responses to these chemicals have been reported. Cell stress responses are highly conserved responses to environmental changes with transient reprogramming of transcriptional, translational, and post-translational activities (2). Thus, culture conditions are critical for correct and reproducible studies using cultured cells.

In this study, we investigated the effect of MHB

*Address correspondence to:

Dr. Hidenori Tani, Environmental Management Research Institute, National Institute of Advanced Industrial Science and Technology (AIST), 16-1, Onogawa, Tsukuba, Ibaraki 305-8569, Japan.

E-mail: h.tani@aist.go.jp

in the incubator water bath on the cell viability, and performed deep sequencing analyses (RNA-seq) on mouse embryonic stem cells (mESCs) cultured with MHB to determine the effects of MHB exposure on genome-wide gene expression. We chose mESCs because mESCs are basic cells and have a normal karyotype, maintain high telomerase activity, and exhibit remarkable long-term proliferative potential. We also examined two chemicals listed in the Japan Pollutant Release and Transfer Register as a class I designated chemical substances.

2. Materials and Methods

2.1. Chemicals

MHB, benzene, and chloroform were obtained from Wako, Osaka, Japan. MHB was used in a water bath. Benzene and chloroform were dissolved in dimethyl sulfoxide (DMSO) (Wako) and diluted in culture medium at a 0.1% vol/vol final concentration.

2.2. Cell culture

The mESC line H-1 was isolated from C3H/He mice by Kitani *et al.* (3). mESCs were maintained in Dulbecco's modified Eagle's medium (4.5 g/L glucose) with L-glutamine, without sodium pyruvate, (Nacalai Tesque, Kyoto, Japan) supplemented with 15% fetal bovine serum (Gibco, MA, USA), 1,000 U/mL Stem Sure Leukemia Inhibitory Factor (mouse, recombinant, solution; Wako), 0.1 mM Stem Sure 2-mercaptoethanol solution (Wako), and penicillin-streptomycin (Gibco). Cells were grown on mitomycin C (Kyowa Kirin, Tokyo, Japan)-treated mouse embryonic fibroblast feeder cells (C57BL/6J) at 37°C in a humidified incubator with 5% CO₂ without MHB. For the feeder-free culturing, mESCs were cultured in ESGRO complete plus serum-free clonal grade medium (Merck Millipore, Darmstadt, Germany) on gelatin (Sigma, MO, USA)-coated dishes without feeder cells at 37°C in a humidified incubator with 5% CO₂ without MHB for 4 days (pre-culture). In the following experiments, mESCs without feeder-free cells were used for chemical stress treatments. For chemical stress treatments, mESCs were cultured with or without 2% MHB (4 g in 200 mL sterilized water) in the incubator water bath, which is the concentration of MHB used commonly in our lab.

2.3. Chemical stress treatments

Cells without feeder cells (pre-culturing without MHB for 4 days) were seeded at 3.8×10^5 cells per well (6-well plate) in 2 mL medium or at 1.9×10^4 cells per well (96-well plate) in 100 μ L medium. The cells were incubated overnight at 37°C with 5% CO₂ with

or without MHB for 24 h. In separate analyses, cells were treated with 2 μ L benzene (final concentration of 1,000 μ M) or 2 μ L chloroform (1,000 μ M) for 24 h. Total RNA was extracted from cells in the 6-well plate with 400 μ L RNAiso Plus (Takara, Kyoto, Japan) according to the manufacturer's instructions. The amount of total RNAs were analyzed using Nano Drop 2000c spectrophotometer (Thermo scientific, MA, USA). The numbers of viable cells in the 96-well plate were counted using a Cell Counting Kit-8 (Dojindo, Kumamoto, Japan) in accordance with the manufacturer's instructions.

2.4. RNA-seq and data analysis

RNA-seq analyses were performed by Takara, Japan. First, ribosomal RNA was removed using a Ribo-Zero Magnetic Gold Kit (Human/Mouse/Rat) (Illumina, CA, USA) from 6 μ g total RNA. An RNA-seq library was constructed using the TruSeq Standard mRNA Sample Prep Kit (Illumina). One hundred base pair-end read RNA-seq tags were generated using an Illumina HiSeq 2500 sequencer according to the standard protocol. Fluorescence images were processed to sequences using the analysis pipeline supplied by Illumina. RNA-seq tags were mapped to the mouse genome (hg19) from the National Center for Biotechnology Information using TopHat mapping software. Genic representations using fragments per kilobase of exon per million mapped fragments (FPKM) to normalize for gene length and depth of sequencing were calculated. RNA-seq tags were assigned to corresponding RefSeq transcripts when their genomic coordinates overlapped. We used RNA sequences available from public databases: mRNA from NM of RefSeq and lncRNA candidates from NR of RefSeq.

2.5. Data access

Short-read sequence archive data in this study are registered in GenBank (<http://www.ncbi.nlm.nih.gov/genbank/>)/DDBJ (<http://dbj.sakura.ne.jp>). The data to determine the expression levels of transcripts are registered as follows: accession nos. DRA005417; DRX076620, DRX076621, DRX076628, DRX076629, DRX076638, and DRX076638 (with MHB; MHB +), and DRX076650, DRX076651, DRX076658, DRX076659, DRX076668, and DRX076669 (without MHB; MHB -).

3. Results

3.1. Effect of MHB on cell viability

First, to examine the effect of MHB in the incubator water bath on the cell viability of cultured cells, mESCs were cultured with or without MHB for 24 h.

Figure 1 shows a phase-contrast image of the mESCs. No floating cells (dead cells) were observed under microscopic observation (data not shown). Moreover, the amounts of isolated RNAs from one well (6-well plate) in duplicate with or without MHB were 5.1 ± 0.3 or $5.8 \pm 0.3 \mu\text{g}$ (mean \pm errors, $n = 2$), respectively. Taken together, after culture with MHB, the number of mESCs was significantly decreased compared with the number of mESCs after culture without MHB.

3.2. Effect of MHB on genome-wide gene expression

To examine the effect of MHB on genome-wide gene expression patterns, we performed deep sequencing analyses (RNA-seq) on mESCs cultured with (MHB +) or without MHB (MHB -) for 24 h. We then analyzed more than 40 million RNA-seq tags from each sample. Genic representations were calculated using FPKM to normalize for gene length and depth of sequencing. Sequencing tags were then mapped to the mouse reference genome sequence using mapping software, allowing no mismatches. In total, 32,586 RNAs from the NM and NR categories of the Reference Sequence (RefSeq) Database were used for RNA annotation. The above examinations were also conducted for cultured cells under control conditions (DMSO only in the culture medium) and under benzene-treated conditions, and chloroform-treated conditions. This is a simplified simulation cell-based toxicity assay.

To quantify the effect of MHB on gene expression patterns, correlation coefficients of the logarithms of FPKMs were determined, both between MHB + and MHB -, and between replicated samples of MHB -, respectively, in the control conditions and in the chemical-treated conditions (the benzene- and chloroform-treated conditions). Figure 2 shows that the correlation coefficient between MHB + and MHB - was significantly lower than that of the replicated MHB - in the control conditions by approximately 0.1. A similar tendency was observed for the benzene-treated conditions (Figure 3) and for the chloroform-treated conditions (Figure 4). Moreover, cell viabilities were

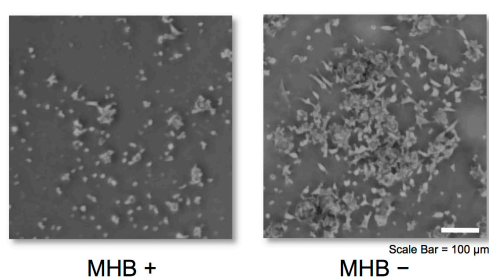


Figure 1. Phase-contrast microscopic observation of mESCs. mESCs were cultured at 37°C in a humidified CO₂ incubator with or without 2% methyl p-hydroxybenzoate (MHB) for 24 h. MHB + or MHB - indicates that mESCs were cultured with or without MHB in the incubator water bath, respectively.

measured after exposure to 1,000 μM benzene and 1,000 μM chloroform for 24 h without MHB. Cell viabilities were decreased to $79 \pm 13\%$ and $66 \pm 10\%$ (mean \pm SD, $n = 4$) after exposure to 1,000 μM benzene and 1,000 μM .

3.3. Gene ontology term classification of mRNAs

A two-sample t-test between MHB + and MHB - in the control conditions was conducted, and the RNAs having the 10 lowest p-values were extracted. We then categorized the RNAs according to their Gene Ontology

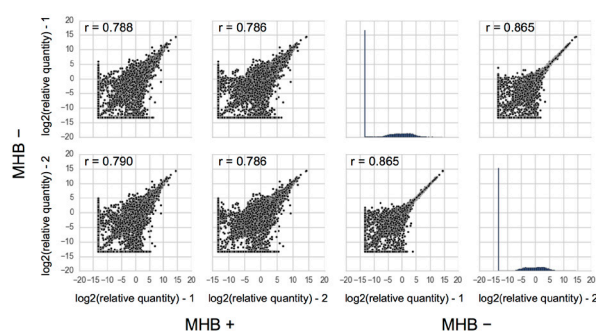


Figure 2. Scatter plot for gene expression pattern determined by RNA-seq under DMSO (control) conditions. mESCs were cultured at 37°C in a humidified CO₂ incubator with DMSO and with or without 2% MHB for 24 h. MHB + or MHB - indicates that mESCs were cultured with or without MHB in the incubator water bath, respectively. The relative quantitative values (FPKMs from RNA-seq data) of 32,586 RNAs were plotted on MHB + versus MHB - ($n = 2$; left four panels), and between replicated samples of MHB - ($n = 2$; right four panels), respectively. MHB + and MHB - experiments were performed in duplicate, and each "r" indicates correlation coefficient. Same experiments (MHB - "-1 versus -1" or "-2 versus -2"; right two panels) also indicates that histogram of relative quantitative values.

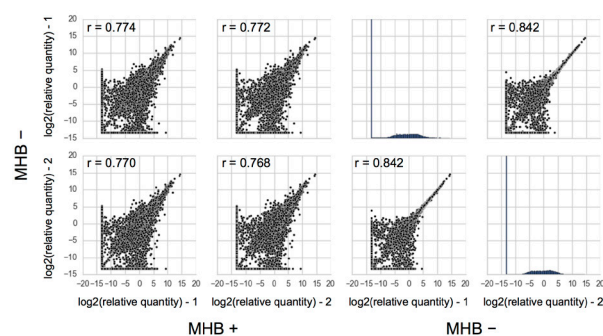


Figure 3. Scatter plot for gene expression pattern determined by RNA-seq under benzene conditions. mESCs were cultured at 37°C in a humidified CO₂ incubator with 1,000 μM benzene and with or without 2% MHB for 24 h. MHB + or MHB - indicates that mESCs were cultured with or without MHB in the incubator water bath, respectively. The relative quantitative values (FPKMs from RNA-seq data) of 32,586 RNAs were plotted on MHB - versus MHB + ($n = 2$; left four panels), and between replicated samples of MHB - ($n = 2$; right four panels), respectively. MHB + and MHB - experiments were performed in duplicate, and each "r" indicates correlation coefficient. Same experiments (MHB - "-1 versus -1" or "-2 versus -2"; right two panels) also indicates that histogram of relative quantitative values.

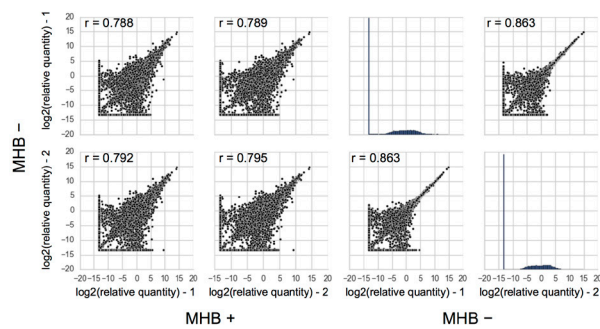


Figure 4. Scatter plot for gene expression pattern determined by RNA-seq under chloroform conditions. mESCs were cultured at 37°C in a humidified CO₂ incubator with 1,000 μM chloroform and with or without 2% MHB for 24 h. MHB + or MHB - indicates that mESCs were cultured with or without MHB in the incubator water bath, respectively. The relative quantitative values (FPKMs from RNA-seq data) of 32,586 RNAs were plotted on MHB - versus MHB + ($n = 2$; left four panels), and between replicated samples of MHB - ($n = 2$; right four panels), respectively. MHB + and MHB - experiments were performed in duplicate, and each "r" indicates correlation coefficient. Same experiments (MHB - "-1 versus -1" or "-2 versus -2"; right two panels) also indicates that histogram of relative quantitative values.

(GO) term. We observed significant differences for the GO terms classified as poly(A) RNA binding, chromatin binding, and RNA splicing between MHB + and MHB -. Moreover, cell maturation was also present in the list of GO terms (Table 1). These results suggest that MHB affects not only basic molecular processes but also cell growth. We also conducted the same analysis for the chemical-treated conditions. For the benzene-treated conditions, we observed significant differences for the GO terms classified as cell cycle, RNA splicing, and cell proliferation between MHB + and MHB - (Table 2). On the other hand, for the chloroform-treated conditions, we observed significant differences for the GO terms classified as cell cycle, positive regulation of cell migration, and programmed necrotic cell death between MHB + and MHB - (Table 3). We also examined the FPKM values of cell growth-related genes between duplicated samples of MHB -. We focused on the genes in Tables 1-3 [tumor suppressor candidate 2 (*Tusc2*), centrosomal protein 131(*Cep131*), RB transcriptional corepressor like 1 (*Rbl1*), transcription factor Dp-1

Table 1. Functional classification of RNAs having the 10 lowest P-values under DMSO (control) conditions

Refseq	Gene name	MHB +/MHB -	p-value	GO term	Definition
NM_025669	<i>Pnlsr</i>	111954	7.29×10^{-10}	0044822	poly(A) RNA binding
NM_025891	<i>Smarcd3</i>	26184	8.08×10^{-10}	0003682	chromatin binding
NM_173441	<i>Iws1</i>	81056	1.53×10^{-9}	0008380	RNA splicing
NM_008717	<i>Zfp638</i>	141698	2.39×10^{-9}	0003677	DNA binding
NM_053182	<i>Pag1</i>	6244	4.60×10^{-9}	0042169	SH2 domain binding
NR_073524	<i>Slfn10-ps</i>	4809	3.02×10^{-8}	-	-
NM_001204333	<i>Cyp4f14</i>	1060	5.40×10^{-8}	0050544	arachidonic acid binding
NM_172728	<i>Creb5</i>	3700	7.91×10^{-8}	0003677	DNA binding
NM_001024922	<i>Ddx49</i>	344879	1.06×10^{-7}	0005524	ATP binding
NM_019742	<i>Tusc2</i>	27527	1.34×10^{-7}	0048469	cell maturation

Table 2. Functional classification of RNAs having the 10 lowest P-values under benzene conditions

Refseq	Gene name	MHB +/MHB -	p-value	GO term	Definition
NM_009734	<i>Cep131</i>	20390	1.58×10^{-9}	0007049	cell cycle
NM_001162922	<i>Zfp931</i>	7742	3.37×10^{-9}	0008150	biological process
NM_011249	<i>Rbl1</i>	27763	4.71×10^{-9}	0007049	cell cycle
NM_008717	<i>Zfp638</i>	58978	7.96×10^{-9}	0008380	RNA splicing
NR_037683	<i>Snord42b</i>	74957	1.07×10^{-8}	-	-
NM_001164769	<i>Fbxw2</i>	0.000032	2.58×10^{-8}	0005515	protein binding
NM_007460	<i>Ap3d1</i>	0.000054	3.91×10^{-8}	0072657	protein localization to membrane
NM_010832	<i>Msl3</i>	3004	4.21×10^{-8}	0006325	chromatin organization
NM_011661	<i>Tyr</i>	43861	4.90×10^{-8}	0008283	cell proliferation
NM_001040072	<i>Nynrin</i>	0.000009	5.27×10^{-8}	0003676	nucleic acid binding

Table 3. Functional classification of RNAs having the 10 lowest P-values under chloroform conditions

Refseq	Gene name	MHB +/MHB -	p-value	GO term	Definition
NM_001291768	<i>Tfdp1</i>	80940	1.69×10^{-7}	0007049	cell cycle
NM_134087	<i>Fam83h</i>	44282	1.84×10^{-7}	0030335	positive regulation of cell migration
NM_001142697	<i>Tpgs2</i>	38260	1.86×10^{-7}	0005575	cellular_component
NM_027777	<i>Pex1</i>	11049	2.06×10^{-7}	0005524	ATP binding
NM_001004142	<i>Nlrp1a</i>	72514	2.21×10^{-7}	0097300	programmed necrotic cell death
NM_001033378	<i>A430078G23Rik</i>	8986	2.31×10^{-7}	-	-
NM_028815	<i>Cep97</i>	7395	2.55×10^{-7}	0030030	cell projection organization
NM_001162973	<i>Lrrc51</i>	4377	2.58×10^{-7}	0005575	cellular_component
NM_133907	<i>Ube3c</i>	177872	2.67×10^{-7}	0004842	ubiquitin-protein transferase activity
NM_001004066	<i>Zfp386</i>	16820	3.12×10^{-7}	0006355	regulation of transcription, DNA-templated

(*Tfdp1*), and tyrosinase (*Tyr*)]. The FPKM values of cell maturation-related gene, *Tusc2*, were 3.7 and 3.8 in duplicate. Those of cell cycle-related genes, *Cep131*, *Rb11*, and *Tfdp1*, were 0.55 and 0.53, 3.1 and 3.0, and 25.9 and 29.0, respectively. Those of cell proliferation-related gene, *Tyr*, were 7.8 and 8.4. These results indicate that cell growth-related genes were not significantly different between duplicated samples of MHB –.

4. Discussion

Our results show that MHB has a growth inhibitory effect on cultured mESCs and that the use of MHB also affects gene expression patterns both in control conditions and in chemical-treated conditions. In our experiments, MHB was not directly added into the culture medium; therefore, we considered that aerosol of MHB from the water bath of incubator affected those above-mentioned effects to cultured cells. The GO term analyses indicate that MHB clearly affects cell growth pathways in both control conditions and chemical-treated conditions. Moreover, the effect of MHB cannot be accounted for by subtracting the gene expression pattern under control conditions from those under chemical-treated conditions. This is because the GO terms that appeared under the control conditions (Table 1) are not identical to those under the chemical-treated conditions (Tables 2 and 3). Therefore, the simple setting of control conditions in cell-based assays is not adequate.

This study is the first to demonstrate the inconvenient

effect of MHB on cultured mammalian cells used for gene expression analyses in cell-based toxicity assays. This effect has, to date, been neglected. We suggest that other chemicals commonly used as incubator water bath preservatives should be reconsidered in terms of their biological effects on cultured cells.

Acknowledgements

The mouse ES cell line H-1 and murine embryo fibroblast feeder cells, C57BL/6J, were provided by the RIKEN BRC through the Project for Realization of Regenerative Medicine and the National Bio-Resource Project of the MEXT, Japan. Deep sequencing and data analysis were performed by TaKaRa.

References

1. Soni MG, Taylor SL, Greenberg NA, Burdock GA. Evaluation of the health aspects of methyl paraben: A review of the published literature. *Food Chem Toxicol.* 2002; 40:1335-1373.
2. Kültz D. Molecular and evolutionary basis of the cellular stress response. *Annu Rev Physiol.* 2005; 67:225-257.
3. Kitani H, Takagi N, Atsumi T, Kawakura K, Imamura K, Goto S, Kusakabe M, Fukuta K. Isolation of a germline-transmissible embryonic stem (ES) cell line from C3H/He mice. *Zoolog Sci.* 1996; 13:865-871.

(Received October 9, 2017; Revised October 25, 2017; Accepted October 28, 2017)

Ethanol extracts of *Aster yomena* (Kitam.) Honda inhibit adipogenesis through the activation of the AMPK signaling pathway in 3T3-L1 preadipocytes

Min Ho Han¹, Ji-Suk Jeong², Jin-Woo Jeong^{3,4}, Sung Hyun Choi⁵, Sung Ok Kim⁶, Su Hyun Hong⁴, Cheol Park⁷, Byung Woo Kim⁸, Yung Hyun Choi^{3,8,*}

¹National Marine Biodiversity Institute of Korea, Seochon, Republic of Korea;

²Gurye Wild Flower Institute and Gurye-gun Agricultural Center, Gurye, Republic of Korea;

³Anti-Aging Research Center, Dongeui University, Busan, Republic of Korea;

⁴Open Laboratory for Muscular and Skeletal Disease, and Department of Biochemistry, Dongeui University College of Korean Medicine, Republic of Korea;

⁵Department of System Management, Korea Lift College, Geochang, Republic of Korea;

⁶Department of Food Science & Biotechnology, College of Engineering, Kyungsung University, Busan, Republic of Korea;

⁷Department of Molecular Biology, College of Natural Sciences, Dongeui University, Busan, Republic of Korea;

⁸Biopharmaceutical Engineering Major, Division of Applied Bioengineering, College of Engineering, Dongeui University, Busan, Republic of Korea.

Summary

The leaves of *Aster yomena* (Kitam.) Honda have long been used as a traditional herb for treating disorders including coughs, asthma, and insect bites. According to recent studies, *A. yomena* leaf extracts have several pharmacological properties, including anti-inflammatory, antioxidant, and anti-asthmatic activities. However, little information is available regarding their anti-obesity effect. In this study, we investigated the inhibitory effect of the ethanol extracts of *A. yomena* leaves (EEAY) on adipocyte differentiation and adipogenesis using 3T3-L1 preadipocytes. When 3T3-L1 preadipocytes were treated with various concentrations of EEAY (ranging from non-toxic), the number of lipid droplets, lipid content, and triglyceride production, the typical characteristics of adipocytes, were suppressed in a concentration-dependent manner. During this process, EEAY significantly reduced the expression of adipogenic transcription factors, including peroxisome proliferator-activated receptor- γ , CCAAT/enhancer-binding protein α and β , and sterol regulatory element-binding protein-1c. In addition, EEAY was also found to potently inhibit the expression of adipocyte-specific genes, including adipocyte fatty acid-binding protein and leptin. In particular, EEAY treatment effectively enhanced the activation of the AMP-activated protein kinase (AMPK) signaling pathway; however, the co-treatment with compound C, an inhibitor of AMPK, significantly restored the EEAY-induced inhibition of pro-adipogenic transcription factors and adipocyte-specific genes. These results indicate that EEAY may exert an anti-obesity effect by controlling the AMPK signaling pathway, suggesting that the leaf extract of *A. yomena* may be a potential anti-obesity agent.

Keywords: *Aster yomena* (Kitam.), 3T3-L1 preadipocytes, adipocyte differentiation, adipogenesis, AMPK

Released online in J-STAGE as advance publication October 11, 2017.

*Address correspondence to:

Dr. Yung-Hyun Choi, Department of Biochemistry, College of Korean Medicine, Dongeui University, Busan, 47227, Republic of Korea.

E-mail: choiyh@deu.ac.kr

1. Introduction

Obesity is a metabolic disorder caused by an imbalance in the energy intake and expenditure. It is a major risk factor for several chronic diseases, including hypertension, atherosclerosis, and type 2 diabetes

(1,2). Obesity is characterized by an overgrowth of the adipocytes, indicated by an increase in the number of adipocytes, resulting from their division and differentiation. Adipocytes also play a crucial role in storing excess energy in the form of triglycerides (TGs) and releasing energy in the form of glycerol and fatty acids (3,4). In particular, pre-adipocytes differentiate into mature adipocytes owing to high caloric intake and various stimulatory factors such as insulin and glucocorticoids (5,6). The differentiation of pre-adipocytes into mature adipocytes is accompanied by the sequential expression and activation of adipogenic transcription factors, including peroxisome proliferator-activated receptor- γ (PPAR γ), CCAAT/enhancer-binding proteins (C/EBPs), and sterol regulatory element-binding protein-1c (SREBP-1c) in a coordinated manner (6,7). In the final stages of the differentiation, adipocytes secrete adipose tissue-specific products, including adipocyte-specific fatty acid binding protein (aP2) and leptin (8-11). After differentiation, they regulate the lipid metabolism by synthesizing lipolytic enzymes such as fatty acid synthase (FAS), acetyl-CoA carboxylase (ACC), and hormone-sensitive lipase (12,13). Therefore, the inhibition of the differentiation of preadipocytes into adipocytes would reduce the mass of adipose tissue and reduce the incidence of obesity. Further, the identification of a factor that inhibits differentiation would be useful for treating obesity and related metabolic diseases.

Furthermore, the AMP-activated protein kinase (AMPK), a serine/threonine kinase, is a key sensory protein that controls energy metabolism (14,15). Once AMPK is activated *via* phosphorylation by the upstream AMPK kinases, it functions as a cellular energy sensor through the regulation of fatty acid and glucose homeostasis (16,17). The activated AMPK increases glucose transport and fatty acid oxidation; it also inhibits the energy-consuming processes such as lipogenesis, protein synthesis, and gluconeogenesis (18,19). AMPK also induces inactivation by phosphorylating ACC, the key enzyme for fatty acid oxidation and biosynthesis (13,20). Further, when AMPK is activated, it may protect preadipocyte differentiation with the inhibition of the transcription factors such as PPAR γ and C/EBPs. In particular, low levels of AMPK activation are associated with the onset of obesity and diabetes (21,22); therefore, AMPK has been identified as a potential target for treating obesity and the related metabolic disorders (14,22,23).

Plant-based materials have been used since a long time as traditional medicines in many cultures and are well-known sources for developing anti-obesity compounds. In this study, *Aster yomena* (Kitam.) Honda was selected from among traditional Korean medicine resources for the development of a new anti-obesity active substance. *A. yomena* is a perennial herb widely distributed throughout Asia that has been used in traditional medicine to treat several diseases such as

cough, asthma, and insect bites (24). Several previous studies have shown that the leaf extracts or compounds of *A. yomena* have many pharmacological activities, including anti-microbial (25,26), antioxidant (27-29) and anti-coagulant (30) actions. Kim *et al.* (31) showed that the phenolic compounds extracted from the leaves of this plant significantly inhibited the production of interleukin-6 by stimulating tumor necrosis factor- α in the osteoblasts, indicating an anti-inflammatory activity. We recently reported that the ethanol extract of *A. yomena* leaves (EEAY) inhibited lipopolysaccharide-induced inflammatory responses in the macrophage model owing to the deactivation of the toll like receptor-mediated nuclear factor- κ B signaling pathway (32). However, to our knowledge, the efficacy of EEAY as anti-obesity agents and the underlying molecular mechanisms are still unclear. Therefore, we designed this study to evaluate the anti-obesity effect of EEAY using 3T3-L1 preadipocytes and attempted to study the mechanism associated with the inhibition of the adipogenesis of 3T3-L1 cells.

2. Materials and Methods

2.1. Cell culture

The murine 3T3-L1 preadipocytes were purchased from the American Type Culture Collection (Manassas, VA, USA) and maintained in Dulbecco's modified Eagle's medium (DMEM, Welgene, Daegu, Republic of Korea) containing 4.5 g/L D-glucose (Welgene) supplemented with 10% bovine calf serum (BCS, Welgene) and 1% penicillin/streptomycin (Welgene) at 37°C in a humidified atmosphere comprising 5% CO₂ and 95% air.

2.2. Preparation and treatment of EEAY

The dried leaves of *A. yomena* used in this study were provided by the Gurye Wild Flower Institute (Gurye, Republic of Korea). The EEAY were prepared as per the method described by Kang *et al.* (32). The prepared EEAY were dissolved in dimethylsulfoxide (DMSO; Sigma-Aldrich Chemical Co. St. Louis, MO, USA) to achieve a final concentration of 200 mg/mL (extract stock solution).

2.3. Differentiation of 3T3-L1 preadipocytes

To differentiate the 3T3-L1 preadipocytes into adipocytes, 3T3-L1 preadipocytes were grown in culture plates for 2 d to full confluency. Thereafter, the cells were cultured in a differentiation medium (MDI) containing 5 μ g/mL insulin, 1 mM dexamethasone, and 0.5 mM isobutylmethylxanthine (Sigma-Aldrich Chemical Co.). After 2 d, the medium was changed to DMEM, containing 10% BCS and 5 μ g/mL insulin for 2 d and subsequently cultured in a normal medium for

4 d. Various concentrations of EEAY were added along with the MDI, and 3T3-L1 preadipocytes that induced 8-d differentiation were used for various experimental analyses.

2.4. Assessment of cell viability

To evaluate the cytotoxic ability of EEAY, 3T3-L1 preadipocytes were seeded in 6-well plates at a density of 1×10^4 cells per well. After 24 h, the cells were treated with different concentrations of EEAY for 72 h. Thereafter, 3-(4,5-dimethylthiazol-2-yl)-2,5-diphenyltetrazolium bromide (MTT, Sigma-Aldrich Chemical Co.) was added to each well at a concentration of 0.5 mg/mL, followed by incubation at 37°C in a dark environment for 3 h. The MTT solution was removed, and DMSO (200 μ L) was added to dissolve the formazan complex. The viable cells were detected by reading the absorbance of formazan at 540 nm using an enzyme-linked immunosorbent assay (ELISA) microplate reader (Dynatech Laboratories, Chantilly, VA, USA). The optical density of the formazan formed in the control (untreated) cells was used to represent 100% viability.

2.5. Oil red O staining

The cells were washed gently with ice-cold phosphate-buffered saline (PBS) twice and fixed with 3.7% formalin (Sigma-Aldrich Chemical Co.) at room temperature for 1 h. Thereafter, the cells were stained with Oil Red O solution (0.5% in propylene glycol, Sigma-Aldrich Chemical Co.) for 20 min and rinsed with 70% ethanol and PBS. The stained lipid droplets in the cells were then observed under a microscope (X100, Olympus, Tokyo, Japan).

2.6. Measurement of the intracellular TG content

The cellular TG contents were measured using a commercial TG assay kit (Sigma-Aldrich Chemical Co.) according to the manufacturer's instructions. Briefly, the harvested adipocytes were washed twice with ice-cold PBS and lysed in RIPA lysis buffer. Thereafter, the cells were centrifuged at 13,000 g for 20 min at 4°C, and the supernatants were used to measure the intracellular TG content at 550 nm using a microplate reader.

2.7. Protein isolation and Western blot analysis

As described in a previous study (33), the cells were collected and lysed with a cell lysis buffer. Then, their protein concentrations were determined by using the Bio-Rad protein assay kit (Bio-Rad, Hercules, CA, USA). For Western blotting, equal amounts of protein samples were electrophoretically transferred onto polyvinylidene difluoride membranes (Schleicher & Schuell, Keene, NH, USA) following electrophoretic separation on sodium-

dodecyl sulfate (SDS) gel. Subsequently, the membranes were blocked with 5% non-fat dry milk/Tris-buffered saline containing 0.1% Triton X-100 (TBST, Sigma-Aldrich Chemical Co.) for 1 h and probed overnight with specific primary antibodies at 4°C. After washing the primary antibodies with TBST, the membranes were incubated with the appropriate horseradish peroxidase (HRP)-conjugated secondary antibodies (Amersham Biosciences, Westborough, MA, USA) for 2 h at room temperature. The protein bands were detected using an enhanced chemiluminescence (ECL) kit (Amersham Biosciences) as per the manufacturer's instructions.

2.8. Statistical analyses

All numerical data are expressed using mean \pm standard deviation (SD) values. The significance of the differences between the mean values was analyzed using the Student's *t*-test. All statistical analyses were conducted using the Statistical Package for the Social Sciences version 17.0 software (SPSS Inc., Chicago, IL, USA). Values of $p < 0.05$ were considered statistically significant.

3. Results

3.1. Effect of EEAY on 3T3-L1 preadipocyte viability

3T3-L1 preadipocytes were exposed to various concentrations of EEAY to measure its effect on cell viability using an MTT assay. Our data indicate that EEAY had no cytotoxic effect on the 3T3-L1 cells at concentrations ≤ 500 μ g/mL (Figure 1), and the cells did not show morphological changes (data not shown). Therefore, the maximum concentration of EEAY was set at 200 μ g/mL for future research.

3.2. EEAY inhibits the differentiation of 3T3-L1 preadipocytes

To measure the effects of EEAY on adipogenesis, 3T3-

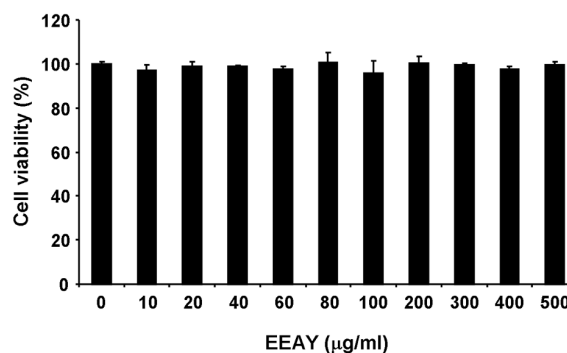


Figure 1. Effects of EEAY on the proliferation of 3T3-L1 mouse preadipocytes. Cells were treated with the indicated concentrations of EEAY for 72 h. Cell viability was determined using an MTT assay. Data of the three independent experiments are expressed as mean \pm SD values.

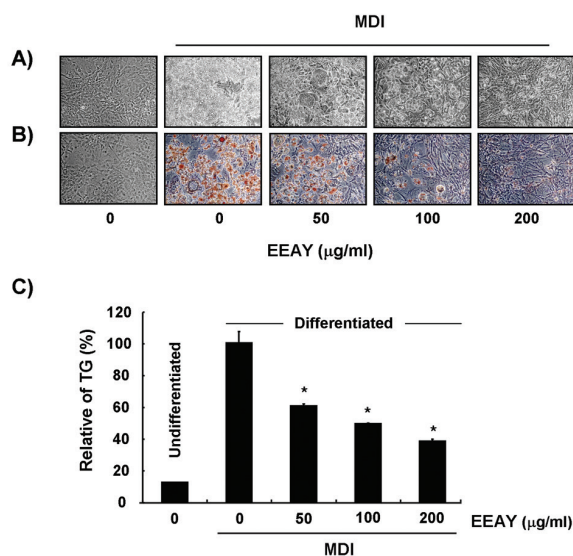


Figure 2. Effects of EEAY on intracellular lipid accumulation and TG content in the differentiated 3T3-L1 cells. The 3T3-L1 preadipocytes were treated with various concentrations of EEAY during differentiation. (A and B) On Day 8, the cells were directly observed via light microscopy (A) or the cells were fixed and stained with Oil Red O to visualize lipid droplets (B) (Magnification, $\times 200$). (C) The TG content was measured to quantify the intracellular lipid content at 500 nm wavelength using the ELISA reader. All values of the three independent experiments are presented as means \pm SD values ($*p < 0.05$ vs. the differentiated cells without treatment).

L1 preadipocytes were differentiated in the presence or absence of EEAY. As shown in Figure 2A and B, EEAY reduced lipid accumulation in 3T3-L1 adipocytes, as evidenced by the decrease in the cell size and number of lipid droplets in the mature adipocytes in a concentration-dependent manner. Further, it is noteworthy that there was about 60% lipid reduction after treatment with 200 $\mu\text{g/mL}$ EEAY (Figure 2C). These data suggest that EEAY could exert an anti-adipogenic effect through inhibition or delay in the differentiation and adipogenesis of the 3T3-L1 preadipocytes.

3.3. EEAY attenuates the expression of adipogenic transcription factors

The differentiation of preadipocytes into adipocytes is coordinated by a complex process that involves the sequential activation of multiple adipogenic transcription factors, including PPAR γ , C/EBP α/β , and SREBP-1c (6,7). To investigate the role of EEAY in reducing fat accumulation during the adipogenesis of 3T3-L1 preadipocytes, we examined the effects of EEAY on the expression of these adipogenic transcription factors. The immunoblotting results indicated that the increased expression of the transcription factors was largely inhibited following EEAY treatment in a concentration-dependent manner (Figure 3A). These results suggest that the inhibition of lipid accumulation by EEAY is associated with the suppression of the expression of adipogenic transcription factors.

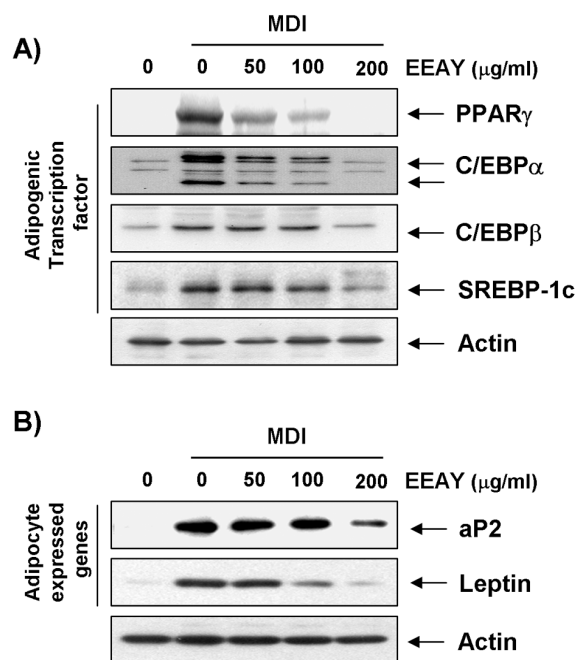


Figure 3. Effects of EEAY on the levels of adipogenic transcription factors (A) and adipocyte expressed genes (B) expression in the differentiated 3T3-L1 cells. At day 0, confluent 3T3-L1 preadipocytes were treated with various concentrations of EEAY in the absence or presence of an MDI differentiation medium for 48 h. On day 8, completely differentiated cells were lysed to extract the total protein. The cellular proteins were separated electrophoretically using SDS-polyacrylamide gels and transferred onto membranes. The membranes were probed with the indicated antibodies. The proteins were visualized using an ECL detection system. Actin was used as an internal control.

3.4. EEAY suppress the expression of adipocyte-related genes

We further examined the influence of EEAY on the expression of adipocyte-related markers such as aP2 and leptin (9,11). As shown in Figure 3B, the increased expression of aP2 and leptin protein in differentiated 3T3-L1 cells decreased in a concentration-dependent manner compared to that in the control group after EEAY administration. These results support the hypothesis that the anti-adipogenic effect of EEAY is associated with the downregulation of the expression of adipocyte-related markers involved in lipid metabolism.

3.5. EEAY induces the phosphorylation of AMPK and ACC

AMPK plays a central role in regulating the cellular metabolism and energy balance in the adipose tissue. The activation of AMPK inhibits preadipocyte differentiation and adipogenesis through increased phosphorylation of ACC, a substrate of AMPK (13,17). To investigate whether AMPK is activated by EEAY during 3T3-L1 differentiation, we analyzed the levels of phosphorylated AMPK and ACC and found that EEAY remarkably enhanced the phosphorylation of AMPK and ACC

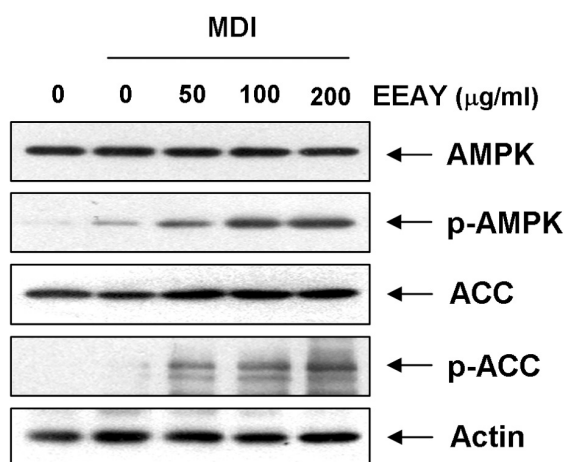


Figure 4. Effects of EEAY on the phosphorylation of AMPK and ACC in the differentiated 3T3-L1 cells. The proteins were isolated cells grown under the same conditions (as shown in Figure 3), and the total protein levels of AMPK and ACC, and their phosphorylated states (p-AMPK and p-ACC, respectively) were determined using the indicated antibodies and an ECL detection system. Actin was used as an internal control.

without altering the expression of their total protein expression, indicating the activation of the AMPK pathway. (Figure 4). However, when compound C, an AMPK specific inhibitor, was pretreated in the 3T3-L1 cells, the phosphorylation of both, AMPK and ACC induced by EEAY was significantly reduced (Figure 5A).

3.6. Activation of the AMPK signaling pathway is involved in the inhibitory effects of EEAY on 3T3-L1 adipogenesis

We aimed to analyze the relationship between the activation of the AMPK signaling pathway and EEAY-mediated inhibition of adipogenesis. Therefore, we evaluated the EEAY-induced reduction in the effect of compound C on the expression of adipogenic transcription factors such as PPAR γ , C/EBP α , C/EBP β , and SREBP-1c. As shown in Figure 5B, the expression of these transcription factors that was repressed by EEAY was increased again in the presence of compound C. These results suggest that the EEAY-induced inhibition of adipogenesis in the 3T3-L1 cells is achieved by the activation of at least the AMPK signaling pathway.

4. Discussion

In this study, we investigated the anti-adipogenesis effect of EEAY using 3T3-L1 preadipocytes. According to the results of this study, the lipid accumulation and TG content in the cytoplasm of differentiated 3T3-L1 cells was actively increased and was significantly inhibited by EEAY treatment in a concentration-dependent manner. Adipocyte differentiation is accompanied by lipid and TG accumulation; therefore, the results indicate that EEAY

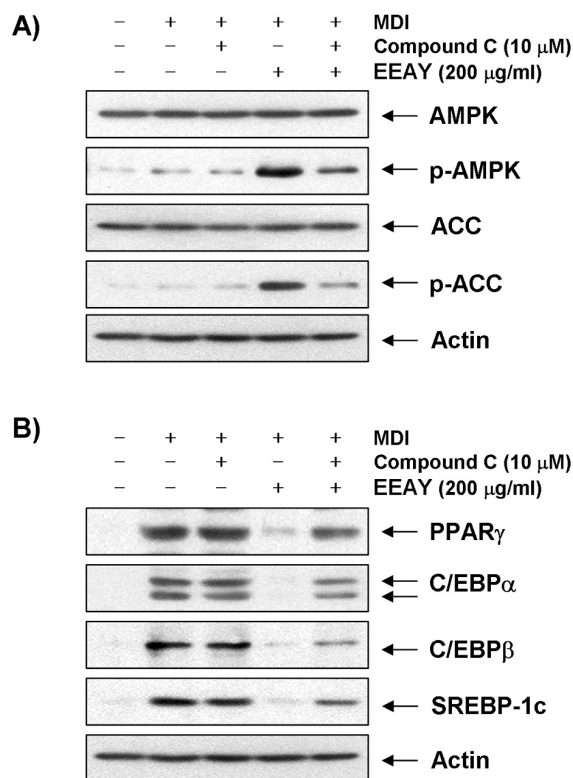


Figure 5. Effects of AMPK inhibitor on the EEAY-induced reduction in the expression of adipogenic transcription factors in the differentiated 3T3-L1 cells. Cells were pretreated with compound C, an AMPK inhibitor, for 1 h, and then treated with 200 mg/mL EEAY. On day 8, completely differentiated cells were lysed, and the cellular proteins were separated electrophoretically using SDS-polyacrylamide gels and transferred onto membranes. The membranes were probed with the indicated antibodies. Proteins were observed using an ECL detection system. Actin was used as an internal control.

treatment significantly suppressed the differentiation of 3T3-L1 preadipocytes.

The differentiation of preadipocytes into adipocytes is regulated by a complicated process that is sequentially co-ordinated by various transcription factors. Among them, C/EBP β is induced in the early stages of differentiation and is known to induce the expression of PPAR γ and C/EBP α , major regulators of adipogenesis and lipogenesis in the late stage differentiation (6,7). In addition, SREBP-1c is involved in lipid metabolism and is a further regulator of fatty acid synthesis enzymes. This transcription factor also enhances the differentiation of preadipocytes and the expression of down-stream genes associated with fatty acid metabolism (34,35). In addition to the activation of adipogenic transcription factors, transactivating adipocyte-specific genes such as aP2 and leptin are also critically important for the differentiation of preadipocytes into mature adipocytes (8,10). Therefore, the inhibition of adipogenic transcription and adipocyte-specific factors would decrease the adipocyte differentiation associated biosynthesis of fatty acids and TGs. In order to investigate the role of EEAY in regulating the expression level of the adipogenic transcription factors during adipogenesis of 3T3-

L1 cells, we compared their expression levels in the presence and absence of EEAY. As shown in Figure 3A, our immunoblotting data indicated that EEAY treatment of 3T3-L1 adipocytes significantly diminished the expression of the four transcription factors that were examined during adipocyte differentiation. These results indicated that EEAY blocked adipocyte differentiation by suppressing the expression of transcriptional factors involved in the different stages of differentiation. In addition, EEAY also reduced the expression of adipocyte markers aP2 and leptin on the 3T3-L1 cells. aP2 is a carrier protein that can trigger the accumulation of lipid droplets in the cytoplasm of differentiating adipocytes (36,37), and leptin upregulates the adipocyte genes involved in lipid oxidation, enhancing lipid accumulation in the adipocytes (38,39); therefore, our results also suggest that EEAY strongly suppress the de novo synthesis of TGs and differentiation of adipocytes.

Accumulating evidence suggests that the AMPK signaling pathway is a target for the energy balance and metabolic disorders involved in the maintenance of lipid and cholesterol homeostasis. During preadipocyte differentiation and adipogenesis, AMPK is inactivated by lower phosphorylation levels (17,19). In addition, AMPK activation by phosphorylation can reduce the degree of obesity by inhibiting adipocyte differentiation by changing the expression and activity of the enzymes and proteins involved in lipid metabolism (16,19). Furthermore, ACC, a downstream substrate of AMPK, is a rate-limiting enzyme that limits the critical rates in fatty acid synthesis and oxidation, reducing the fatty acid and lipid synthesis to inhibit the onset and progression of obesity (13,18). Therefore, AMPK signaling has gained the attention of researchers as a molecular target for fighting obesity. To determine whether AMPK activation is involved in EEAY-mediated attenuation of adipocyte differentiation and adipogenesis, we examined whether EEAY can activate AMPK. According to our results, EEAY markedly elevates the phosphorylation level of AMPK in a dose-dependent manner. Moreover, ACC phosphorylation was also increased, indicating that the AMPK signaling pathway was activated following EEAY administration. To investigate whether EEAY directly weakens adipocyte differentiation and adipogenesis through AMPK activation, the effect of compound C, an AMPK inhibitor, on the reduced adipogenic transcription factors in cultured 3T3-L1 cells in the presence of EEAY was evaluated. As expected, the elevated phosphorylation of ACC and AMPK was inhibited simultaneously by treatment with compound C (Figure 5A). In addition, the EEAY-induced reduction in the expression of transcription factors such as PPAR γ , C/EBP members, and SREBP-1c was reversed by the suppression of AMPK activity by compound C (Figure 5B). The results collectively indicate that EEAY stimulated AMPK activity, suppressing the adipocyte differentiation regulators and consequently their target

lipogenic enzymes and proteins, ultimately resulting in reduced lipid accumulation.

In summary, our results indicate that EEAY reduced adipocyte differentiation and adipogenesis in the 3T3-L1 cells by suppressing the adipogenic transcriptional factors and their downstream target genes without cytotoxicity. Further, EEAY also increased the phosphorylation of AMPK and ACC; however, the artificial blockage of AMPK activity suppressed the inhibitory effects of EEAY on the expressions of adipogenic transcriptional factors, demonstrating that EEAY has significant anti-adipogenic effect that function *via* the AMPK pathway. Thus, the activation of the AMPK pathway by EEAY may be a potential strategy for preventing obesity.

Acknowledgements

This research was supported by Basic Science Research Program through the National Research Foundation of Korea (NRF) grant funded by the Korea government (2015R1A2A2A01004633) and Blue-Bio Industry Regional Innovation Center (RIC08-06-07) at Donggeui University as a RIC program under Ministry of Trade, Industry & Energy and Busan city.

References

1. Bonomini F, Rodella LF, Rezzani R. Metabolic syndrome, aging and involvement of oxidative stress. *Aging Dis.* 2015; 6:109-120.
2. Catanzaro R, Cuffari B, Italia A, Marotta F. Exploring the metabolic syndrome: Nonalcoholic fatty pancreas disease. *World J Gastroenterol.* 2016; 22:7660-7675.
3. Berk PD, Verna EC. Nonalcoholic fatty liver disease: Lipids and insulin resistance. *Clin Liver Dis.* 2016; 20:245-262.
4. Frühbeck G, Méndez-Giménez L, Fernández-Formoso JA, Fernández S, Rodríguez A. Regulation of adipocyte lipolysis. *Nutr Res Rev.* 2014; 27:63-93.
5. Ali AT, Hochfeld WE, Myburgh R, Pepper MS. Adipocyte and adipogenesis. *Eur J Cell Biol.* 2013; 92:229-236.
6. Mota de Sá P, Richard AJ, Hang H, Stephens JM. Transcriptional regulation of adipogenesis. *Compr Physiol.* 2017; 7:635-674.
7. Guo L, Li X, Tang QQ. Transcriptional regulation of adipocyte differentiation: A central role for CCAAT/enhancer-binding protein (C/EBP) β . *J Biol Chem.* 2015; 290:755-761.
8. Kralisch S, Fasshauer M. Adipocyte fatty acid binding protein: A novel adipokine involved in the pathogenesis of metabolic and vascular disease? *Diabetologia.* 2013; 56:10-21.
9. Pandit R, Beerens S, Adan RAH. Role of leptin in energy expenditure: The hypothalamic perspective. *Am J Physiol Regul Integr Comp Physiol.* 2017; 312:R938-R947.
10. Stern JH, Rutkowski JM, Scherer PE. Adiponectin, leptin, and fatty acids in the maintenance of metabolic homeostasis through adipose tissue crosstalk. *Cell Metab.* 2016; 23:770-784.
11. Wang S, Moustaid-Moussa N, Chen L, Mo H, Shastri

- A, Su R, Bapat P, Kwun I, Shen CL. Novel insights of dietary polyphenols and obesity. *J Nutr Biochem*. 2014; 25:1-18.
12. Nakamura MT, Yudell BE, Loor JJ. Regulation of energy metabolism by long-chain fatty acids. *Prog Lipid Res*. 2014; 53:124-144.
 13. Coles CA. Adipokines in healthy skeletal muscle and metabolic disease. *Adv Exp Med Biol*. 2016; 900:133-160.
 14. Jeon SM. Regulation and function of AMPK in physiology and diseases. *Exp Mol Med*. 2016; 48:e245.
 15. Garcia D, Shaw RJ. AMPK: Mechanisms of cellular energy sensing and restoration of metabolic balance. *Mol Cell*. 2017; 66:789-800.
 16. Coughlan KA, Valentine RJ, Ruderman NB, Saha AK. Nutrient excess in AMPK downregulation and insulin resistance. *J Endocrinol Diabetes Obes*. 2013; 1:1008.
 17. Marín-Aguilar F, Pavillard LE, Giampieri F, Bullón P, Cordero MD. Adenosine monophosphate (AMP)-activated protein kinase: A new target for nutraceutical compounds. *Int J Mol Sci*. 2017; 18:E288.
 18. Bijland S, Mancini SJ, Salt IP. Role of AMP-activated protein kinase in adipose tissue metabolism and inflammation. *Clin Sci (Lond)*. 2013; 124:491-507.
 19. Angin Y, Beauloye C, Horman S, Bertrand L. Regulation of carbohydrate metabolism, lipid metabolism, and protein metabolism by AMPK. *EXS*. 2016; 107:23-43.
 20. Mount P, Davies M, Choy SW, Cook N, Power D. Obesity-related chronic kidney disease-The role of lipid metabolism. *Metabolites*. 2015; 5:720-732.
 21. Kadowaki T, Yamauchi T, Waki H, Iwabu M, Okada-Iwabu M, Nakamura M. Adiponectin, adiponectin receptors, and epigenetic regulation of adipogenesis. *Cold Spring Harb Symp Quant Biol*. 2011; 76:257-265.
 22. Feng S, Reuss L, Wang Y. Potential of natural products in the inhibition of adipogenesis through regulation of PPAR γ expression and/or its transcriptional activity. *Molecules*. 2016; 21:E1278.
 23. Baek JH, Kim NJ, Song JK, Chun KH. Kahweol inhibits lipid accumulation and induces glucose-uptake through activation of AMP-activated protein kinase (AMPK). *BMB Rep*. 2017. pii: 3779.
 24. Sim JH, Lee HS, Lee S, Park DE, Oh K, Hwang KA, Kang HR, Ye SK, Kim HR. Anti-asthmatic activities of an ethanol extract of *Aster yomena* in an ovalbumin-induced murine asthma model. *J Med Food*. 2014; 17:606-611.
 25. Park SH, Eom AH. Effects of mycorrhizal and endophytic fungi on plant community: A microcosm study. *Mycobiology*. 2007; 35:186-190.
 26. Yun J, Lee H, Ko HJ, Woo ER, Lee DG. Fungicidal effect of isoquercitrin *via* inducing membrane disturbance. *Biochim Biophys Acta*. 2015; 1848:695-701.
 27. Heo BG, Park YS, Chon SU, Lee SY, Cho JY, Gorinstein S. Antioxidant activity and cytotoxicity of methanol extracts from aerial parts of Korean salad plants. *Biofactors*. 2007; 30:79-89.
 28. Nugroho A, Kim KH, Lee KR, Alam MB, Choi JS, Kim WB, Park HJ. Qualitative and quantitative determination of the caffeoylquinic acids on the Korean mountainous vegetables used for chwinamul and their peroxynitrite-scavenging effect. *Arch Pharm Res*. 2009; 32:1361-1367.
 29. Lee W, Woo ER, Lee DG. Phytol has antibacterial property by inducing oxidative stress response in *Pseudomonas aeruginosa*. *Free Radic Res*. 2016; 50:1309-1318.
 30. Choi JH, Kim DW, Park SE, Choi BS, Sapkota K, Kim S, Kim SJ. Novel thrombolytic protease from edible and medicinal plant *Aster yomena* (Kitam.) Honda with anticoagulant activity: Purification and partial characterization. *J Biosci Bioeng*. 2014; 118:372-377.
 31. Kim AR, Jin Q, Jin HG, Ko HJ, Woo ER. Phenolic compounds with IL-6 inhibitory activity from *Aster yomena*. *Arch Pharm Res*. 2014; 37:845-851.
 32. Kang HJ, Jeong JS, Park NJ, Go GB, Kim SO, Park C, Kim BW, Hong SH, Choi YH. An ethanol extract of *Aster yomena* (Kitam.) Honda inhibits lipopolysaccharide-induced inflammatory responses in murine RAW 264.7 macrophages. *Biosci Trends*. 2017; 11:85-94.
 33. You MK, Kim HJ, Rhyu J, Kim HA. Pear pomace ethanol extract improves insulin resistance through enhancement of insulin signaling pathway without lipid accumulation. *Nutr Res Pract*. 2017; 11:198-205.
 34. Xu X, So JS, Park JG, Lee AH. Transcriptional control of hepatic lipid metabolism by SREBP and ChREBP. *Semin Liver Dis*. 2013; 33:301-311.
 35. Zhou X, Xu J, Shi Y, Ye JM. Discovery of novel anti-diabetic drugs by targeting lipid metabolism. *Curr Drug Targets*. 2015; 16:1372-1380.
 36. Tian X, Kang DS, Benovic JL. β -arrestins and G protein-coupled receptor trafficking. *Handb Exp Pharmacol*. 2014; 219:173-186.
 37. Hotamisligil GS, Bernlohr DA. Metabolic functions of FABPs-mechanisms and therapeutic implications. *Nat Rev Endocrinol*. 2015; 11:592-605.
 38. Harris RB. Direct and indirect effects of leptin on adipocyte metabolism. *Biochim Biophys Acta*. 2014; 1842:414-423.
 39. Ma X, Lee P, Chisholm DJ, James DE. Control of adipocyte differentiation in different fat depots; implications for pathophysiology or therapy. *Front Endocrinol (Lausanne)*. 2015; 6:1.

(Received September 7, 2017; Revised October 2, 2017; Accepted October 5, 2017)

Evaluation of the innate immune-stimulating activity of amazake using a silkworm muscle contraction assay

Hiroko Maruki-Uchida¹, Masahiko Sai¹, Kazuhisa Sekimizu^{2,3,*}

¹Research and Development Department, Health and Wellness Headquarters, Morinaga and Company Limited, Yokohama, Japan;

²Institute of Medical Mycology, Teikyo University, Tokyo, Japan;

³Genome Pharmaceuticals Institute Co., Ltd., Tokyo, Japan.

Summary

We evaluated the innate immune-stimulating activity of amazake using a silkworm muscle contraction assay. Sake cake, a raw material used to make amazake, had high innate immunity-stimulating activity, whereas rice malt, another raw material used to make amazake, did not, even after fermentation. These results suggest that the silkworm muscle contraction assay is a useful tool to screen foods with high innate immune-stimulating activity and that amazake made from sake cake has immunomodulatory potential.

Keywords: Amazake, sake cake, sake lees, rice malt, silkworm, innate immunity

1. Introduction

The immune system is comprised of two elements: acquired immunity and innate immunity. The innate immune system, which mediates rapid responses to challenges using germline-encoded components, is a biological defense system against pathogens. The complement system, natural killer (NK) cells, and macrophages play important roles in innate immune defense. The innate immune system cooperates with the acquired immune system, which is developed through responses to antigens in order to protect the body. The innate immune capabilities of modern humans are declining due to stress, and environmental and dietary changes.

The development of a system to evaluate innate immunity is important for research on the prevention and treatment of disease. The evaluation of cells *in vitro* has limited use because the systems do not reflect the complexity of innate immunity. The evaluation of immunity in animals is undesirable from both cost and ethics perspectives. Therefore, we focused on the

silkworm as a model organism. The silkworm is an invertebrate that has no antibody formation organs. Therefore, in the silkworm, responses to pathogens depend on the innate immune system. The mechanisms of innate immunity are highly conserved from invertebrates to vertebrates, which makes the silkworm suitable for the evaluation of the innate immune system. We previously reported the use a basic silkworm-based research model for drug discovery and the investigation of new immunostimulators (1-3).

Amazake is a traditional, sweet, Japanese beverage that originated from "Amanotamazake", which was mentioned in the Chronicles of Japan from 720. Rice malt (koji) amazake is made from glycosylated starch by the action of amylase in rice malt. Sake cake amazake is made using sake cake, which contains fermented yeast and various nutrients, and sugar. Amazake can also be made using both rice malt and sake cake. Generally, amazake contains healthy ingredients, such as sugars, amino acids, and vitamin B, and it is sometimes called a "drinking drip". In Japan, amazake is thought beverage to prevent summer weariness and winter colds. Amazake contains many bioactive substances, including the fermentation products of rice malt fungi and yeasts obtained from rice malt and sake cakes. Amazake reportedly has antihypertensive effects (4) and tyrosinase-inhibiting activity (5), while there are few scientific reports on its effects on immunity.

Released online in J-STAGE as advance publication October 30, 2017.

*Address correspondence to:

Dr. Kazuhisa Sekimizu, Teikyo University Institute of Medical Mycology, 359 Ohtsuka, Hachioji, Tokyo, 192-0395, Japan.

E-mail: sekimizu@main.teikyo-u.ac.jp

In this study, we used a silkworm muscle contraction assay to evaluate the immunomodulatory activity of the amazake ingredients sake cake and rice malt. We also examined the effects of glycosylation on the activity of rice malt.

2. Materials and Methods

2.1. Sample preparation

Sake cake and rice malt were obtained from Morinaga & Co., Ltd. (Tokyo, Japan); they were frozen at -30°C and freeze-dried (200 g) overnight with an Eyela FDU-2110 freeze dryer (Tokyo Rikakikai, Tokyo, Japan). The samples were ground in a mortar, and dissolved in physiological saline (Otsuka Pharmaceutical, Tokyo, Japan) at 6.3 mg sake cake/mL and 3.2 mg rice malt/mL. For rice malt glycosylation, the rice malt was dissolved in water (2-fold dilution, w/v) and glycosylated by general method.

2.2. Silkworm muscle contraction assay

We measured the effects of various samples on silkworm muscle contraction activity, as previously reported (6). Briefly, samples (50 μL) were injected into the body fluid of silkworms with a 1-mL syringe via a 27-gauge needle (Terumo, Tokyo, Japan). The muscle contraction value (C) was calculated by measuring the maximum length of each silkworm before (x cm) and after (y cm) the injection, such that $C = (x - y)/x$. Physiological saline was used as a negative control, and 0.2 mL air was used as a positive control ($C: 0.43 \pm 0.03$). The concentration that caused $C = 0.15$ (one unit) was calculated using a dose-response curve.

3. Results and Discussion

The compositions of sake cake and rice malt are presented in Table 1. The moisture content of sake cake was higher than that of rice malt. The levels of glucose and sugars with a high degree of polymerization were lower in sake cake than in rice malt. The results of amazake-induced muscle contraction activity are summarized in Table 2. Sake cake showed four times higher immunity-stimulating activity than green tea, which is a traditional beverage that is well known in Japan for its health effects. Rice malt did not show immunity-stimulating activity, even when glycosylated. The immunomodulatory activity of sake cake was not affected by rice malt.

Polysaccharides have been reported to have immunity-stimulating activity based on silkworm assays (7). Our results indicated that the carbohydrates in amazake did not contribute to its immunity-stimulating activity, whereas sake cake appeared to have contributed to its activity. Okuda *et al.* reported

Table 1. Compositions of sake cake and rice malt

g/100g	Sake cake	Rice malt
Moisture	54.5	15.5
Fat	1.5	0.5
Protein	9.5	6.9
Ash	0.3	0.3
Glucose	6.7	28.4
Maltose	2.8	2.1
Maltotriose	1.5	< 0.1
Dietary fiber	2.8	1.3
Alcohol	2.8	1.3

Table 2. Immunity-stimulating activity of sake cake, rice malt, glycosylated rice malt

Sample	Relative activity (units/mg)
sake cake	25 ± 5
rice malt	< 6.3
glycosylated rice malt	< 6.3
sake cake + glycosylated rice malt	17 ± 3
green tea	6 (1)

Values were mean \pm standard deviation. One unit of activity was defined as the activity required to decrease the length of silkworm muscle specimens by 15% (6).

that sake cake has natural immunity-stimulating activity, based on NK cell activity (unpublished data). Therefore, the evidence suggests that sake cake amazake may stimulate innate immunity.

In larval hemocytes, immunologic stimulants can induce the production of reactive oxygen species, followed by the activation of serine proteases, thereby mediating the paralytic peptide processing reaction and leading to defense responses in the silkworm (6). In humans, NK cell activity is commonly assessed as a measure of natural immune activation. Broccoli extract was shown to have immunity-stimulating activity in the silkworm and to cause NK cell activation in humans (unpublished data). NK cell activity is lower in the elderly (8) and is also related to the risk of cancer (9). Therefore, natural and safe foods that stimulate NK cell activity would be beneficial, and further studies on sake cake amazake are needed to verify its NK cell-related activity.

The most well-known immunity-stimulating food is yogurt containing *Lactobacillus* species. *Lactobacillus* species improve the gut environment and stimulates NK cell activity in humans (10-13). Although we did not directly compare the efficacy of *Lactobacillus* species and amazake, lactic acid bacteria reportedly have high immunity-stimulating activity (250-460 units/mg) in the same silkworm muscle contraction assay (14). The amount of sake cake ingested at one time is about fifty times higher than that of lactic acid bacteria. Considering the levels ingested, sake cake is expected to exert high immunomodulatory activity. Kawamoto *et al.* reported that sake cake fermented with lactic acid bacteria prevents allergic rhinitis in mice (15); thus,

combining these health-promoting components is an attractive strategy.

In conclusion, the silkworm muscle contraction assay is an easy method to evaluate the innate immunity-stimulating activities of foods, and amazake made from sake cake is one of the expected immunity-stimulating foods. Studies in human systems will be required to confirm and extend our findings.

Acknowledgements

We thanked Dr. Kana Hashimoto for her technical support.

References

1. Dhital S, Hamamoto H, Urai M, Ishii K, Sekimizu K. Purification of innate immunostimulant from green tea using a silkworm muscle contraction assay. *Drug Discov Ther.* 2011; 5:18-25.
2. Fujiyuki T, Hamamoto H, Ishii K, Urai M, Kataoka K, Takeda T, Shibata S, Sekimizu K. Evaluation of innate immune stimulating activity of polysaccharides using a silkworm (*Bombyx mori*) muscle contraction assay. *Drug Discov Ther.* 2012; 6:88-93.
3. Sekimizu K, Hamamoto H. Using silkworms as a laboratory animal to evaluate medicines and foods. *Drug Discov Ther.* 2016; 10:1-2.
4. Saito Y, Wanezaki K, Kawato A, Imayasu S. Antihypertensive effects of peptide in sake and its by-products on spontaneously hypertensive rats. *Biosci Biotechnol Biochem.* 1994; 58:812-816.
5. Jeon HJ, Noda M, Maruyama M, Matoba Y, Kumagai T, Sugiyama M. Identification and kinetic study of tyrosinase inhibitors found in sake lees. *J Agric Food Chem.* 2006; 54:9827-9833.
6. Ishii K, Hamamoto H, Kamimura M, Sekimizu K. Activation of the silkworm cytokine by bacterial and fungal cell wall components *via* a reactive oxygen species-triggered mechanism. *J Biol Chem.* 2008; 283:2185-2191.
7. Fujiyuki T, Hamamoto H, Ishii K, Urai M, Kataoka K, Takeda T, Shibata S, Sekimizu K. Evaluation of innate immune stimulating activity of polysaccharides using a silkworm (*Bombyx mori*) muscle contraction assay. *Drug Discov Ther.* 2012; 6:88-93.
8. Myśliwska J, Myśliwski A, Romanowski P, Bigda J, Sosnowska D, Foerster J. Monocytes are responsible for depressed natural killer (NK) activity in both young and elderly low NK responders. *Gerontology.* 1992; 38:41-49.
9. Imai K, Matsuyama S, Miyake S, Suga K, Nakachi K. Natural cytotoxic activity of peripheral-blood lymphocytes and cancer incidence: an 11-year follow-up study of a general population. *Lancet.* 2000; 356:1795-1799.
10. De Simone C, Vesely R, Bianchi Salvadori B, Jirillo E. The role of probiotics in modulation of the immune system in man and in animals. *Int J Immunother.* 1993; 9:23-28.
11. Link-Amster H, Rochat F, Saudan KY, Mignot O, Aeschlimann JM. Modulation of a specific humoral immune response and changes in intestinal flora mediated through fermented milk intake. *FEMS Immunol Med Microbiol.* 1994; 10:55-63.
12. Nagao F, Nakayama M, Muto T, Okumura K. Effects of a fermented milk drink containing *Lactobacillus casei* strain Shirota on the immune system in healthy human subjects. *Biosci Biotechnol Biochem.* 2000; 64:2706-2708.
13. Lee A, Lee YJ, Yoo HJ, Kim M, Chang Y, Lee DS, Lee JH. Consumption of dairy yogurt containing *Lactobacillus paracasei* ssp. *paracasei*, *Bifidobacterium animalis* ssp. *lactis* and heat-treated *Lactobacillus plantarum* improves immune function including natural killer cell activity. *Nutrients.* 2017; 9:558.
14. Ishii M, Nishida S, Kataoka K, Nishiyama Y, Abe S, Sekimizu K. Lactic acid bacteria of the *Leuconostoc* genus with high innate immunity-stimulating activity. *Drug Discov Ther.* 2017; 11:25-29.
15. Kawamoto S, Kaneoke M, Ohkouchi K, Amano Y, Takaoka Y, Kume K, Aki T, Yamashita S, Watanabe K, Kadowaki M, Hirata D, Ono K. Sake lees fermented with lactic acid bacteria prevents allergic rhinitis-like symptoms and IgE-mediated basophil degranulation. *Biosci Biotechnol Biochem.* 2011; 75:140-144.

(Received October 3, 2017; Revised October 19, 2017; Accepted October 21, 2017)

Early small bowel perforation due to aflibercept

Toufic Moussallem, Chetana Lim, Michael Osseis, Francesco Esposito, Eylon Lahat, Liliana Fuentes, Chady Salloum, Daniel Azoulay*

Department of Hepato-Biliary and Pancreatic Surgery and Liver Transplantation, AP-HP Henri Mondor Hospital, Créteil, France.

Summary

In patients with malignancy who receive aflibercept based chemotherapy, gastrointestinal perforation is among the reported adverse events with a prevalence of 1.9%. This complication may lead to mortality up to 10.8%. We here report a case of small bowel perforation that occurred fifteen days after the first cycle of aflibercept in a 58-year old female who had metachronous colorectal liver metastases. Emergency laparotomy was performed and revealed a small bowel perforation without any anastomotic dehiscence. Surgery was followed by uneventful outcome. The use of aflibercept in patients with malignancy may be associated with very early gastrointestinal perforation and this should be known by oncologist and surgeons.

Keywords: Aflibercept, chemotherapy, gastrointestinal, perforation, angiogenesis inhibitor

1. Introduction

Spontaneous gastrointestinal perforation is a well-known and potentially life-threatening adverse event associated with Bevacizumab-based chemotherapy (1). Aflibercept, a new angiogenesis inhibitor targeting the vascular endothelial growth factor (VEGF) pathway, is currently used in combination with FOLFIRI in metastatic colorectal cancer patients progressing following an oxaliplatin-based chemotherapy since 2012 (2). As expected, Aflibercept may be also associated with increased risk of gastrointestinal perforation. The incidence of gastrointestinal perforation associated with Aflibercept has been estimated to be 1.9% with an associated mortality of 10.8% (3). We report here a case of small bowel perforation that occurred early in a patient receiving aflibercept for the treatment of metachronous colorectal liver metastases.

2. Case Report

Eight months after right colectomy and pancreaticoduodenectomy for a PT4N0M0 right colon adenocarcinoma, a 58-year old female developed metachronous liver metastasis. There was no evidence of tumor recurrence in all small intestine segments or peritoneal carcinomatosis. Neoadjuvant chemotherapy included FOLFIRI in combination with Aflibercept. Fifteen days after the first cycle of FOLFIRI/aflibercept combination, the patient complained for acute abdominal pain with nausea. The patient did not report any corticosteroid or nonsteroidal anti-inflammatory drug use. In physical examination, there were no signs of abdominal hernia. Computed tomography showed a pneumoperitoneum due to small bowel perforation. There were no signs of small intestine volvulus or occlusion, or internal hernia. In addition, the preoperative imaging confirmed patency of the superior mesenteric artery and vein. Emergent laparotomy confirmed the spontaneous mid-gut perforation (Figure 1A). Primary direct suture of the perforation was performed. Because of the softness of the small bowel wall with a risk of tearing and subsequent risk of secondary perforation, an obliteration of the perforation was performed using the round ligament (Figure 1B). The round ligament was dissected, divided and the umbilical portion of the round ligament was sutured on the small bowel. The postoperative course was uneventful. Aflibercept was

Released online in J-STAGE as advance publication October 11, 2017.

*Address correspondence to:

Dr. Daniel Azoulay, Department of Hepato-Biliary and Pancreatic Surgery and Liver Transplantation, AP-HP Henri Mondor Hospital, 51 Avenue du Marechal de Lattre de Tassigny, 94010 Créteil, France.

E-mail: daniel.azoulay@aphp.fr

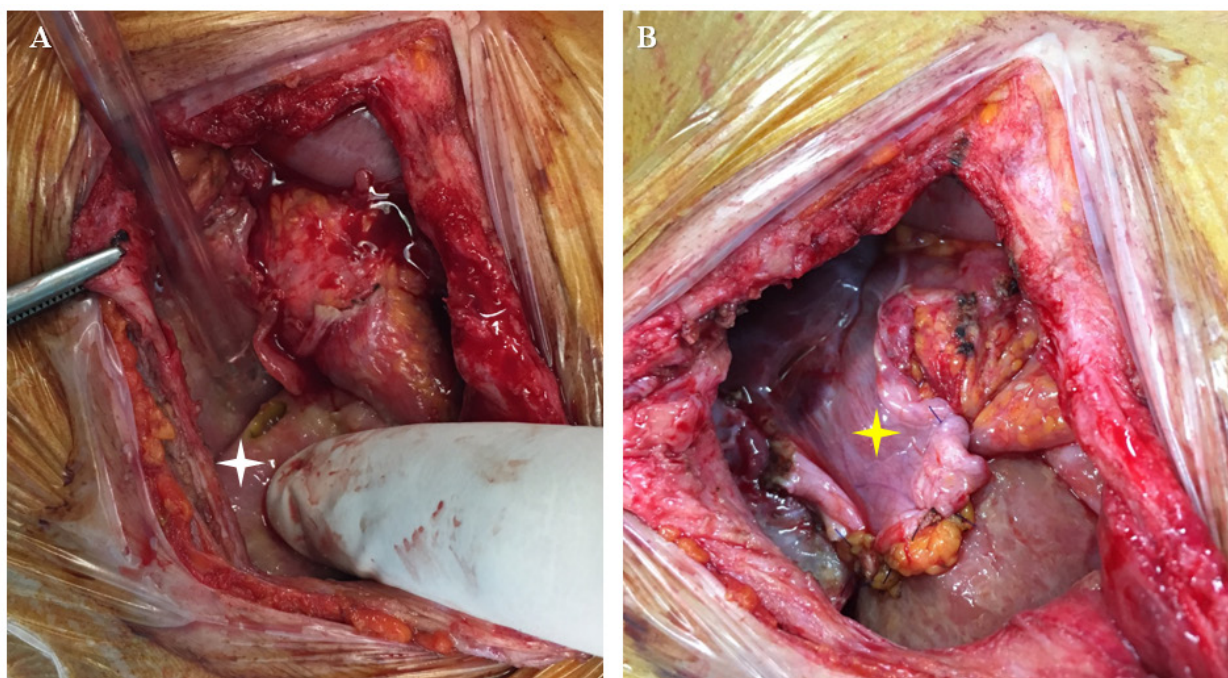


Figure 1. Intraoperative view of the small bowel perforation due to Aflibercept. A. Before obliteration by the round ligament (white star). B. After primary surgical suture and obliteration by the round ligament (yellow arrow).

discontinued postoperatively. The patient underwent liver resection 3 months later. She is doing well 3 months after hepatectomy with normal bowel function.

3. Discussion

Gastrointestinal perforation during or after treatment with Aflibercept was reported in patients with metastatic colorectal cancer (4,5). The present report has important clinical implications. First, in the present case, small bowel perforation occurred fifteen days after the first cycle of aflibercept. In the literature, time of occurrence of this complication has, to the best of our knowledge, never been described (4,5). Second, gastrointestinal perforation does not usually mean anastomotic dehiscence.

In the present case, the surgical treatment of the perforated small bowel consisted in performing simple surgical suture combined with the interposition of the round ligament. The use of the round ligament has been reported in the treatment of perforated peptic ulcer (6), but its use for obliteration of small bowel perforation has, to the best of our knowledge, never been reported.

In conclusion, the present report shows that the use of aflibercept in patients with malignancy may be associated with very early gastrointestinal perforation and this should be known by oncologist and surgeons.

References

1. Hapani S, Chu D, Wu S. Risk of gastrointestinal perforation in patients with cancer treated with bevacizumab: a meta-analysis. *Lancet Oncol.* 2009; 10:559-568.
2. FDA approves aflibercept (zaltrap) for metastatic colorectal cancer. *Oncology (Williston Park).* 2012; 26:842, 873.
3. Qi WX, Shen F, Qing Z, Xiao-Mao G. Risk of gastrointestinal perforation in cancer patients treated with aflibercept: a systematic review and meta-analysis. *Tumor Biol.* 2014; 35:10715-10722.
4. Van Cutsem E, Tabernero J, Lakomy R, Prenen H, Prausová J, Macarulla T, Ruff P, van Hazel GA, Moiseyenko V, Ferry D, McKendrick J, Polikoff J, Tellier A, Castan R, Allegra C. Addition of aflibercept to fluorouracil, leucovorin, and irinotecan improves survival in a phase III randomized trial in patients with metastatic colorectal cancer previously treated with an oxaliplatin-based regimen. *J Clin Oncol.* 2012; 30:3499-3506.
5. Tang PA, Cohen SJ, Kollmannsberger C, Bjarnason G, Virik K, MacKenzie MJ, Lourenco L, Wang L, Chen A, Moore MJ. Phase II clinical and pharmacokinetic study of aflibercept in patients with previously treated metastatic colorectal cancer. *Clin Cancer Res.* 2012; 18:6023-6031.
6. Costalat G, Dravet F, Alquier Y, Noel P, Vernhet J. Treatment of perforated peptic ulcer using the round ligament under coeloscopy. *J Chir (Paris).* 1991; 128:91-93.

(Received July 17, 2017; Revised September 18, 2017; Accepted September 22, 2017)

Erratum

DOI: 10.5582/ddt.2017.E1

In the article entitled "Sushi repeat-containing protein X-linked 2 promotes angiogenesis through the urokinase-type plasminogen activator receptor dependent integrin $\alpha\beta 3$ /focal adhesion kinase pathways" by Liu KL *et al.* (*Drug Discov Ther.* 2017; 11(4):212-217.), a mistake in Figure 3a ($\alpha\beta 3$) has been identified. Figure 3 is printed below.

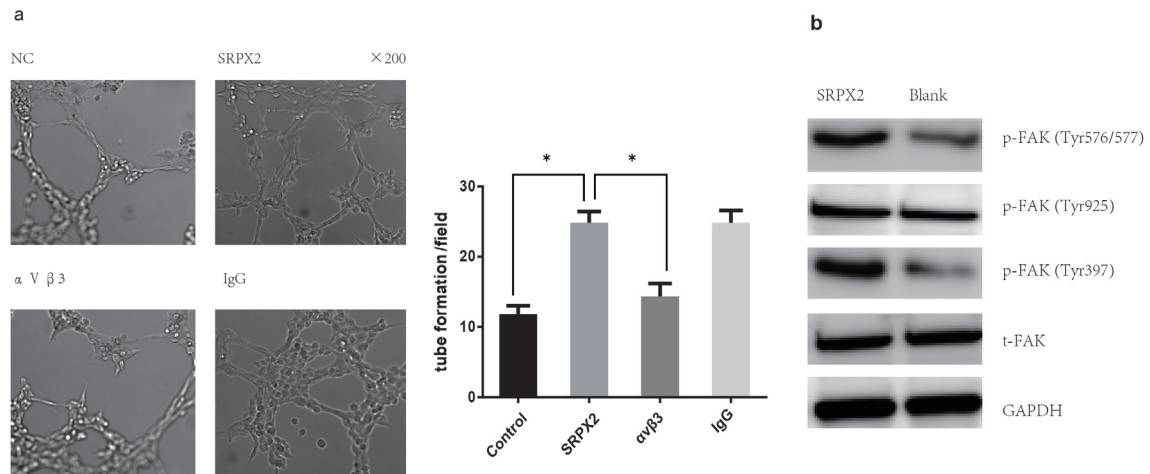


Figure 3. SRPX2 recombinant protein promoted tube formation of HUVECs on matrigel and pretreatment of integrin $\alpha\beta 3$ neutralizing antibody in HUVECs ($\alpha\beta 3$ group) significantly attenuated this effect (a). IgG group: pretreatment of HUVECs with control mouse IgG antibody. SRPX2 recombinant protein increased phosphorylation of FAK at sites of Tyr 397 and Tyr 576/577 in HUVECS after 4h culture compared with NC and Blank group (b). $*p < 0.001$.

Guide for Authors

1. Scope of Articles

Drug Discoveries & Therapeutics welcomes contributions in all fields of pharmaceutical and therapeutic research such as medicinal chemistry, pharmacology, pharmaceutical analysis, pharmaceuticals, pharmaceutical administration, and experimental and clinical studies of effects, mechanisms, or uses of various treatments. Studies in drug-related fields such as biology, biochemistry, physiology, microbiology, and immunology are also within the scope of this journal.

2. Submission Types

Original Articles should be well-documented, novel, and significant to the field as a whole. An Original Article should be arranged into the following sections: Title page, Abstract, Introduction, Materials and Methods, Results, Discussion, Acknowledgments, and References. Original articles should not exceed 5,000 words in length (excluding references) and should be limited to a maximum of 50 references. Articles may contain a maximum of 10 figures and/or tables.

Brief Reports definitively documenting either experimental results or informative clinical observations will be considered for publication in this category. Brief Reports are not intended for publication of incomplete or preliminary findings. Brief Reports should not exceed 3,000 words in length (excluding references) and should be limited to a maximum of 4 figures and/or tables and 30 references. A Brief Report contains the same sections as an Original Article, but the Results and Discussion sections should be combined.

Reviews should present a full and up-to-date account of recent developments within an area of research. Normally, reviews should not exceed 8,000 words in length (excluding references) and should be limited to a maximum of 100 references. Mini reviews are also accepted.

Policy Forum articles discuss research and policy issues in areas related to life science such as public health, the medical care system, and social science and may address governmental issues at district, national, and international levels of discourse. Policy Forum articles should not exceed 2,000 words in length (excluding references).

Case Reports should be detailed reports of the symptoms, signs, diagnosis, treatment, and follow-up of an individual patient. Case reports may contain a demographic profile of the patient but usually describe an unusual or novel occurrence. Unreported or unusual side effects or adverse interactions involving medications will also be considered. Case

Reports should not exceed 3,000 words in length (excluding references).

News articles should report the latest events in health sciences and medical research from around the world. News should not exceed 500 words in length.

Letters should present considered opinions in response to articles published in Drug Discoveries & Therapeutics in the last 6 months or issues of general interest. Letters should not exceed 800 words in length and may contain a maximum of 10 references.

3. Editorial Policies

Ethics: Drug Discoveries & Therapeutics requires that authors of reports of investigations in humans or animals indicate that those studies were formally approved by a relevant ethics committee or review board.

Conflict of Interest: All authors are required to disclose any actual or potential conflict of interest including financial interests or relationships with other people or organizations that might raise questions of bias in the work reported. If no conflict of interest exists for each author, please state "There is no conflict of interest to disclose".

Submission Declaration: When a manuscript is considered for submission to Drug Discoveries & Therapeutics, the authors should confirm that 1) no part of this manuscript is currently under consideration for publication elsewhere; 2) this manuscript does not contain the same information in whole or in part as manuscripts that have been published, accepted, or are under review elsewhere, except in the form of an abstract, a letter to the editor, or part of a published lecture or academic thesis; 3) authorization for publication has been obtained from the authors' employer or institution; and 4) all contributing authors have agreed to submit this manuscript.

Cover Letter: The manuscript must be accompanied by a cover letter signed by the corresponding author on behalf of all authors. The letter should indicate the basic findings of the work and their significance. The letter should also include a statement affirming that all authors concur with the submission and that the material submitted for publication has not been published previously or is not under consideration for publication elsewhere. The cover letter should be submitted in PDF format. For example of Cover Letter, please visit <http://www.ddtjournal.com/downloadcentre.php> (Download Centre).

Copyright: A signed JOURNAL PUBLISHING AGREEMENT (JPA) must be provided by post, fax, or as a scanned file before acceptance of the article. Only forms with a hand-written signature are accepted. This copyright will ensure the widest possible dissemination of information. A form facilitating transfer of copyright can be downloaded by clicking the appropriate link and can be returned to the e-mail address or fax number noted on the form (Please visit

Download Centre). Please note that your manuscript will not proceed to the next step in publication until the JPA form is received. In addition, if excerpts from other copyrighted works are included, the author(s) must obtain written permission from the copyright owners and credit the source(s) in the article.

Suggested Reviewers: A list of up to 3 reviewers who are qualified to assess the scientific merit of the study is welcomed. Reviewer information including names, affiliations, addresses, and e-mail should be provided at the same time the manuscript is submitted online. Please do not suggest reviewers with known conflicts of interest, including participants or anyone with a stake in the proposed research; anyone from the same institution; former students, advisors, or research collaborators (within the last three years); or close personal contacts. Please note that the Editor-in-Chief may accept one or more of the proposed reviewers or may request a review by other qualified persons.

Language Editing: Manuscripts prepared by authors whose native language is not English should have their work proofread by a native English speaker before submission. If not, this might delay the publication of your manuscript in Drug Discoveries & Therapeutics.

The Editing Support Organization can provide English proofreading, Japanese-English translation, and Chinese-English translation services to authors who want to publish in Drug Discoveries & Therapeutics and need assistance before submitting a manuscript. Authors can visit this organization directly at <http://www.iacmhr.com/iac-eso/support.php?lang=en>. IAC-ESO was established to facilitate manuscript preparation by researchers whose native language is not English and to help edit works intended for international academic journals.

4. Manuscript Preparation

Manuscripts should be written in clear, grammatically correct English and submitted as a Microsoft Word file in a single-column format. Manuscripts must be paginated and typed in 12-point Times New Roman font with 24-point line spacing. Please do not embed figures in the text. Abbreviations should be used as little as possible and should be explained at first mention unless the term is a well-known abbreviation (*e.g.* DNA). Single words should not be abbreviated.

Title page: The title page must include 1) the title of the paper (Please note the title should be short, informative, and contain the major key words); 2) full name(s) and affiliation(s) of the author(s); 3) abbreviated names of the author(s); 4) full name, mailing address, telephone/fax numbers, and e-mail address of the corresponding author; and 5) conflicts of interest (if you have an actual or potential conflict of interest to disclose, it must be included as a footnote on the title page of the manuscript; if no conflict of interest exists for each author, please state "There is no conflict of interest to disclose"). Please visit [Download Centre](#) and refer to the title page of the manuscript sample.

Abstract: The abstract should briefly state the purpose of the study, methods, main findings, and conclusions. For article types including Original Article, Brief Report, Review, Policy Forum, and Case Report, a one-paragraph abstract consisting of no more than 250 words must be included in the manuscript. For News and Letters, a brief summary of main content in 150 words or fewer should be included in the manuscript. Abbreviations must be kept to a minimum and non-standard abbreviations explained in brackets at first mention. References should be avoided in the abstract. Key words or phrases that do not occur in the title should be included in the Abstract page.

Introduction: The introduction should be a concise statement of the basis for the study and its scientific context.

Materials and Methods: The description should be brief but with sufficient detail to enable others to reproduce the experiments. Procedures that have been published previously should not be described in detail but appropriate references should simply be cited. Only new and significant modifications of previously published procedures require complete description. Names of products and manufacturers with their locations (city and state/country) should be given and sources of animals and cell lines should always be indicated. All clinical investigations must have been conducted in accordance with Declaration of Helsinki principles. All human and animal studies must have been approved by the appropriate institutional review board(s) and a specific declaration of approval must be made within this section.

Results: The description of the experimental results should be succinct but in sufficient detail to allow the experiments to be analyzed and interpreted by an independent reader. If necessary, subheadings may be used for an orderly presentation. All figures and tables must be referred to in the text.

Discussion: The data should be interpreted concisely without repeating material already presented in the Results section. Speculation is permissible, but it must be well-founded, and discussion of the wider implications of the findings is encouraged. Conclusions derived from the study should be included in this section.

Acknowledgments: All funding sources should be credited in the Acknowledgments section. In addition, people who contributed to the work but who do not meet the criteria for authors should be listed along with their contributions.

References: References should be numbered in the order in which they appear in the text. Citing of unpublished results, personal communications, conference abstracts, and theses in the reference list is not recommended but these sources may be mentioned in the text. In the reference list, cite the names of all authors when there are fifteen or fewer authors; if there are sixteen or more authors, list the first three followed by *et al.* Names of journals should

be abbreviated in the style used in PubMed. Authors are responsible for the accuracy of the references. Examples are given below:

Example 1 (Sample journal reference):
Nakata M, Tang W. Japan-China Joint Medical Workshop on Drug Discoveries and Therapeutics 2008: The need of Asian pharmaceutical researchers' cooperation. *Drug Discov Ther.* 2008; 2:262-263.

Example 2 (Sample journal reference with more than 15 authors):
Darby S, Hill D, Auvinen A, *et al.* Radon in homes and risk of lung cancer: Collaborative analysis of individual data from 13 European case-control studies. *BMJ.* 2005; 330:223.

Example 3 (Sample book reference):
Shalev AY. Post-traumatic stress disorder: Diagnosis, history and life course. In: *Post-traumatic Stress Disorder, Diagnosis, Management and Treatment* (Nutt DJ, Davidson JR, Zohar J, eds.). Martin Dunitz, London, UK, 2000; pp. 1-15.

Example 4 (Sample web page reference):
World Health Organization. The World Health Report 2008 – primary health care: Now more than ever. http://www.who.int/whr/2008/whr08_en.pdf (accessed September 23, 2010).

Tables: All tables should be prepared in Microsoft Word or Excel and should be arranged at the end of the manuscript after the References section. Please note that tables should not in image format. All tables should have a concise title and should be numbered consecutively with Arabic numerals. If necessary, additional information should be given below the table.

Figure Legend: The figure legend should be typed on a separate page of the main manuscript and should include a short title and explanation. The legend should be concise but comprehensive and should be understood without referring to the text. Symbols used in figures must be explained.

Figure Preparation: All figures should be clear and cited in numerical order in the text. Figures must fit a one- or two-column format on the journal page: 8.3 cm (3.3 in.) wide for a single column, 17.3 cm (6.8 in.) wide for a double column; maximum height: 24.0 cm (9.5 in.). Please make sure that artwork files are in an acceptable format (TIFF or JPEG) at minimum resolution (600 dpi for illustrations, graphs, and annotated artwork, and 300 dpi for micrographs and photographs). Please provide all figures as separate files. Please note that low-resolution images are one of the leading causes of article resubmission and schedule delays. All color figures will be reproduced in full color in the online edition of the journal at no cost to authors.

Units and Symbols: Units and symbols conforming to the International System of Units (SI) should be used for physicochemical quantities. Solidus notation (*e.g.* mg/kg, mg/mL, mol/mm²/min) should be used. Please refer to the SI Guide www.bipm.org/en/si/ for standard units.

Supplemental data: Supplemental data might be useful for supporting and enhancing your scientific research and Drug Discoveries & Therapeutics accepts the submission of these materials which will be only published online alongside the electronic version of your article. Supplemental files (figures, tables, and other text materials) should be prepared according to the above guidelines, numbered in Arabic numerals (*e.g.*, Figure S1, Figure S2, and Table S1, Table S2) and referred to in the text. All figures and tables should have titles and legends. All figure legends, tables and supplemental text materials should be placed at the end of the paper. Please note all of these supplemental data should be provided at the time of initial submission and note that the editors reserve the right to limit the size and length of Supplemental Data.

5. Submission Checklist

The Submission Checklist will be useful during the final checking of a manuscript prior to sending it to Drug Discoveries & Therapeutics for review. Please visit [Download Centre](#) and download the Submission Checklist file.

6. Online submission

Manuscripts should be submitted to Drug Discoveries & Therapeutics online at <http://www.ddtjournal.com>. The manuscript file should be smaller than 5 MB in size. If for any reason you are unable to submit a file online, please contact the Editorial Office by e-mail at office@ddtjournal.com

7. Accepted manuscripts

Proofs: Galley proofs in PDF format will be sent to the corresponding author *via* e-mail. Corrections must be returned to the editor (proof-editing@ddtjournal.com) within 3 working days.

Offprints: Authors will be provided with electronic offprints of their article. Paper offprints can be ordered at prices quoted on the order form that accompanies the proofs.

Page Charge: A page charge of \$140 will be assessed for each printed page of an accepted manuscript. The charge for printing color figures is \$340 for each page. Under exceptional circumstances, the author(s) may apply to the editorial office for a waiver of the publication charges at the time of submission.

(Revised February 2013)

Editorial and Head Office:

Pearl City Koishikawa 603
2-4-5 Kasuga, Bunkyo-ku
Tokyo 112-0003
Japan
Tel: +81-3-5840-9697
Fax: +81-3-5840-9698
E-mail: office@ddtjournal.com

JOURNAL PUBLISHING AGREEMENT (JPA)

Manuscript No.:

Title:

Corresponding author:

The International Advancement Center for Medicine & Health Research Co., Ltd. (IACMHR Co., Ltd.) is pleased to accept the above article for publication in Drug Discoveries & Therapeutics. The International Research and Cooperation Association for Bio & Socio-Sciences Advancement (IRCA-BSSA) reserves all rights to the published article. Your written acceptance of this JOURNAL PUBLISHING AGREEMENT is required before the article can be published. Please read this form carefully and sign it if you agree to its terms. The signed JOURNAL PUBLISHING AGREEMENT should be sent to the Drug Discoveries & Therapeutics office (Pearl City Koishikawa 603, 2-4-5 Kasuga, Bunkyo-ku, Tokyo 112-0003, Japan; E-mail: office@ddtjournal.com; Tel: +81-3-5840-9697; Fax: +81-3-5840-9698).

1. Authorship Criteria

As the corresponding author, I certify on behalf of all of the authors that:

- 1) The article is an original work and does not involve fraud, fabrication, or plagiarism.
- 2) The article has not been published previously and is not currently under consideration for publication elsewhere. If accepted by Drug Discoveries & Therapeutics, the article will not be submitted for publication to any other journal.
- 3) The article contains no libelous or other unlawful statements and does not contain any materials that infringes upon individual privacy or proprietary rights or any statutory copyright.
- 4) I have obtained written permission from copyright owners for any excerpts from copyrighted works that are included and have credited the sources in my article.
- 5) All authors have made significant contributions to the study including the conception and design of this work, the analysis of the data, and the writing of the manuscript.
- 6) All authors have reviewed this manuscript and take responsibility for its content and approve its publication.
- 7) I have informed all of the authors of the terms of this publishing agreement and I am signing on their behalf as their agent.

2. Copyright Transfer Agreement

I hereby assign and transfer to IACMHR Co., Ltd. all exclusive rights of copyright ownership to the above work in the journal Drug Discoveries & Therapeutics, including but not limited to the right 1) to publish, republish, derivate, distribute, transmit, sell, and otherwise use the work and other related material worldwide, in whole or in part, in all languages, in electronic, printed, or any other forms of media now known or hereafter developed and the right 2) to authorize or license third parties to do any of the above.

I understand that these exclusive rights will become the property of IACMHR Co., Ltd., from the date the article is accepted for publication in the journal Drug Discoveries & Therapeutics. I also understand that IACMHR Co., Ltd. as a copyright owner has sole authority to license and permit reproductions of the article.

I understand that except for copyright, other proprietary rights related to the Work (e.g. patent or other rights to any process or procedure) shall be retained by the authors. To reproduce any text, figures, tables, or illustrations from this Work in future works of their own, the authors must obtain written permission from IACMHR Co., Ltd.; such permission cannot be unreasonably withheld by IACMHR Co., Ltd.

3. Conflict of Interest Disclosure

I confirm that all funding sources supporting the work and all institutions or people who contributed to the work but who do not meet the criteria for authors are acknowledged. I also confirm that all commercial affiliations, stock ownership, equity interests, or patent-licensing arrangements that could be considered to pose a financial conflict of interest in connection with the article have been disclosed.

Corresponding Author's Name (Signature):

Date:

